School of Engineering

UNIVERSIDAD CARLOS III DE MADRID

Department of Continuum Mechanics
and Structural Analysis

APPLICABILITY TO A PRE-DESIGN TOOL OF ANALYTICAL MODELS ON THE IMPACT OF COMPOSITE LAMINATES

Senior Thesis

Author:
David Rodríguez Martínez

Advisor:
Dr. Carlos Navarro Ugena
Continuum Mechanics and Structural Analysis
Universidad Carlos III de Madrid

Co-advisor:
Dr. Ever J. Barbero
Mechanical and Aerospace Engineering
West Virginia University

Leganés, 2015

Only those who attempt the absurd
can achieve the impossible,

Albert Einstein (1879-1955)

Acknowledgements

In the first place, I would like to express my heartfelt gratitude to all the people that have helped me to reach where I am today. Special gratitude to all those with whom I have not spent enough time during this long journey. Thank you all for always come through for me and be my biggest support, helping me to get over every hurdle along the way.

Second, I would like to thank my advisors, Professors Carlos Navarro and Ever J. Barbero, who provided the insight and expertise that greatly assisted this project. Thank you both for providing me the incredible opportunity to perform this work abroad. Special thanks to Professor Ever Barbero and his family for the enormous care and hospitality I received during the time I spent in the United States. The things I learned and the awe-inspiring people I met while I was there, make of this time something I will never forget.

I also take this opportunity to express my sense of gratitude to both *Universidad Carlos III de Madrid* and the *West Virginia University* for all the effort in providing an environment where I was able to pursuit my best, laying the groundwork for an amazing and exciting future.

Last but not least, I would like to place on record, my gratitude to one and all, who directly or indirectly, have helped to the completion of this project.

Abstract

Development of composite materials has caused that innovative features and capabilities are being sought for their use in new technology applications. Catastrophic events, like high velocity impacts, are likely to appear in fields where composite materials are being lately applied. Lightweight headgear for modern military ground forces, structural shielding for a knew orbiter spacecraft, or blades intended for high-efficiency wind turbines, are just some examples.

The dynamic response of composite materials has become an essential knowledge. New set of tools need to be developed in order to spread this knowledge and decrease design cost. As compared to experimental testing and numerical methods, analytical models stand out as the cheapest and fastest way to provide preliminary results that successfully assist early design stages. The main goal of this project relies on laying the basics for the development of a pre-design tool on the implementation of this latter type of models. This tool will support the early design of composite material structural components likely subjected to impact situations.

During the last three decades, a great number of analytical models have being developed intended to theoretically predict the behavior under impact of composite materials. The present work covers the basics findings on the field. Two models, based on the impact over carbon fiber, and glass and polymer fiber composites, are selected and thoroughly described in order to evaluate their applicability into a pre-design tool. Description of both models are provided with the needed background and theoretical foundations.

In order to evaluate the applicability of analytical models, a simple requirements-based method is presented. It is based on three broad requirements: good predictions, broad applicability and event sensitivity. Both analytical models are evaluated against these requirements. Results of this evaluation show how the first model (carbon fiber model) reproduces one specific case with accuracy. In spite of this good agreement, there is no possibility to reproduce further environments. This makes the model non optimal to be implemented into a design tool. The second model (glass and polymer fiber model) appears to successfully meet the three established requirements. Finally, some guidelines in the development of future analytical models under the method here described, and some possible paths to be followed in the implementation of the pre-design tool, are presented.

Contents

Chapter 1

Introduction

1.1 Motivation

Materials have always been developed and improved accordingly to the needs of the time. Back in the Middle Ages (from A.D. 400 to c.e. 1500), leather coats turned into full cast iron harness and chain mails in order to protect knights' torso in combat (Starley, 1999). At this time, materials research was aimed to improve the strength and flexibility of knights' protection armor. Today's needs demand new and improved materials features. Engineers work for structures to endure complex loads, land vehicles to run faster, and aircrafts to flight higher.

Structures and components have to be designed to endure not only the effects produced by their daily use, but also complex effects caused by rarely situations. Impacts and other types of dynamic loads are not but one more of these needs to be fulfilled. New current and future applications must consider impact loads alongside the conventional ones. Meteoroid colliding against a spacecraft, a fan blade impacting on its engine containment, a vehicle crashing into a obstacle, or the blast of an improvised explosive device (IED), are just some examples of the new capabilities sought in materials (Navarro (1998) and Kulkarni et al. (2013)).

For all this new set of applications, advanced materials have been developed during the last century. Composite materials have turned out to be one of nowadays more popular and highly-applied materials due to their capacity to tailor their properties to the needs of the final application.

A great example of the importance of impact resistance in the use of advanced materials can be found in the structural design of the International Space Station (ISS). The ISS is one of the largest and most ambitious space vehicle design and on-orbit construction program ever executed. Because of its huge dimensions, the long planned lifetime, and the high velocity and low altitude at which the ISS orbits, there are high probabilities of colliding against natural micrometeoroids and man-made space debris; such as defunct satellites, slag from solid rocket motors, explosion fragments or spent rockets stages (Nahra, 1989). These objects are a real threat to the ISS structural integrity. Due to their low dimensions, they cannot be detected by either optical or radar instruments. In order to ensure crew safety, ISS modules and critical components are protected against impact by a variety of shield types specifically designed. The so-called stuffed whipple shield developed by NASA, protects sections of the ISS exposed to

the highest concentration of orbital debris and meteoroids impacts. In order to do so, it incorporates a blanket, between the outer aluminum bumper and the inner pressure wall, made of a ceramic cloth called Nextel® followed by a high strength Kevlar® fabric (Christiansen and Kerr, 2001).

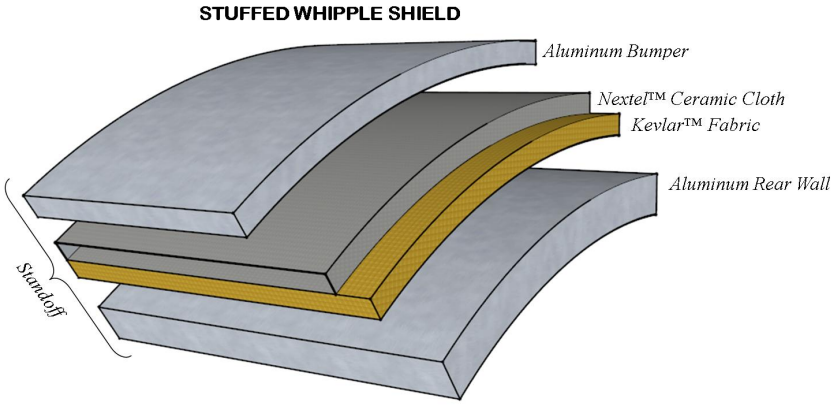

Figure 1.1: Stuffed whipple shield structural diagram.

This is just an example of the union between advanced materials and new featured capabilities. In order to acquire the background needed to develop and implement such kind of structures, scientist and engineers make use of different approaches. Experimental testing is established as one of the most followed paths. Full-scale tests are carried out in order to learn about the material behavior and verify the correct functionality of the structure. This approach gives the opportunity to reproduce the environment and conditions of the system in use, providing a precise overview of the event. An experimental device comprising a gas gun and a cryogenic chamber, is shown in Figure 1.2. This device was specifically designed by López-Puente et al. (2002a) in order to carry out impact tests at very low temperatures (up to -150 °C).

Figure 1.2: Gas gun experimental device, (López-Puente et al., 2002a)

Nevertheless, the empirical approach is, in many cases, expensive and time-consuming. Accordingly to the in-use conditions of the specimen under study, specific devices have to be designed and manufactured in order to measure certain parameters of interest. Two different approaches provide a cheapest and fastest alternative to reach such valuable knowledge. Many times, experimental tests result in mathematical models allowing others to avoid the need of testing. These models, by solving the basic equations of mechanics, provide a broadest approach to the system behavior, but enough precise for certain design stages. On the one hand, full-numerical methods make use of a computer-based treatment in order to solve complex problems. By the so-called simplified engineering modeling, numerical methods predict with suitable accuracy the behavior of materials under different situations. In Figure 1.3, a numerical simulation of an ice cylinder colliding at high velocity, is illustrated. The figure displays the impact event at three different stages by using three different integration procedures (Lagrangian, arbitrary Lagrangian Eulerian (ALE), and smoothed particles hydrodynamic (SPH)) (Pernas-Sánchez et al., 2012).

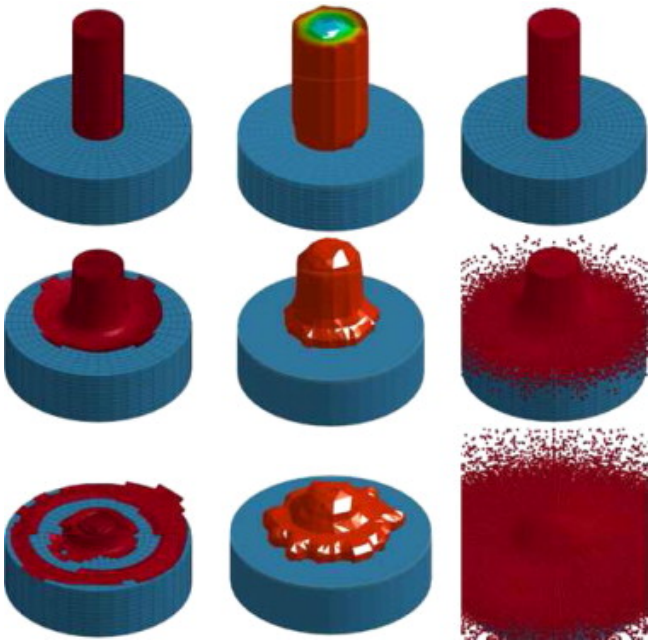

Figure 1.3: Ice projectile impact sequence using three integration methods: left Lagrangian, center ALE, right SPH, (Pernas-Sánchez et al., 2012)

Numerical modeling is an exceptional and low-cost approach to understand and verify the behavior of materials and structures. However, the complexity of the equations involved, requires, in many cases, of an enormous amount of computing time. It is possible to simplified the basics of these models so that a simple closed-form solution is obtained without the need of computer-based methods. This is the case of analytical models. This latter type of models relies on simple constitutive relationships and by taking into account just the main physical aspects of the event, they provide a generic approach to the problem solution.

Despite the lack of accuracy, less time-consuming and low cost make analytical models a suitable approach at early design stages. At first, engineers need of a reliable, agile and inexpensive tool in order to provide a benchmark for incoming design stages. With that aim,

the creation of a pre-design tool on the design of composite materials subjected to high-velocity impact situations, was proposed. In order to successfully design and implement such a tool, a thorough examination of the content need to be accomplished at first. The present work encompasses the basics to understand, analyze and settle the mainstay for the future creation of a pre-design tool on the impact of composite material laminates.

1.2 Background

The high demand of composite materials to low and high technology applications has caused that, during the last three decades, a great number of analytical models have been created intended to theoretically predict the behavior of such materials under different loading conditions. In the late 1980s, numerous experimental works were published regarding the behavior of composite materials under impact situations (e.g., Takeda et al. (1980); Manders and Harris (1986); Akay (1987); Stellbrink (1987); Rechak and Sun (1987); Hong and Liu (1989); and Curson et al. (1990)). Most of these works were motivated by their direct application to the military field. The continuous development of advanced materials and their use to a wider range of applications have caused that, on our days, the scientific scene is still filled with experimental works regarding the behavior under impact of these new set of materials (e.g., Carrillo et al. (2012); Shaktivesh et al. (2013); Yashiro et al. (2013); and Woo and Kim (2014)).

Along with the empirical approach, many authors based their scientific production on the research for a theoretical solution to the problem of impact in composite materials (e.g., Naik and Shrirao (2004); Naik et al. (2005, 2006); Naik and Kavala (2008); and Naik et al. (2010)). One of the first works on the field was performed by Smith et al. (1958). Smith's seminal works are focussed on the transverse impact of individual textile yarns. His work set up the basics for future developments concerning wave propagation throughout the impacted material. Further details on the propagation of stress waves are presented in Chapter 3 of the present work.

Following Smith's findings, Florence and Ahrens (1967) and Florence (1969) presented experimental and theoretical results on the interaction between projectiles and lightweight composite armor. These works present an extraordinary survey, mainly on the behavior under impact of ceramic tiles either backed and unbacked by flexible composite plates. Later on, Roylance (1973) proposed a semi-empirical approach to the impact of textile composites; describing master-curves for a set of different types of fibers.

By this time, several parameters define the jargon in the field of impacts of materials. One of the most relevant, the so-called ballistic limit, was thoroughly studied in Misey (1978). Ballistic limit is defined as the minimum velocity needed to be achieved by a given projectile in order to completely defeat the target. In relation with this limit, a statistical variable was also defined. Named mean ballistic limit velocity or V50, defines the velocity at which the impacting projectiles are expected to defeat a system 50% of the time (Cunniff, 1999). This term is useful on handling experimental data, having less, if any, application from a design point of view.

Based on the kinetic energy of the impactor, impacts events can be divided into three segments: low velocity, high velocity, and hyper-velocity impacts. Low velocity impacts can be defined as the impact event where the time for the projectile in contact with the target exceeds

the period of the lowest vibrational mode (Kulkarni et al., 2013). In a more generic way, low impacts can be considered those cases where the impactor speed is below 100 m/s (Navarro, 1998). At low impact velocities, the boundary conditions of the structural component are important in order to accurately describe the impact event. This is due to the fact that stress waves generated outward from the point of impact have enough time to reach the edges of the structural component, turning the support conditions crucial to determine its full response (Cantwell and Morton, 1991). The basics of dynamic loads and low velocity impacts in composite materials are carefully studied and presented in the excellent books written by Zukas (1982), Meyers (1994), and Abrate (1998). An example of an impact within this regime would be the collision of a ground vehicle during maintenance and loading operations on aircrafts. Ground service equipment (GSE), as the one shown in Figure 1.4, accounts for a significant percentage of damage taking place over commercial transport aircrafts. This could take place during cargo movement while loading the aircraft, or docking of the GSE around the aircraft doors (Kim et al., 2010).

Figure 1.4: Ground vehicles, luggage carts and cargo containers account to be an important aircraft structural threat, (Source: wikimedia.org)

On the other hand, local material behavior around the impacted zone governs the structural response at high impact velocities. This localized form of material response makes it independent of the system support conditions. Low and high velocity impacts will create different levels of damage with different consequences on the impacted material (Cantwell and Morton, 1989). Examples of impact within this velocity regime would be a low caliber bullet fired against a protective vest, a hail storm around an airplane in flight, or a damage blade of a propeller impacting over the hull ship. The analytical models presented throughout this project are focussed on the ballistic response of the material when low mass projectiles impact at high velocities.

Finally, hyper-velocity impacts are those cases where the locally impacted material behaves like a fluid. When a hyper-velocity impact occurs, very high stresses are induced upon the material. An excellent survey on hyper-velocity impacts in composites was made by Katz et al.

(2008). Katz and his co-workers presented valuable experimental data by using a laser driven flyer plate (LDFP) system that allows to generate debris impact up to velocities of 3 km/s. Typical impacts comprising space debris can reach velocities up to 15 km/s, and even higher in the case of meteoroids collisions (impacts around 72 km/s have been accounted (ESA, 2013)). The catastrophic effects caused in the material by an impact at hyper-velocity are shown in the following figure.

Figure 1.5: Effects of a hyper-velocity impact, (Photo provided by ESA)

It is already mentioned how the material response changes when variations on the projectile velocity are applied. The response under impact of composite materials is also influenced by the type of fiber and matrix used. A great number of authors performed experimental studies and developed analytical models on the impact of a variety of fiber-matrix combinations.

Carbon fiber-reinforced composites have been extensively studied due to their steadily increasing applicability on different industry sectors. An excellent set of works regarding high velocity impact on carbon fiber composites can be found in Cantwell and Morton (1985, 1986, 1989, 1990). Following Cantwell and Morton's work, analytical models developed by Sun and Potti (1996), Bland and Dear (2001), Hosur et al. (2001), López-Puente et al. (2002a,b, 2007), Tanabe et al. (2003), Hazzel et al. (2008), and López-Puente et al. (2009), are also focussed on the ballistic response of carbon fiber-reinforced composites. Most of these models are based on an energy balance criteria, assuming a quasi-static behavior of the material. Abrate (2001) presented the basics for a spring-mass model that accounts for the dynamics of the structure in a simplified manner. Chapter 2 presents a thorough description of the impact in carbon fiber composites at high velocities, along with a detail examination of the analytical model developed by López-Puente (2003).

The response under impact of glass fiber-reinforced composites has also motivated grand part of the scientific production. Some examples of the study on high velocity impacts in glass fiber composites are the papers due to Wu and Chang (1995), Naik and Shrirao (2004), Naik et al. (2006), Naik and Doshi (2008), García-Castillo et al. (2009), and Shaktivesh et al. (2013). Along with glass fibers, the dynamic behavior of polymeric fibers and the ballistic response of flexible fiber composite armors have been extensively studied (e.g., Zhu et al. (1992a,b); Iremonger and Went (1996); Morye et al. (2000); Gu (2003); Patel et al. (2004); Reis et al. (2012); and Carrillo et al. (2012)). Chapter 3 of the present work focusses on the behavior against impact of these two types of reinforcements. An analytical model intended to theoretically predict the behavior of glass and polymer fiber composites subjected to impact loads, is described as well.

Apart from the type of composites already mentioned, the dynamic response of other types of advanced materials has been widely studied. Those are the cases of metal fiber-reinforced composites (Morinière et al., 2014), ceramic clothing shields (Hayhurst et al., 1999), or polymer matrix nano-composites (Sun et al., 2009).

The selection of the type of constituent affects the ballistic behavior of composite materials. Together with the type of constituent and the impact velocity regime, a number of parameters influence the overall ballistic behavior of the material (López-Puente et al., 2009). This is due to the complexity of the projectile-composite interaction. Those parameters include: the composite stacking sequence (Will et al., 2002) and ply orientation (Wang et al., 2015), thickness of the target material (Atas et al., 2013; Naik and Doshi, 2008), obliquity of the collision (Hazzel et al., 2008; Pernas-Sánchez et al., 2014), weathering effects caused by extreme low temperatures (López-Puente et al., 2002a) or exposure to gamma radiation (Alves et al., 2005), shape of the impactor (Mines et al., 1999; Wen, 2000; Tan et al., 2003), nature of the impactor (e.g., collision of ice spheres (Kim et al., 2003)), curvature of the target plate (Kistler and Waas (1998a,b, 1999)), and effects caused by impacts over preloaded plates (Khalili et al., 2007; García-Castillo et al., 2009).

Apart from the parameters just mentioned, design against impact of composite materials is complicated due to the exhibition of coupling effects among membrane, torsion, and bending strains, weak transverse shear strength, and discontinuity of the mechanical properties along the thickness of composite laminates (Patel et al., 2004).

Chapter 2

Analytical description of the impact event in carbon fiber composites

The present chapter focuses on the description of the dynamic process that occurs when a small projectile strikes over a thin composite plate reinforced by continuous carbon fibers. Carbon fiber composites are today employed in a wide range of applications. From amateur sporting goods to complex and expensive spatial structures, carbon fiber composites are used to achieve lightweightness and high mechanical performance. Owing to the latter, the behavior of the material under different types of loads and environmental conditions must be thoroughly known; whether it is a tennis ball in a warm day of summer or a small wreckage of a comet the one colliding with the composite structure.

One of the common paths followed by scientist and engineers to achieve such level of knowledge is through the development of experimental testings. Based on experimentation, one is likely able to understand and describe the main factors responsible of the material behavior. In some cases, experimental observations result in mathematical models. Models developed with the aim of spreading the knowledge accomplished so that others can use them avoiding the need for experimental testing. The main goal of this work lies on this latter fact. Hence, a detailed description of an analytical model based on carbon fiber composites impacted by a projectile traveling at high velocity is presented.

Besides the mathematics demanded by the analytical modeling, one must understand first what happens to the material when a projectile impacts at high velocity. Therefore, the following section describes, based on different experimental observations, the damage and failure processes that take place when a carbon fiber composite plate is subjected to an impact within the high velocity regime.

Following the empirical assessments, the analytical model developed by López-Puente (2003) is described. This model depicts the impact event by the use of a differential analysis based on energy balance criteria; whereby a closed-form solution for the ballistic limit, residual velocity, and extent of the damaged area is obtained. First, the mathematical formulation can be found, followed by a complete description of its resolution. Last, a thorough discussion of the benefits and limitations of the model are presented.

2.1 The impact process on CFRPs

In order to completely understand the equations of the model, a qualitative description of the physical phenomenon is presented. A number of aspects must be kept in mind regarding the behavior of the material under impact conditions. The type of constituents, their internal arrangement, the velocity and obliquity of the collision, and the projectile properties are the major, but not unique, factors that influence the material behavior. One can find differences in the results obtained when varying just one of the previous aspects. The present section deals with this hurdle by presenting an overview of the process; focalising attention on the impact behavior of the so-called CFRP laminates. CFRP refers to carbon fiber reinforced plastics. Plastics that could be either based on thermoset or thermoplastic polymers. Thus, CFRP laminates are a specific class encompassed within the wide group of polymer matrix composites (PMC) (Barbero, 2010).

The bibliography regarding the behavior of CFRPs under different impact conditions is extensive. A good literature review concerning experimental observations on the impact of CFRP laminates can be found in López-Puente et al. (2009). Some of these works are underlined below.

In the context of impact processes, behavior of the material commonly means the description of different energy absorption and damage mechanisms taking place during the impact event. The experimental observations accomplished in Tanabe et al. (2003), López-Puente et al. (2009) and Pernas-Sánchez et al. (2014) reveal that CFRP laminated plates subjected to high velocity impacts dissipate the kinetic energy of the projectile mainly by the following five processes: laminate crushing, shear-out, delamination, linear momentum transfer, and tensile failure of fibers. The magnitude of each mechanism is dependent on the impact velocity and the instant of the process evaluated. Most authors distinguish thus, in one way or another, between two cases. On each case the laminate behavior is dominated by a different damage mechanism.

On the one hand, there is a first case in which the behavior is dominated by tensile failure of fibers. This failure pattern appears when the projectile velocity is below or slightly over the ballistic limit. In this case, perforation of the target does not always occur. On the other hand, there is a second case where the behavior of the material is dominated by the so-called plugging process, which appears when the projectile velocity is much higher than the ballistic limit. Plugging process comes out as a result of the combination of crushing and shear-out mechanisms. In this second case, perforation always happens along with the formation of the plug. The different mechanisms appear on both cases are thoroughly described below.

When the projectile firstly contacts the upper layers of the material, the laminate is damaged by compression. This process is called laminate crushing and appears on both cases (fiber failure or plugging). The spread of crushing through the thickness of the target depends on the velocity of the projectile. This initial failure could be named also matrix crushing, due to the fact that transverse compression is a matrix-dominated process. This will be treated in detail in Section 2.3. Because of this initial crushing, detached parts of the material accelerates from rest to a certain velocity considered to be equal to that of the projectile. This last statement is also revealed by the experimental tests performed in Hazzel et al. (2008).

If the velocity of the projectile is such that crushing occurs under the conditions of the plug-dominated case, the rest of the plies below the crushed zone start to break through a shearing process. This compression/shear process results in the formation of the plug. The kinetic energy involved in propelling the plug and small detached parts of the material is the energy absorbed by linear momentum transfer. Further description regarding the formation and geometry of the plug can be found in the following section.

On the other hand, if the velocity of the impactor is not high enough to shear out the fibers, experimental observations suggest an energy dissipation mechanism by which the fibers break due to tensile stresses.

A graphic sketch of the impact process in both tensile fiber failure and plug-dominated cases are shown in the following figure.

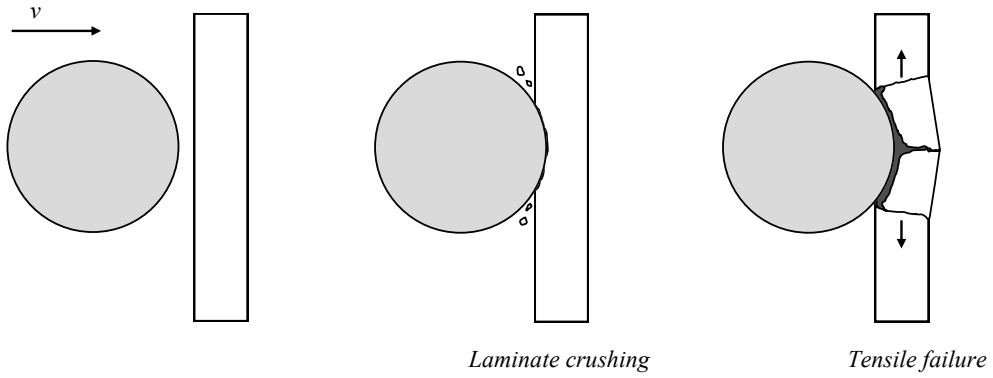

(a) Impact process at velocities near the ballistic limit

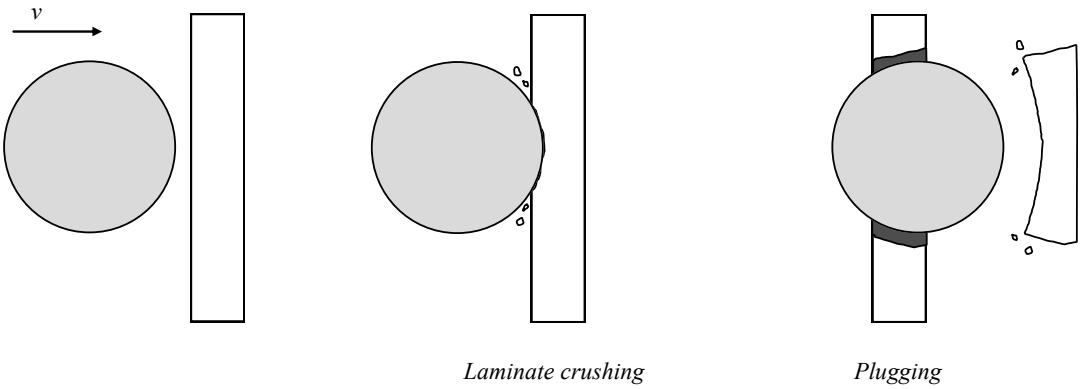

(b) Impact process at velocities above the ballistic limit

Figure 2.1: Description of the material breakage patterns at different velocity regimens.

Finally, a last damage mechanism appears upon the impacted material. This damage mechanism is related to the energy absorbed by delamination. Delamination is a failure mechanism

caused by the split of the plies as a result of local bending and through-the-thickness wave propagation (Cantwell and Morton, 1990). Although a portion of the energy dissipated by the material during a high velocity impact is always related to this failure mechanism, delamination is of major importance when collisions occur over thick laminates or unidirectional laminates formed by plies of different orientations. The reason for the latter lies on the increased difference in the bending stiffness between plies. Greater the number of plies or the variability in the apparent bending stiffness, greater the number of interfaces available for delamination (Sebaey et al., 2013). Delamination also plays a major role on the residual capability of defeated targets due to the overall reduction of the laminate stiffness (Abrate, 1998).

When perforation occurs, different postmortem aspect of the laminate is revealed for each case. This variation in the aspect of the defeated target is illustrated in Figure 2.2. In the case dominated by tensile fiber failure the penetration channel is not visible due to relaxation effects that come out upon the plies. In the plug-dominated case, the channel is an entirely visible through-the-thickness hole (Hazzel et al., 2008). Remarkable is the remaining shape appearing in the back face of the plate when it is impacted at velocities near the ballistic limit (Figure 2.2(a)). This deformation pattern is also observed by other authors for impacts on polymer matrix composites reinforced by polymeric fibers. This is due to the fact that the breakage process of this latter type of materials is dominated by tensile fiber failure when subjected to transverse impact loads (Morye et al., 2000).

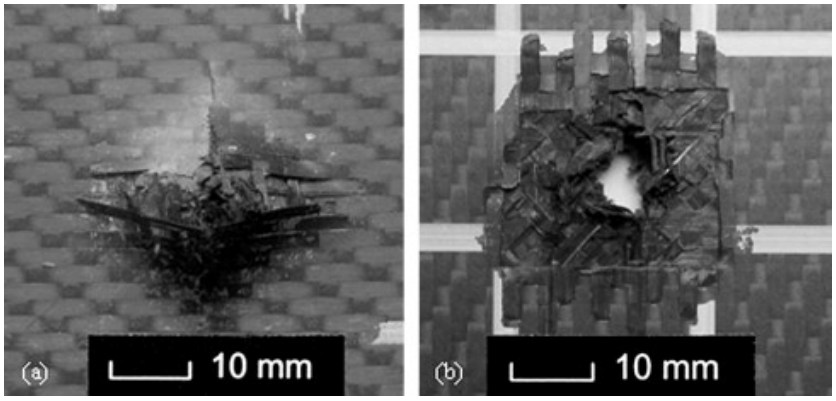

Figure 2.2: Rear face of a CFRP laminated panel struck at a velocity (a) right above the ballistic limit (tensile failure of fibers) and (b) two times greater than the ballistic limit (plugging), (Hazzel et al., 2008)

Apart from this two cases, several authors report the existence of a third case. This third case can be considered as an intermediate case between the tensile fiber failure and plug-dominated cases. In this intermediate case the material simultaneously breaks by crushing/shear of the upper layers and tensile failure of the rear fibers. Cantwell and Morton (1990) relate this process to the failure pattern of thick (8 mm) laminates. The same pattern is observed in the ballistic tests carried out by Hazzel et al. (2008). An ejected plug recovered after the impact of a steel sphere on a 6 mm CFRP laminate is shown in Figure 2.3. The white arrows indicate sharp surfaces located at the top of the plug as a result of the shear-out process. The white oval indicates jagged edges relate with the tensile failure and subsequent pull-out of the fibers located at the bottom of the plug. Hazell and his colleagues state that the combined

shear/tensile failure is only possible if dishing occur in the sample during the impact.

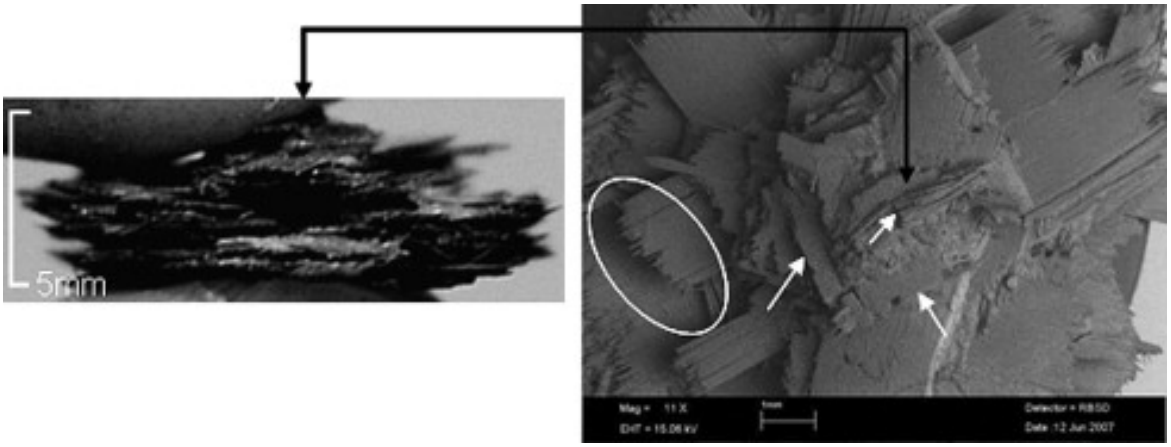

Figure 2.3: Ejected plug from an impact on a 6 mm CFRP laminate at high velocity, (Hazzel et al., 2008)

2.2 Analytical modeling

The analytical model described below was developed by López-Puente (2003). By leaning on the law of conservation of energy the model is able to predict the ballistic limit, residual velocity of the projectile, damaged area caused on the material, and the amount of energy absorbed by each damage mechanism.

The behavior of a composite material plate subjected to impact loads depends on an endless list of features, including the type of constituents, its internal arrangement, impact conditions, and projectile parameters. The present model focuses on the dynamic process taking place when a spherical steel projectile impacts a thin CFRP woven laminate at high velocity.

The kinetic energy of the impactor (E_{ke}) is considered to be absorbed by three mechanisms: *laminate crushing* (E_{lc}) , *linear momentum transfer* (E_{mt}), and *tensile fiber failure* (E_{tf}).

Considering these three energy absorption mechanisms involves the following assumptions.

i. The projectile is considered to be a perfectly-rigid solid. It has been experimentally observed (López-Puente, 2003) that for this type of materials the projectile does not suffer any permanent deformations. Therefore, the energy absorbed by the projectile deformation may be neglected.

ii. The impact is normal to the target. A spherical projectile is used to validate the model in order to avoid external ballistic problems, e.g. tumbling caused by yaw, precession, and nutation displacements of the projectile in flight (Manzano-Trovamala et al., 2001).

iii. Elastic deformation of the target material may be neglected due to the low amount of energy absorbed by this process as compared to other absorption mechanisms when an impact occurs over brittle materials (Zukas, 1982).

iv. The energy absorbed by delamination neither is considered. It has been experimentally observed that woven composite plates impacted at high velocities are not seriously affected by this type of interlaminar failure (López-Puente et al., 2002b).

In order to find a closed-form solution, the basic equation of the model is simplified by the application of a perturbation technique. The perturbation technique used is encompassed within the branch of regular perturbation analysis (Godoy, 1999). An overview of this technique is presented later on in this chapter.

2.2.1 Problem formulation

Once the energy terms involved in the impact event are identified, it is possible to describe the basic balance equation of the model. This fundamental equation is described as follows, where the sum of every energy absorption mechanism must be equal to the kinetic energy of the projectile at any instant of time.

$$-\mathrm{d}E_{ke} = \mathrm{d}E_{lc} + \mathrm{d}E_{mt} + \mathrm{d}E_{tf} \tag{2.1}$$

In order to simplify the mathematical description of the event a spatial rather than temporal integration will be chosen. Being v_i the initial velocity of the projectile, x the variable used to describe the projectile position, and establishing the origin of the movement at the upper side of the laminate, the initial condition is further illustrated by Figure 2.4.

Following this reasoning, the analysis of each energy term is presented below.

- *Kinetic energy of the projectile*: Being m_p the projectile mass and $v(x)$ the projectile velocity as a function of its displacement, the kinetic energy lost by the movement of the projectile through the woven laminated plate between x and $x + \mathrm{d}x$ is given by

$$\mathrm{d}E_{ke} = \frac{1}{2} m_p \mathrm{d}(v(x)^2) \tag{2.2}$$

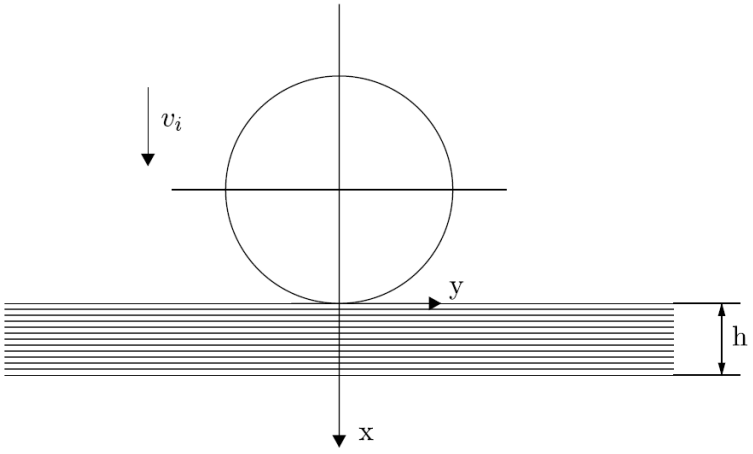

Figure 2.4: Projectile and target configuration for null projectile displacement, (López-Puente et al., 2007)

- *Energy absorbed by laminate crushing*: When contact between the projectile and the composite takes place, compressive loading arises in the target. It is possible to describe the crushing process in terms of the product of the out-of-plane compressive strength Z_c (see Section 2.4 for a detailed description of this property) multiplied by the frontal projectile area that contacts the non-crushed laminate $A(x)$, and the distance covered by the projectile.

$$\mathrm{d}E_{lc} = Z_c A(x)\mathrm{d}x \tag{2.3}$$

  Due to the spherical geometry of the impactor the value of $A(x)$ varies with the depth of penetration. A detailed description of this function can be found in Appendix A.

- *Energy absorbed by linear momentum transfer*: After compressive breakage of a differential laminate volume $A(x)dx$, detached parts are driven along with the projectile with a certain velocity considered equal to that of the projectile. The energy required to speed up a differential laminate volume from rest to the projectile velocity is defined as

$$\mathrm{d}E_{mt} = \frac{1}{2}\left[A(x)\mathrm{d}x\rho_l\right] v(x)^2 \tag{2.4}$$

  in which ρ_l is the laminate density, thus the term in brackets represents the accelerated mass.

- *Energy absorbed by tensile fiber failure*: Considering the last two absorption mechanisms, the model offers good correlation with experimental data for velocities sufficiently over the ballistic limit (2,3 times, approximately; see Section 2.3). However, for lower velocities it has been experimentally observed a third energy absorption process consisting on the creation of a 65° troncoconic collapsed zone dominated by the tensile failure of fibers (Figure 2.5(a)).

  To be highlighted how similar this type of failure is to that formed in materials with similar brittleness behavior such as ceramics subjected to transverse impact. Description of this failure pattern can be seen in the seminal studies made by Florence (1969), Woodward (1990) and den Reijer (1991); as well as in the later works made by Zaera and Sánchez-Gálvez (1998) and Benloulo and Sánchez-Gálvez (1998). These studies are focused on the analytical modelling of defeated mixed armors (ceramic tile faced by a metallic or composite plate). An alumina tile impacted by spherical steel projectile is shown in Figure 2.5(b). As can be seen, CFRP laminates presents a conical deformation pattern resembling that appearing on ceramics when subjected to transverse impact loads.

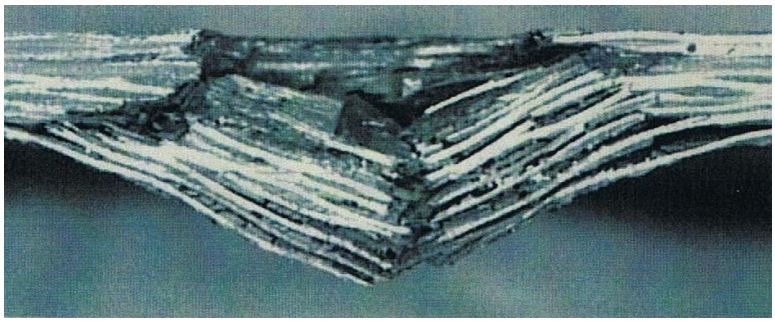

(a) CFRP woven laminate impacted at 92 m/s, (López-Puente et al., 2007)

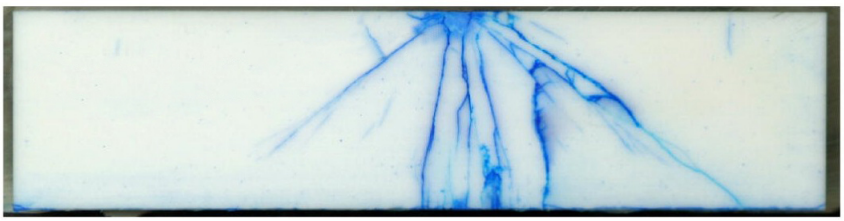

(b) Alumina tile impacted at 586 m/s, (Compton et al., 2013)

Figure 2.5: Cross section view of the conoid formation in different materials

In order to show up this type of failure mechanism, non-penetrated plies need to have enough time to develop tensile stress along the fiber direction. This happens at slow impact velocities. Numerical simulations performed by López-Puente et al. (2002a) display that the estimated time needed by the laminate, so that this breakage situation occurs, is approximately equal to that needed by the elastic wave to reach the lower face of the laminate and bounce back through the total thickness of the plate. This time is

$$t_0 = \frac{2h}{\sqrt{E_3/\rho_l}} \tag{2.5}$$

where E_3 is the through-thickness elastic modulus and h is the total thickness of the laminate.

The amount of energy associated with this failure mechanism can be approximated by

$$\mathrm{d}E_{tf} = \omega_f \mathrm{d}V \tag{2.6}$$

in which ω_f is the breakage specific energy and $\mathrm{d}V$ the affected material volume at any $\mathrm{d}x$. Assuming that the fiber behavior is linear and elastic up to failure, the specific energy is estimated as

$$\omega_f = 2\left(\frac{1}{2}X_t\varepsilon_f\right) \tag{2.7}$$

where X_t is the tensile strength of the laminate and ε_f is the ultimate strain. The equation is multiplied by two, given the biaxial nature of the tensional field (López-Puente et al., 2007).

For the complete description of this energy absorption mechanism, it is required to define the region affected by this type of failure. As has been mentioned, the fiber breakage is located in a troncoconic volume, with a semiangle $\alpha = 65°$, whose diagonals are aligned through the warp and fill directions of the composite laminate. Figure 2.6 depicts a diagram where the affected volume $\mathrm{d}V$ is defined, where x_0 is the projectile position at t_0. According to the figure the differential volume can be expressed as

$$\mathrm{d}V = 2l^2\mathrm{d}x = 2\mathrm{d}x(r + (x - x_0)\tan\alpha)^2 \tag{2.8}$$

A cut-off function $c_r(x)$ is required, so that the tensile failure term becomes zero at $t < t_0$ and when the projectile perforates the laminate.

$$c_r(x) = \begin{cases} 0 & \text{if} \quad 0 < x < x_0; \\ 1 & \text{if} \quad x_0 < x < h; \\ 0 & \text{if} \quad x \geq h. \end{cases} \tag{2.9}$$

Therefore, the energy differential absorbed by tensile failure is

$$\mathrm{d}E_{tf} = X_t\varepsilon_f 2\mathrm{d}x(r + (x - x_0)\tan\alpha)^2 c_r(x) \tag{2.10}$$

It is important to emphasize that $\mathrm{d}E_{tf}$ depends on the unknown parameter x_0, since it depends on the projectile velocity function; this problem will be solved later (see Section 2.2.2 , Equation 2.30).

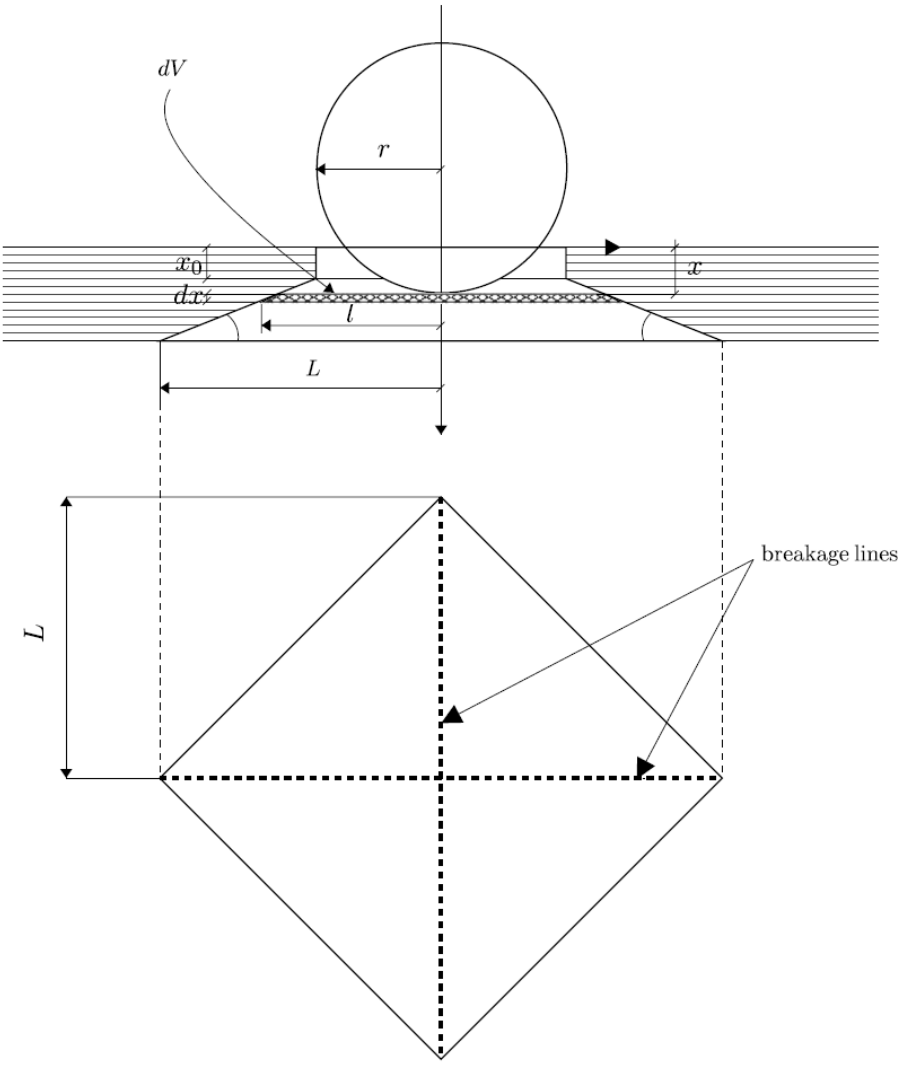

Figure 2.6: Volume affected by tensile fiber failure, (López-Puente et al., 2007)

Returning to the fundamental equation, by introducing every energetic term, the basic balance equation is described as follows

$$-\frac{1}{2}m_p \mathrm{d}(v(x)^2) = Z_c A(x)\mathrm{d}x + \frac{1}{2}(A(x)\mathrm{d}x\rho_l)v(x)^2 + X_t\varepsilon_f 2\mathrm{d}x(r + (x - x_0)\tan\alpha)^2 c_r(x) \quad (2.11)$$

Adding an initial condition, the main differential equation of the model is obtained

$$\begin{cases} -\frac{1}{2}m_p \mathrm{d}(v(x)^2) = Z_c A(x)\mathrm{d}x + \frac{1}{2}(A(x)\mathrm{d}x\rho_l)v(x)^2 + X_t\varepsilon_f 2\mathrm{d}x(r + (x - x_0)\tan\alpha)^2 c_r(x) \\ v(0) = v_i \end{cases} \quad (2.12)$$

Following simplifications are carried out with the aim of finding a simple way to obtain a closed-form solution to the previous equation. Hereinafter the dependence of the main functions are going to be omitted.

$$\begin{cases} -\frac{1}{2}m_p\frac{\mathrm{d}v^2}{\mathrm{d}x} = Z_c A(x) + \frac{1}{2}(A(x)\rho_l)v^2 + X_t\varepsilon_f 2(r + (x - x_0)\tan\alpha)^2 c_r \\ \\ v(0) = v_i \end{cases} \tag{2.13}$$

2.2.2 Equation resolution. Perturbation analysis

The problem resolution described below is based on the application of a perturbation technique. Perturbation techniques involve a large number of mathematical tools established around the use of asymptotic series to describe the solution of complex problems. Complex problems might be non-linear problems, problems without exact solution, or problems in which the exact solution is available but due to the intricate dependency between terms they are hard to handle as such. Besides from solving complex problems, the use of perturbation techniques provides in many cases the opportunity to classify the solutions obtained and hence, identify different features of the behavior of the system involved.

Perturbations were first regarded by Newton in his *Principia* (1687) by treating the basics of planetary motion. Further development in the use of perturbation techniques yielded to the definition of the basics of the so-called Lunar Theory and the broad Celestial Mechanics (Moulton, 1914). The main goal pursued by the use of perturbation techniques consists on finding an approximate solution to a given complex problem; that could be for instance the relative motion of the Moon and the Earth. The approximate solution can be found by solving a problem or a set of problems that are similar but easier to solve. These problems differ in a small amount, that is the perturbation, to the one of interest; in the case of the Moon's movement that is the influence of the gravitational attraction caused by the Sun. By omitting the variability in the gravitational effects appearing on both the Moon and the Earth, one is able to predict approximately the position of the Moon relative to the Earth.

Similar approach can be used to solve Equation 2.13. The technique used in this work is called explicit substitution technique, applied when the concerned problem is of the type of regular perturbation. Regular perturbation analysis implies that the set of straightforward problems can be defined and the solution obtained meet the characteristics of the real solution of the problem. The literature on different perturbation techniques is extensive; a good review when applied to non-linear systems can be found in Godoy (1999).

Firstly, a brief overview focused on a mathematical description of regular perturbation analysis is presented, so that the subsequent application of this technique to the concerned problem can be understood clearly.

Consider the problem of finding the solution to the generic equation $\varphi(x, \varepsilon) = 0$, which contains the parameter ε. If this parameter is sufficiently small $|\varepsilon| \ll 1$, the generic problem just described could be seen as a perturbation of the problem $\varphi(x, 0) = 0$, called the unperturbed problem in which ε tends towards zero. If $x(\varepsilon)$, which is denoted as the solution to the generic problem, approaches to the solution $x_{(0)}$ of the unperturbed problem, the equation $\varphi(x, \varepsilon) = 0$ could be named as a perturbation type problem, and regular perturbation analysis could be applied (Tolano, 2008).

On this basis, the solution to the above described perturbed problem could be written by means of an asymptotic power expansion $x(\varepsilon) = x_{(0)} + x_{(1)}\varepsilon + x_{(2)}\varepsilon^2 + \ldots + x_{(n)}\varepsilon^n + O(\varepsilon^{n+1})$; where $x_{(0)}$ is the solution to the unperturbed problem, also called the zero-order problem, and $(x_{(1)}, x_{(2)}, \ldots, x_{(n)})$ are the specific solutions to the high-order problems.

For sake of completeness the fundamental theorem of perturbation theory is presented.

Theorem 1. *(Fundamental Theorem of Perturbation Theory)*

If an asymptotic expansion satisfies

$$A_0 + A_1\varepsilon + A_2\varepsilon^2 + \ldots + A_n\varepsilon^n + O(\varepsilon^{n+1}) \tag{2.14}$$

for all sufficient small ε and the coefficients $\{A_j\}$ are independent of ε, then

$$A_0 = A_1 = \ldots = A_n = 0. \tag{2.15}$$

In order to apply this technique to the equation of the model, first step consist on finding which term of the equation produces small changes in the system behavior, that is the perturbation factor. By the nondimensionalization of the problem, one is able to carry out a dimensional comparison between the different involved terms. Dimensionless velocity and displacement of the projectile are defined as $v^* = v/v_i$ and $x^* = x/h$ respectively, where v_i is the impact velocity and h is the thickness of the impacted plate. The frontal projectile area $A(x)$ can be defined as $A(x) = A_0 A_c(x^*)$, where $A_0 = \pi r^2$ and $A_c(x^*)$ is the non-dimensional frontal projectile area further described in Appendix A. These changes lead to

$$\begin{cases} -\frac{1}{2} m_p \frac{v_i \mathrm{d}v^{*2}}{h \mathrm{d}x^*} = Z_c A_0 A_c(x^*) + \frac{1}{2}(A_0 A_c(x^*)\rho_l)(v_i v^*)^2 + X_t \varepsilon_f 2(r + (hx^* - x_0)\tan\alpha)^2 c_r(x^*) \\ \\ v^*(0) = 1 \end{cases} \tag{2.16}$$

By applying the change of variable $w^* = v^{*2}$ and reorganizing the terms, previous equation leads to

$$\begin{cases} -\frac{\mathrm{d}w^*}{\mathrm{d}x^*} = \frac{2hZ_c A_0 A_c(x^*)}{m_p v_i^2} + \frac{A_0 A_c(x)\rho_l h}{m_p} w^* + \frac{4hX_t \varepsilon_f r^2}{m_p v_i^2}(1 + (\frac{hx^*}{r} - \frac{x_0}{r})\tan\alpha)^2 c_r(x^*) \\ \\ w^*(0) = 1 \end{cases} \tag{2.17}$$

Hereinafter, asterisks are going to be omitted. Therefore, the basic equation of the present model can be rewritten as follows

$$-\frac{\mathrm{d}w}{\mathrm{d}x} = \frac{2hZ_c A_0}{m_p v_i^2} A_c + \frac{A_0 \rho_l h}{m_p} A_c w + \frac{4hX_t \varepsilon_f r^2}{m_p v_i^2}(1 + (\frac{hx}{r} - \frac{x_0}{r})\tan\alpha)^2 c_r \tag{2.18}$$

The above simplifications allow to define the characteristic values of the different energetic terms by the analysis of the order-of-magnitude estimate for the main variables involved in the

problem (Table 2.1). The dimensional terms for each energy absorption mechanism, and their characteristic value as a function of the impact velocity, is presented below.

Variable	Order of Magnitude
$h\ [m]$	10^{-3}
$Z_c\ [N/m^2]$	10^{8}
$A_0\ [m^2]$	10^{-5}
$m_p\ [kg]$	10^{-3}
$\rho_l\ [kg/m^3]$	10^{3}
$r\ [m]$	10^{-3}
$X_c\ [N/m^2]$	10^{9}
$\varepsilon_f\ [N/m^2]$	10^{-2}

Table 2.1: Order-of-magnitude estimate for the main variables involved in the problem.

Energetic Ratios	
$R_{lc} = \frac{2hZ_cA_0}{m_pv_i^2} \sim \frac{10^3}{v_i^2}$	Laminate crushing
$R_{mt} = \frac{A_0\rho_l h}{m_p} \sim 10^{-2}$	Linear momentum transfer
$R_{tf} = \frac{4hX_t\varepsilon_f r^2}{m_pv_i^2} \sim \frac{10}{v_i^2}$	Tensile failure

Table 2.2: Characteristic values for the different energetic terms.

It can be seen that the ratio R_{tf}, corresponding to the tensile failure as compared with the projectile initial kinetic energy, is always lower than the others at any impact velocity within the range of high velocity impacts ($v_i > 100\ m/s$). Thereby R_{tf} can be considered as the perturbation factor $\varepsilon = R_{tf}$, and the simplified perturbed equation of the problem can be written as

$$-w' = R_{lc}A_c + R_{mt}A_cw + \varepsilon(1 + (\frac{hx}{r} - \frac{x_0}{r})\tan\alpha)^2c_r \tag{2.19}$$

By means of the regular perturbation analysis, the solution to the previous equation might be written in terms of the following asymptotic power expansion

$$w = w_{(0)} + w_{(1)}\varepsilon + O(\varepsilon^2) \tag{2.20}$$

where $w_{(0)}$ is the solution of the unperturbed problem, and $w_{(1)}$ represents the first-order term. By choosing a linear approximation, that is not taking into account order terms higher than first, we assume an approximate error of $\varepsilon^2 \sim 100/v_i^4$.

The next step is based on the application of the premises defined by the explicit substitution technique, whereby the expanded solution (Equation 2.20) is directly substituted into Equation 2.19.

$$-(w'_{(0)} + \varepsilon w'_{(1)}) = R_{lc}A_c + R_{mt}A_c(w_{(0)} + w_{(1)}\varepsilon) + \varepsilon(1 + (\frac{hx}{r} - \frac{x_0}{r})\tan\alpha)^2 c_r + O(\varepsilon^2) \quad (2.21)$$

by grouping terms of the same power of ε

$$(w'_{(0)} + R_{lc}A_c + R_{mt}A_c w_{(0)}) + (w'_{(1)} + R_{mt}A_c w_{(1)} + (1 + (\frac{hx}{r} - \frac{x_0}{r})\tan\alpha)^2 c_r)\varepsilon + O(\varepsilon^2) = 0 \quad (2.22)$$

Appealing to the fundamental theorem of perturbation theory (Theorem 1), each independent term corresponding to powers of ε must be set equal to zero.

$$w'_{(0)} + R_{lc}A_c + R_{mt}A_c w_{(0)} = 0 \quad (2.23)$$

$$w'_{(1)} + R_{mt}A_c w_{(1)} + (1 + (\frac{hx}{r} - \frac{x_0}{r})\tan\alpha)^2 c_r = 0 \quad (2.24)$$

Equation 2.23 represents the differential equation for the zero-order term which can be completely defined by

$$\begin{cases} -w'_{(0)} = R_{lc}A_c + R_{mt}A_c w_0 \\ \\ w_{(0)}(0) = 1 \end{cases} \quad (2.25)$$

In a like manner, Equation 2.24 represents the differential equation for the first-order term

$$\begin{cases} -w'_{(1)} = R_{mt}A_c w_1 + \varepsilon(1 + (\frac{hx}{r} - \frac{x_0}{r})\tan\alpha)^2 c_r \\ \\ w_{(1)}(0) = 1 \end{cases} \quad (2.26)$$

Both are first-order lineal differential equations that could be simply solved in order to find a closed-form solution to the impact problem. The solution to the zero-order and first-order terms are given by

$$w_0(x) = -\frac{R_{lc}}{R_{mt}} + \left(1 + \frac{R_{lc}}{R_{mt}}\right) exp(-R_{mt}\hat{A}_c) \quad (2.27)$$

$$w_{(1)}(x) = -exp(-R_{mt}\hat{A}_c)\left[\int_0^x c_r \left(1 + \frac{h\kappa - x_0}{r}\tan\alpha\right)^2 exp(R_{mt}\hat{A}_c)\mathrm{d}\kappa\right] \quad (2.28)$$

in which $\hat{A}_c(x)$ defines the primitive of $A_c(x)$ (see Appendix A).

One important issue must be underlined in order to obtain the ballistic limit equation and completely define the one-order solution. The zero-order solution provides the complete

definition of the cut-off function c_r, this is due to the fact that for displacement values outside the tensile-failure range ($x < x_0$ and $x \geq h$) the full differential equation (Equation 2.17) and the zero-order equation (Equation 2.25), are exactly the same.

$$w(x^*) = \begin{cases} w_{(0)} + O(\varepsilon^2) & \text{if} \quad 0 < x < x_0; \\ w_{(0)} + w_{(1)}\varepsilon + O(\varepsilon^2) & \text{if} \quad x_0 < x < h; \\ w_{(0)} + O(\varepsilon^2) & \text{if} \quad x \geq h. \end{cases} \tag{2.29}$$

This fact gives the opportunity to define the tensile failure starting point x_0 by solving the following equation

$$t_0 \equiv \int_0^{x_0} \frac{\mathrm{d}\chi}{v_i\sqrt{w_{(0)}(\chi)}} = \frac{2h}{\sqrt{E_3/\rho}} \tag{2.30}$$

Likewise, by means of the zero-order solution, it is possible to obtain the closed-form solution for the residual velocity by defining $w_{(0)}$ when $x \geq (h + r)$, and subsequently back dimensionalizing the velocity and displacement projectile variables

$$v_r = v_i\sqrt{exp(-\frac{\pi r^2\rho_l h}{m_p})\left(1 - \frac{2Z_c}{\rho_l v_i^2}(exp(\frac{\pi r^2\rho_l h}{m_p}) - 1)\right)} \qquad \text{Residual velocity} \tag{2.31}$$

By employing this last equation, the ballistic limit as a function of projectile and material properties, and geometric parameters, is completely defined. Equaling the residual velocity v_r to zero and isolating the impact velocity v_i, the formula for the ballistic limit turns out.

$$v_{bl} = \sqrt{\frac{2Z_c}{\rho_l}(exp(\frac{\pi r^2\rho_l h}{m_p}) - 1)} \qquad \text{Ballistic limit} \tag{2.32}$$

2.3 Results and validation

In the present section results provided by the analytical model for a specific type of composite laminate are presented. Along with these results, the validation of the model is carried out by comparing the previous results with experimental data available for the same type of material.

In order to obtain the results provided by the analytical model, code containing its basic equations was implemented in Mathcad 14. Material properties used to validate the model belong to a carbon-epoxy plain weave laminate with ten laminas. The reinforcement is based on AS4 carbon fabric industrially named as AGP193-PW, whilst the matrix corresponds to an Hexply® 8552. This laminate was selected because experimental data can be used to validate the model (López-Puente et al., 2007). Properties of an AGP193-PW/8552 woven laminate are reported in Table 2.3.

Property	Unit	Value
E_1	[GPa]	68.5
E_2	[GPa]	68.5
E_3	[GPa]	9
G_{12}	[GPa]	3.7
ν_{12}		0.11
X_t	[MPa]	860
X_c	[MPa]	795
Y_t	[MPa]	860
Y_c	[MPa]	795
S_t	[MPa]	98
Z_c	[MPa]	60
ρ_l	[kg/m^3]	1430
ε_f		0.02
h	[mm]	2.2

Table 2.3: Material properties (López-Puente et al., 2007).

Results obtained by the model when the material is impacted by a spherical steel projectile of 7.5 mm in diameter and 1.73 g of mass, are shown in Figures 2.7 and 2.8. The main variable used to evaluate the accuracy of models based on ballistic impacts is the residual velocity of the projectile. Residual velocity versus impact velocity are shown in Figure 2.7. The solution of the model is presented divided into two curves. Each curve belongs to one of the solutions provided by the application of the perturbation analysis, that is the zero-order and one-order solutions.

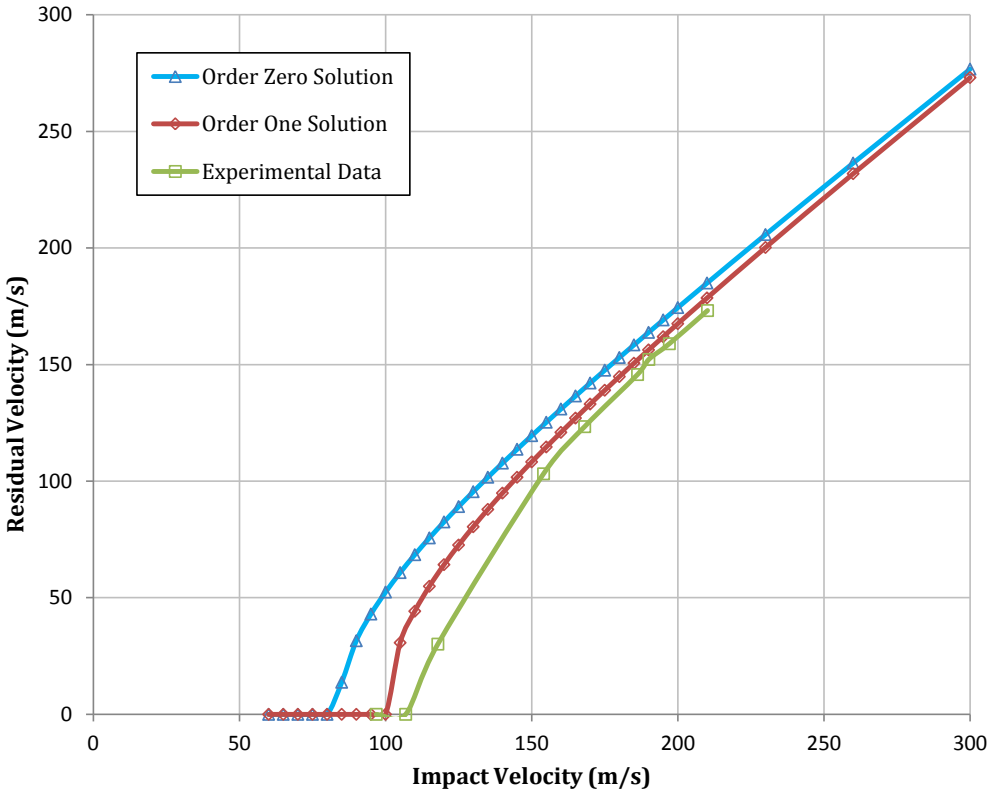

Figure 2.7: Residual velocity versus impact velocity.

The model predicts accurately the response of the selected material for impact velocities over 150 m/s. It is revealed also, the improvement achieved when the first-order solution is included. Further discussion on these results can be found in the next section.

An additional outcome obtained by the model is the one related to the energy absorbed by the different damage and failure mechanisms involved in the process. The energy absorbed by each mechanism during penetration of the target at two different velocities, one in the vicinity of the ballistic limit and the other above the ballistic limit, are shown in Figure 2.8.

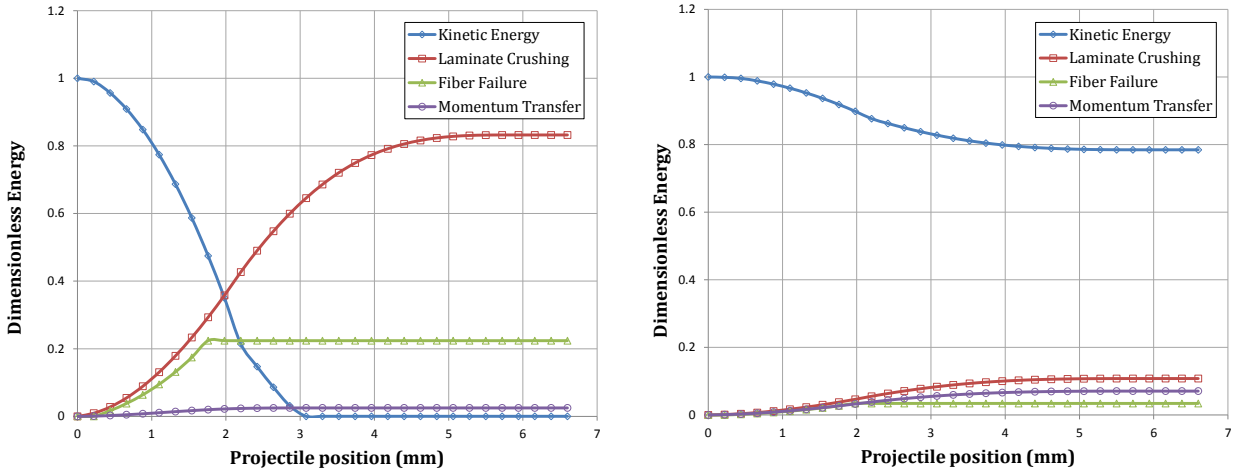

Figure 2.8: Dimensionless energy versus projectile displacement for impact at velocities (a) barely below the ballistic limit (90 m/s) and (b) above the ballistic limit (250 m/s)

Different breakage pattern is observed in both cases. At velocities near the ballistic limit, experimental observations reveal a material behavior dominated by the tensile failure of fibers (Figure 2.8(a)). When the velocity of the impactor is higher than the ballistic limit, a breakage pattern dominated by the plug formation is revealed (Figure 2.8(b)).

2.4 Scope of the model

The results obtained by the model for a specific type of carbon-epoxy woven laminate have been presented. These values seem to be in agreement with the experimental data available. However, whether a constituent of the material changes, the performance of the model is a great unknown. This is based on the strong dependency that the model has to the compressive strength through the thickness direction, Z_c.

None of the main manufacturers available for composite laminates provide values for Z_c. Literature regarding the use of this property are rare; and few are the publications that treat the experimental determination of this property.

One reason for this lack of experimental data relies on the fact that determining the through-thickness properties of composite materials is not a straightforward process; and enormous variability in the results can be obtained (Schubel et al., 2006). Two main factors seem to confirm the latter. First, in order to measure the through-thickness mechanical properties of a given composite one must make sure that a uniform stress state is been produced within the sample. This gives the chance to repeatedly measure the true properties of the material with accuracy. This is hard to achieve due to the difficulty in the manufacturing of composite laminates of uniform quality in sufficiently thick sections. Second, difficulties could be found also when trying to avoid the influence of end effects and stress concentrations during the application of the load (Lodeiro et al., 1999). This undesirable effect might cause splitting or brooming failure

around the load application point (Camponeschi, 1989).

Moreover, the characterization of mechanical properties of materials intended for applications where impacts and collisions likely appear must consider the effects induced by the loading rate. When an impact at high velocity occurs, the material is subjected to strain rates as high as 10^4 or $10^5\,s^{-1}$. Within this range, the response of the material is dominated by its dynamic properties (Rodriguez et al., 2004).

In the field of polymer matrix composites, a number of works have been published and a variety of conclusions and contradictory observations have resulted as well (Jacob et al., 2004). Many authors assume CFRP laminates as a strain-rate insensitive material. This last apply when the material response is dominated by the behavior of the fiber, as happen with the tensile and compression strength along the fiber direction in the range of hundreds strains per second (Daniel et al., 1995). However, when the matrix dominates the response of the material, as it happens for transverse compression, the viscoelastic nature of the polymeric matrix, fiber orientation, time-dependent nature of the accumulating damage, and temperature rise, seem to enhance the overall properties of the material (Hosur et al., 2001). A work regarding the variation in the compressive properties of woven fabric composites in the strain rate range of 680 - 2890 s^{-1} was performed by Naik and Kavala (2008). The variation with the strain rate of the through-thickness compressive strength of a carbon/epoxy plain weave laminate was studied. Results reveal an enhancement of this property of over a forty percent as compared to the quasi-static value. The following figure shows the on-average variation of the main properties for a carbon/epoxy laminate subjected to strain rates up to $10^3\,s^{-1}$. The values were obtained from Hosur et al. (2001), Naik and Kavala (2008), Naik et al. (2010), and López-Puente and Li (2012).

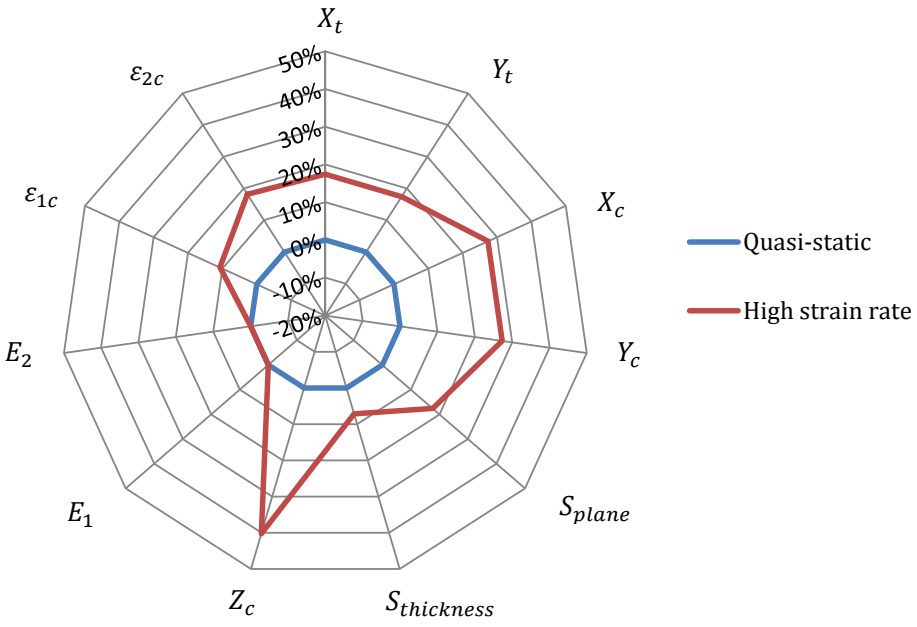

Figure 2.9: Percentage of variation of the main properties at high strain rates for carbon/epoxy woven laminates.

A simple way to incorporate the strain rate effects in models dealing with polymer matrix composites is through the application of the so-called Dynamic Enhancement Factor (DIF). DIF is a factor presented by Xin and Wen (2012) whereby the rate sensitive behavior of the material is characterized. DIF is defined as a function of three empirical constants: A, B and C. The value of each constant is evaluated by curve-fitting technique according to the type of reinforcement. DIF is defined by

$$\text{DIF} = \left\{ \left[\tanh\left(\left(\log\left(\frac{\dot{\varepsilon}}{\dot{\varepsilon_0}} \right) - A \right) \times B \right) \right] \times \left[\frac{2C}{C+1} - 1 \right] + 1 \right\} \times \frac{C+1}{2} \tag{2.33}$$

where $\dot{\varepsilon_0}$ is the reference strain rate, usually taken to be $\dot{\varepsilon_0} = 1\text{s}^{-1}$, and $\dot{\varepsilon}$ is the specific strain rate applied. The strain rate effect could be incorporated to the model by multiplying the given quasi-static value of the strength or modulus by DIF, as shown below

$$S_{RT} = S_0 \times \text{DIF} \tag{2.34}$$

$$E_{RT} = E_0 \times \text{DIF} \tag{2.35}$$

where S_{RT} and E_{RT} could be any strength and any modulus respectively, and S_0 and E_0 are the corresponding static values of the strength and the modulus selected.

As further illustrated in Figure 2.10, DIF consist on an hyperbolic curve in which A is the horizontal coordinate value of the inflection point of the curve in the second ascending stage; B describes the tangent slope of the inflection point of the curve in the second ascending stage; and C represent the limit value of DIF when the strain rate goes to infinity. As mentioned, A, B and C are evaluated according to the type of reinforcement. Xin and Wen (2012) assume that the strength of CFRP laminates remains unchanged when dynamic conditions are applied; that means consider A, B and C equal to zero. As discussed before, this last do not apply to the through-thickness compressive problem. By using the numerical solution provided by López-Puente and Li (2012) as the curve necessary for fitting the constants; A, B, and C are adjusted to values equal to 2, 0.9 and 1.7 respectively. The numerical solution and the value using the DIF approach for the out-of-plane compressive strength of CFRP laminates are shown in Figure 2.10.

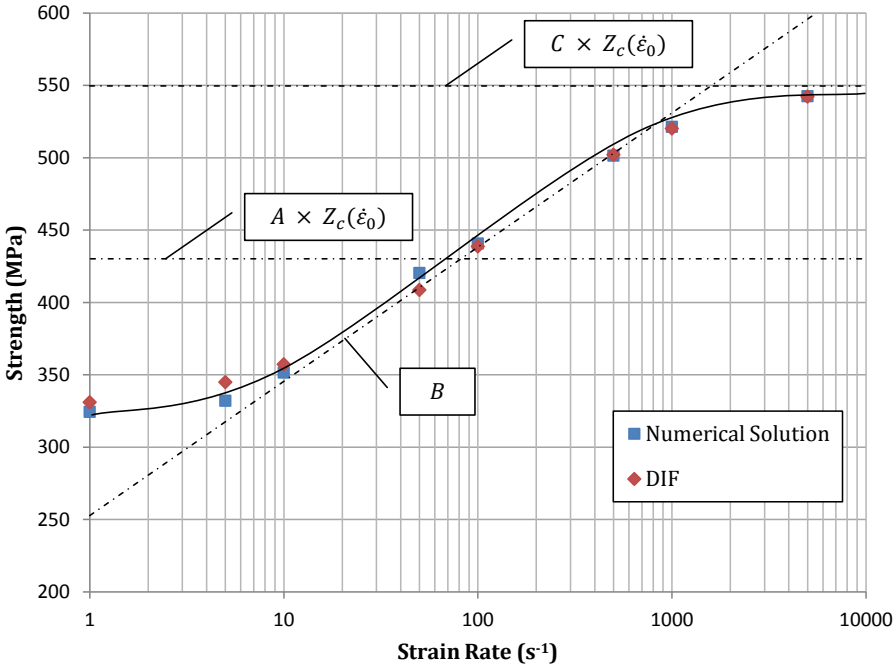

Figure 2.10: Out-of-plane compressive strength versus strain rate.

By using the dynamic enhancement factor one is able to approach with accuracy the variation in the material properties when dynamic conditions are applied.

Chapter 3

Analytical description of the impact event in glass and polymer fiber composites

In the present chapter, the same structure as in Chapter 2 is followed. The behavior of glass and polymer fiber composites when subjected to high velocity impacts is presented firstly, gathering different experimental observations. The formulation and basics of an analytical model intended to predict the ballistic performance of these materials are described afterwards. Finally, results provided by the analytical model are presented along with a comparison against experimental data obtained from the literature.

This chapter focuses on the ballistic performance of glass and polymer fiber composites. Glass and polymer fibers are treated together due to the high failure strain at high strain rates experienced in both types of reinforcements (Naik et al., 2006). Due to the latter, analogous deformation patterns and damage mechanisms are observed when high velocity impacts take place over polymer matrix composites (PMC) reinforced by these two types of fibers.

Glass fiber is the most common reinforcement because its properties can be tailored to meet the specific needs of a wide set of industries. From the honeycomb structure contained in the heat shields of Gemini (NASA spacecraft that led to the Apollo Program) to the hull of simple rigid inflatable boats, fiber glass is used in a variety of environments where different mechanical performance are required (Stickel and Nagarajan, 2012).

On the other hand, polymer fibers encompass a wide group of fibers intended as well for a broad types of applications. Body armor protection, rehabilitation of concrete structures or development of medical implants, are just some examples. Polymer fiber composites are applied in those situations where a high strength-to-weight ratio along with high failure strains are required. Also, there are one of the most extended types of fibers used in ballistic armor protection. At the end of the chapter, a survey of the performance under impact of different polymeric fibers, commonly use in ballistic protection, is presented using results provided by the analytical model.

3.1 The impact process on the basis of wave propagation

The present section describes experimental observations on the impact process over glass and polymer fiber composites. When a body is subjected to an external force, different types of stress waves propagate through the solid in different directions. The rate of change of the applied force establishes the influence that these waves have on the overall response of the material. If the rate of change of the applied force is low, deformation of the solid can be considered under quasi-static conditions. Hence, mechanics of materials fundamental equations can be applied. On the other hand, when the applied force rapidly changes with time, the stresses and strains originated in the material vary in a way that, at a specific time after the impact, some regions have not "realized" about the force, whereas some other regions of the material already did (Meyers, 1994). The latter means that further consideration of static equilibrium within the solid cannot be considered. Under this situation, wave propagation in materials has to be taken into account. A detailed description of wave propagation on the dynamic behavior of materials is presented in Zukas (1982) and Meyers (1994).

The response of sandbags to different loading rates serves as an example of the previous two cases. By applying with just a finger a small amount of pressure, one is able to go through the sandbag without effort. However, if a small-caliber bullet is fired against the same sandbag, it will effectively stop the bullet. For this reason sandbags are commonly used by ground forces in order to build protective walls that prevent soldiers from being hit by enemy fire. How the sandbag is able to stop the bullet and not the finger is due to the different behavior of the material when different loading rates are applied.

Unlike what happens with CFRPs, wave propagation is a major influence in the dynamic behavior of fabric flexible laminates (López-Puente et al., 2007). The present section describes the impact process on plain-weave glass and polymer fiber composites based on the propagation of waves through the material immediately upon the collision.

The process described below is build on the observations resulted from the ballistic tests carried out by Morye et al. (2000), Patel et al. (2004) and Shaktivesh et al. (2013). Based on these works, the material is able to counteract the kinetic energy of the projectile mainly by the following mechanisms: deformation and tensile failure of fibers, transverse compression, formation of a conical frustum on the back face of the target, matrix cracking, delamination, and friction between projectile and target. The shear plugging (characteristic failure process in the impact of CFRPs) is not further observed on thin composite plates reinforced by glass or polymeric fibers (Naik et al. (2006) and García-Castillo (2007)).

The process taking place when a spherical projectile transversely impacts on a thin, flexible fiber composite is shown schematically in Figure 3.1. This process can be divided into three stages: indentation, perforation and exit.

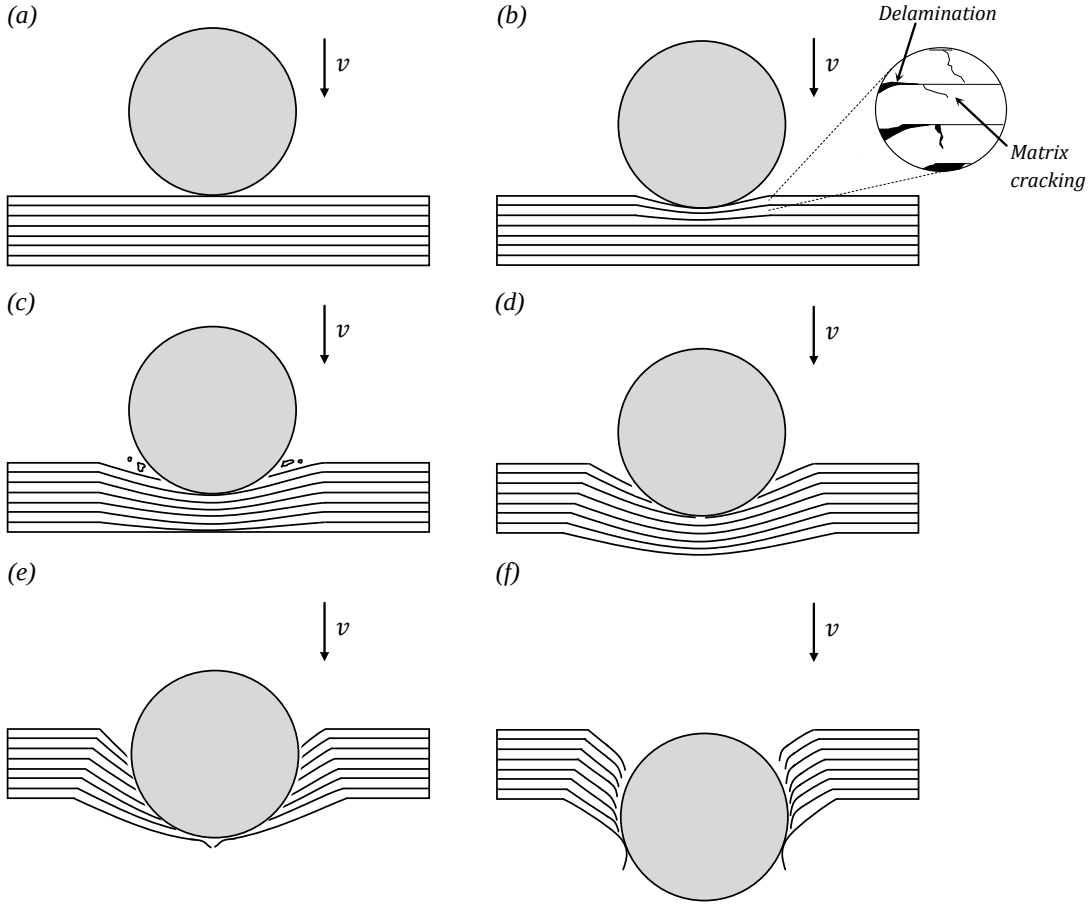

Figure 3.1: Impact process on flexible fiber composites: (a,b) indentation, (c,d,e) perforation and (f) exit.

The indentation stage takes place during the first instants upon collision. Longitudinal and transverse stress waves proceed to spread along the thickness and in-plane directions (Figure 3.1(a)(b)). The layers right below and surrounding the impacted zone undergo compression along the thickness and tension along the in-plane direction. Hence, throughout this stage, fibers can break either by transverse compression or tension. Before the fiber breakage takes place, damage processes comprising matrix cracking and delamination develop along the material near the impacted zone (Figure 3.1(b)). These two processes are of major importance when collisions take place over thick laminates or at low impact velocities (Cantwell and Morton, 1990). Therefore, during this initial stage, the kinetic energy of the projectile is dissipated by deformation, compression, tensile failure of fibers, matrix cracking, and delamination.

The perforation stage begins when the compressive wave reaches the rear face of the composite laminate (Figure 3.1(c)). At this point, the compressive wave is reflected in the form of a tensile wave that increases the damage produced by delamination. Based on the number of layers failed in the first stage and the residual kinetic energy of the projectile, conical deformation may take place on the back face of the material, as depicted in Figure 3.1(d). Delamination continue growing between those plies where fibers remain unbroken. These fibers

undergo tension due to the conical formation and will fail when the induced strain exceed the in-plane failure strain of the material (Figure 3.1(e)). This perforation stage ends up with the total failure of the laminae.

If after the complete failure of the material the projectile remains in movement, a portion of its residual kinetic energy is dissipated by friction between projectile and target. This friction results in local temperature rise, covering the so-called exit stage (Figure 3.1(f)). Finally, if the projectile is still having some kinetic energy, it will exit the target with a certain residual velocity.

The damage and failure processes just described are illustrated in the excellent experimental survey carried out my Morye et al. (2000). In the following figure, the impact between a spherical steel projectile and a composite plate reinforced by Nylon-66, is shown.

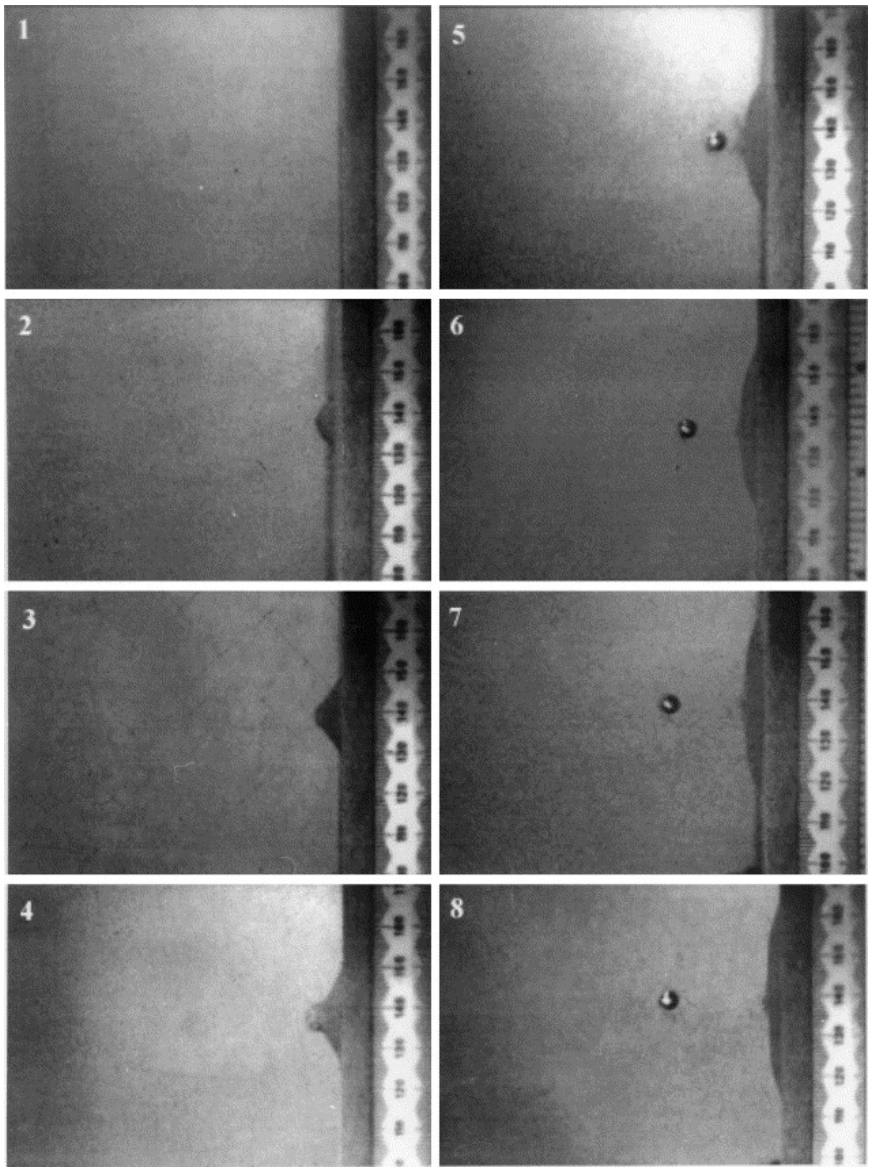

Figure 3.2: High-speed photograph of a Nylon-66 fiber composite impacted by a low-mass steel sphere at 512 m/s (projectile traveling from right to left), (Morye et al., 2000)

3.2 Analytical modeling

The model selected to describe the impact behavior of glass and polymer fiber composites was initially proposed by Vinson and Walker (1997), developed by Morye et al. (2000), completed afterwards in Naik and Shrirao (2004) and Naik et al. (2005, 2006), and finally simplified by García-Castillo (2007). The model draws on the law of conservation of energy and features related with wave propagation are considered. The results provided by the model are able to predict the ballistic limit, residual velocity of the projectile, extent of the damaged area, and amount of energy absorbed by each damage mechanism.

The model is based on the event turned out from the impact between a small projectile traveling at high velocity and a woven composite laminate reinforced by either glass or polymeric fibers. The kinetic energy of the projectile (E_{ke}) is considered to be dissipated by five different mechanisms: *conical frustum formation on the back face of the target* (E_{cf}), *tensile failure of primary yarns* (E_{tf}), *elastic deformation of secondary yarns* (E_{ed}), *delamination* (E_{dl}), and *matrix cracking* (E_{mc}).

Considering these five energy absorption mechanisms involves the following assumptions.

i. The projectile is considered to be a perfectly-rigid solid. The undeformed state of the projectile upon the impact was experimentally observed by Morye et al. (2000).

ii. The projectile reaches the target in its normal direction. A spherical projectile is used to validate the model in order to avoid external ballistic problems, e.g. tumbling caused by yaw, precession, and nutation displacements of the projectile in flight (Manzano-Trovamala et al., 2001).

iii. The velocity of the longitudinal and transverse waves are considered constant on each lamina.

iv. The energy absorbed by the tensile failure of primary yarns and deformation of secondary yarns are treated independently. The latter implies that no interaction between warp and fill yarns is considered.

v. The energy dissipated due to frictional forces and local temperature rise, relative to the interaction between projectile and composite, are neglected (Morye et al., 2000).

vi. The energy absorbed by transverse compression is negligible in the case of composite materials reinforced by flexible fibers. This is confirmed by results obtained in Shaktivesh et al. (2013).

Unlike the model presented in the previous chapter, this model requires of an iterative method to be solved. The impact event is divided into small time intervals, Δt. At the end of each time interval, the energy dissipated by every mechanism has to be calculated along with the projectile velocity. The algorithm required to solve the model is further presented in Section 3.2.2.

3.2.1 Problem formulation

The damage and failure processes arising in the material, when it is subjected to transverse impact, were presented in Section 3.1. The formation of a conical frustum in the back face of the laminate is a characteristic feature in the impact of flexible fiber composites. Vinson and Zukas (1975) were first in defining the parameters regarding the formation of this rear cone.

The geometry of the nose end of the conical frustum, that is the base moving along with the impactor, is determined by the own frontal shape of the projectile. Although the projectile used to validate the model is spherical in shape, for sake of simplicity the frontal face of the conical frustum is assumed to be flat. The depth of the conical frustum is defined thus by the distance traveled by the projectile at any instant of time.

On the other hand, the size of the aft end of the cone, that is the base radius of the conical frustum, is explained on the basis of wave propagation along the target material. Longitudinal and transverse waves spread throughout the material right upon the impact. This phenomenon was thoroughly studied by Smith et al. (1958). Smith and his co-workers presented the equations needed in order to estimate the velocity of longitudinal and transverse waves that propagate along a single yarn transversely struck by a projectile. The velocity of these waves are defined by

$$c_L = \sqrt{\frac{1}{\rho} \cdot \left(\frac{\mathrm{d}\sigma}{\mathrm{d}\varepsilon}\right)_{\varepsilon=\varepsilon_p}} \qquad \text{Longitudinal wave velocity} \tag{3.1}$$

$$c_T = \sqrt{\frac{(1+\varepsilon_p)\sigma_p}{\rho}} - \int_0^{\varepsilon_p} \sqrt{\frac{1}{\rho} \cdot \left(\frac{\mathrm{d}\sigma}{\mathrm{d}\varepsilon}\right)}\,\mathrm{d}\varepsilon \qquad \text{Transverse wave velocity} \tag{3.2}$$

where ρ is the material density, and σ_p and ε_p denote the stress and strain of the material at the yield point, respectively. Assuming that the material has a linear and elastic up-to-failure behavior, the previous equations are simplified as follows

$$c_L = \sqrt{\frac{E}{\rho}} \tag{3.3}$$

$$c_T = \sqrt{\frac{(1+\varepsilon_f)\sigma_f}{\rho}} - \sqrt{\frac{E}{\rho}} \cdot \varepsilon_f \tag{3.4}$$

where E denotes the elastic modulus of the material, and σ_f and ε_f define, in this case, the state of stress and strain at the failure point of the material, respectively. Despite the fact that these equations are encompassed within the so-called rate-independent theory, they are applied in order to simplify the solution of analytical models in which wave propagation have to be considered (Roylance, 1973). An excellent review of the early work on the wave propagation in simple bodies subjected to transverse impact can be found in Rakhmatulin (1966).

Once the velocity of the originated waves are known, the base radius of the conical frustum formed in the back face of the material can be defined. Certain time ($t_i = i \cdot \Delta t$) after the onset of the impact, both waves have traveled a distance defined by the following equations

$$r_{L_i} = \sum_{i=1}^{n} c_L \cdot t_i \tag{3.5}$$

$$r_{T_i} = \sum_{i=1}^{n} c_T \cdot t_i \tag{3.6}$$

where r_{L_i} and r_{T_i} are the distance traveled by the longitudinal and the transverse waves at time t_i, respectively. The distance traveled by the transverse wave defines the size of the region affected by the formation of the conical frustum, $r_{T_i} = r_{c_i}$; where r_{c_i} is the base radius of the cone. The frustum shape formation is illustrated in the following figure.

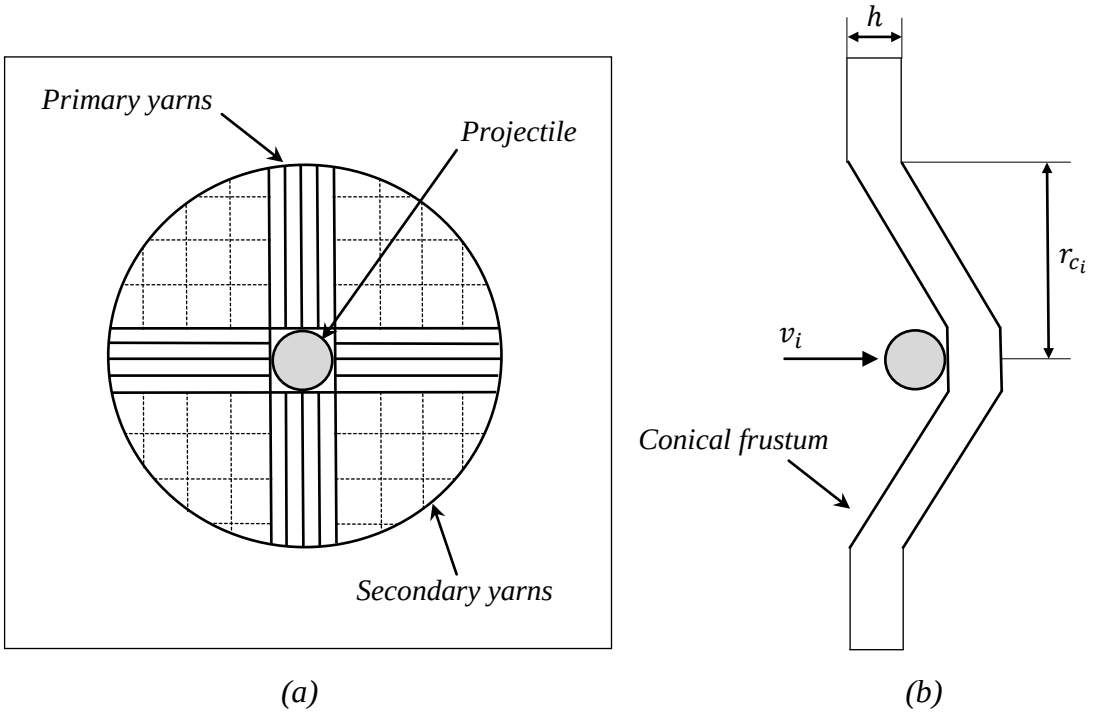

Figure 3.3: Conical frustum shape formed on the back face of the composite laminate impacted by a spherical projectile. (a) Frontal view and (b) side view.

After Vinson and Zukas (1975) defined the parameters regarding the geometry of the conical frustum, Morye et al. (2000) sub-divided the affected zone (region up to which the transverse wave travels) in two regions, as depicted in Figure 3.3(a). When the projectile strikes on the material there is a set of yarns directly impacted by the projectile. These yarns are called primary yarns, and are in charge of providing the force needed to avoid the penetration of the impactor. The primary yarns are arranged along the warp and fill directions. The set of yarns remaining in the affected zone are called secondary yarns. These yarns are not directly impacted by the projectile but they undergo deformation due to the creation of the conical

frustum.

Once the energetic terms involved and the parameters related to the formation and geometry of the cone are identified, it is possible to formulate the law of conservation of energy; whereby the kinetic energy loss by the projectile has to be equal to the sum of every energy absorption mechanism at any instant of time.

$$E_{ke_0} - E_{ke_i} = E_{cf_i} + E_{tf_i} + E_{ed_i} + E_{dl_i} + E_{mc_i} \tag{3.7}$$

where E_{ke_0} is the initial kinetic energy of the projectile ($t = 0\,s$), E_{ke_i} defines the projectile kinetic energy; E_{cf_i}, E_{tf_i}, E_{ed_i}, E_{dl_i}, and E_{mc_i} state the energy absorbed by cone formation, tensile failure of primary yarns, elastic deformation of secondary yarns, delamination, and matrix cracking, respectively. The subscript i denotes the total energy absorbed at an instant of time t_i.

It is possible to define the energy absorbed by each mechanism at the end of ith time interval as

$$E_{AB_i} = \sum_{n=0}^{i} E_{AB_n} = E_{AB_{(i-1)}} + \Delta E_{AB_i} \tag{3.8}$$

where $E_{AB_{(i-1)}}$ defines the energy absorbed by a mechanism up to the end of $(i-1)$th time interval, and ΔE_{AB_i} denotes the energy absorbed by the same mechanism during ith time interval. It can be assumed that the energy absorbed between two consecutive instants of time (t_i and $t_{(i-1)}$) is negligible as compared with the total energy absorbed up to the end of $(i-1)$th interval

$$E_{AB_{(i-1)}} + \Delta E_{AB_i} \approx E_{AB_{(i-1)}} \tag{3.9}$$

Applying the previous assumption to the non-kinetic terms (projectile and conical frustum), the Equation 3.7 is rewritten as

$$E_{ke_0} - E_{ke_i} = E_{cf_i} + E_{tf_{(i-1)}} + E_{ed_{(i-1)}} + E_{dl_{(i-1)}} + E_{mc_{(i-1)}} \tag{3.10}$$

The following defines each energetic term contained in Equation 3.10.

- *Kinetic energy of the projectile*: Being m_p the projectile mass and v_i the projectile velocity, the kinetic energy of the projectile at a time t_i is defined by

$$E_{ke_i} = \frac{1}{2} m_p v_i^2 \tag{3.11}$$

- *Energy absorbed by the conical frustum formed on the back face of the plate*: The energy absorbed by the formation of the conical frustum is defined in terms of its kinetic energy.

$$E_{cf_i} = \frac{1}{2} m_{c_i} v_i^2 \tag{3.12}$$

in which m_{c_i} and v_i is the mass and velocity of the moving cone; considered this velocity to be equal to that of the projectile. The mass of the conical frustum varies during penetration according to the following equation

$$m_{c_i} = \pi r_{c_i}^2 h \rho \tag{3.13}$$

where ρ is the laminate density, h is the laminate thickness, and r_{c_i} is the radius of the moving cone; that it is equal to the distance traveled by the transverse wave.

- *Energy absorbed by the tensile failure of primary yarns*: The energy absorbed by the tensile failure of primary yarns between two consecutive instants of time can be estimated by the following equation

$$\Delta E_{tf_i} = \omega_{f_i} \mathrm{d}V_{t_i} \tag{3.14}$$

in which ω_{f_i} is the breakage specific energy and $\mathrm{d}V_{t_i}$ the volume of the material affected by tensile failure. For sake of simplicity, the following assumptions may be considered.

  i. The projectile is small enough so that the yarn width is considered to be equal to the projectile diameter.
  ii. The thickness of the laminate damaged by tensile failure is equal to the projectile displacement during a given time interval.

These assumptions were first stated by García-Castillo (2007). Considering the previous assumptions, the volume affected by tensile failure of fibers is defined by

$$\mathrm{d}V_{i_t} = \phi \cdot d_i \cdot \mathrm{d}x \tag{3.15}$$

where ϕ is the projectile diameter, d_i is the displacement of the projectile between two consecutive instants of time, and $\mathrm{d}x$ is a differential length measured along the warp direction.

Assuming a linear and elastic up to failure behavior of the material, the breakage specific energy is defined by the following equation

$$\omega_{f_i} = \frac{1}{2} E_t \varepsilon^2 \tag{3.16}$$

where E_t is the tensile modulus of the composite in the warp or fill direction (woven fabric laminate $E_1 \approx E_2$), and ε is the strain endured by the material.

The stress-strain relationship is required to completely define the specific energy absorbed by tensile failure. Despite considering rate-independent theory to describe the velocity of waves in the material, Naik et al. (2006) defines the stress-strain relationship in terms of the so-called stress wave attenuation. This phenomenon was thoroughly studied by Roylance (1973). In the analysis of transverse impacts on single viscoelastic fibers, a decrease in the stress with the distance from the point of impact is observed. Apart from the stress relaxation and creep (characteristic phenomena of the viscous behavior), stress wave attenuation as a result of reflection, transmission and interaction of waves in the material is observed (Roylance (1973) and Naik et al. (2006)).

Stress distribution along the material as a result of stress wave attenuation is shown in the figure below.

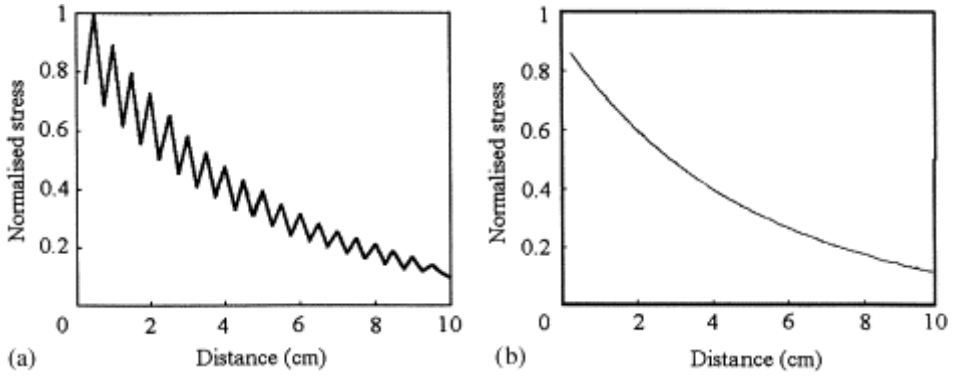

Figure 3.4: (a) Normalized stress distribution in a woven fabric composite, (b) plot generated using a mathematical function, (Naik et al., 2006)

Naik and his colleagues present the following mathematical function in order to estimate the stress distribution along the material (function used in Figure 3.4(b)).

$$y(x) = b^{x/a} \tag{3.17}$$

where x is the distance from the point of impact, a is the width of the yarn impacted, and b is a constant of magnitude less than one referred to as wave transmission factor. This constant is a material property that can be determined by wave transmission studies for a specific material. It is a material property as it depends on the mechanical and physical properties of the matrix and the reinforcing material. An average value of 0.8 can be use for the types of materials concerned herein (Naik et al., 2006). By this approach, the strain distribution in the material as a function of the distance from the point of impact is defined by

$$\varepsilon(x) = \varepsilon_0 b^{x/a} \tag{3.18}$$

where ε_0 is the strain at the point of impact. Once the strain distribution is defined, the energy absorbed by tensile failure of primary yarns between two consecutive instants of time is estimated by

$$\Delta E_{tf_i} = \frac{1}{2}\phi d_i E_t \int_0^x \left(\varepsilon_f b^{\frac{x}{\phi}}\right)^2 \mathrm{d}x \tag{3.19}$$

To be noted that the strain at the point of impact was substituted by the failure strain of the material, and the width of the yarns is considered to be equal to the projectile diameter. Finally, the total energy absorbed by this mechanism at ith time interval is given by

$$E_{tf_i} = \sum_{i=1}^{n} \Delta E_{tf_i} = \sum_{i=1}^{n} \frac{1}{2}\phi d_i E_t \int_0^x \left(\varepsilon_f b^{\frac{x}{\phi}}\right)^2 \mathrm{d}x \tag{3.20}$$

- *Energy absorbed due to deformation of secondary yarns*: The energy absorbed by elastic deformation between two consecutive instants of time can be estimated by the same equation as in the case of tensile failure

$$\Delta E_{ed_i} = \omega_{f_i} \mathrm{d}V_{d_i} \tag{3.21}$$

in which $\mathrm{d}V_{d_i}$ now defines the volume of the material affected by elastic deformation; that is the material encompassed withing the conical frustum zone. Taking into account the cone formation previously depicted in Figure 3.3, the volume of the material subjected to elastic deformation is estimated by

$$\mathrm{d}V_{d_i} = 2\pi h r \mathrm{d}r \tag{3.22}$$

As in the case of tensile failure, in order to completely define the breakage specific energy ω_{f_i}, the strain distribution in the material must be described. Morye et al. (2000) estimates the strain suffered by the material based on the position of the yarns within the affected zone. The yarns that are close to the point of impact experience a strain slightly below the failure strain of the material, while the yarns farther located are not suffering deformation. This is mathematically described by

$$\varepsilon = \begin{cases} \varepsilon_f & \text{at} \quad r \leq \frac{\phi}{2}; \\ \\ 0 & \text{at} \quad r > r_{c_i}. \end{cases} \tag{3.23}$$

Assuming a linear distribution affected by the previous boundary conditions, the strain variation is expressed by the following equation

$$\varepsilon = \frac{2(r_c - r)}{2r_c - \phi} \cdot \varepsilon_f \tag{3.24}$$

Once the strain distribution is defined, the term related to the energy absorbed by elastic deformation of secondary yarns is given by

$$E_{ed_i} = \frac{1}{2} E_t h 2\pi \int_{\frac{\phi}{2}}^{r_{c_i}} \left(\frac{2(r_c - r)}{2r_c - \phi} \cdot \varepsilon_f \right)^2 r \mathrm{d}r \tag{3.25}$$

- *Energy absorbed by delamination and matrix cracking*: Because of the formation of the conical frustum, damage processes in the form of delamination and matrix cracking arise in the material.

  Matrix cracking develops as a consequence of the strain distribution described in Equation 3.24. Material points where the strain is higher than the damage initiation threshold undergo damage in the form of matrix cracking. Owing to the fracture of the matrix, interlaminar strength of the material decreases. As a result, further loading and deformation causes delamination. Experimental observations performed by Takeda et al. (1980) revealed that the delaminated area is quasi-lemniscate in shape (see Figure 3.5). This is due to the fact that, as a result of the anisotropic behavior of the material, delamination propagates more along the warp and fill directions. Some hypothesis were performed afterwards by García-Castillo (2007) in order to simplify the description of this energetic term

  i. The area undergoing delamination and matrix cracking is considered to be circular in shape. The delaminated area between two instants of time is shown in the figure below. The dashed region is the experimentally observed quasi-lemniscate shape, whereas the circular area is the assumption proposed.

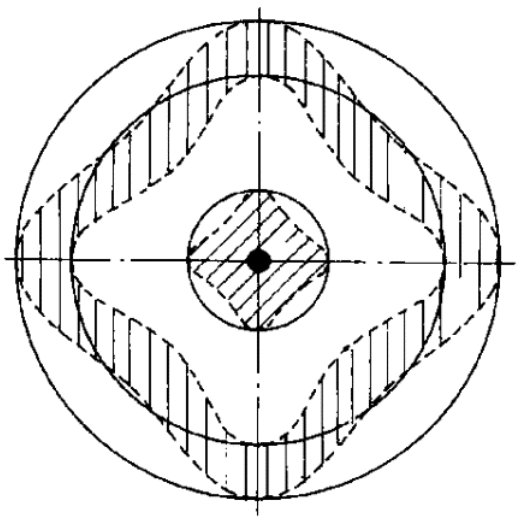

Figure 3.5: Empirically observed and estimated shape of the delaminated region, (Naik et al., 2006)

ii. The area damaged by delamination and matrix cracking is confined inside the region affected by the conical frustum formation.

iii. Delamination and matrix cracking are assumed to affect every layer of the composite.

Following these assumptions the energy dissipated by delamination and matrix cracking are estimated by the following terms

$$E_{dl_i} = \pi r_{c_i}^2 C G_{II_c} \qquad \text{Delamination} \tag{3.26}$$

$$E_{mc_i} = \pi r_{c_i}^2 C E_{MC} h \qquad \text{Matrix cracking} \tag{3.27}$$

where r_{c_i} is the radius of the cone formed, C is a correction factor due to the assumption of circular delaminated area, E_{MC} is the specific matrix breakage energy, and G_{II_c} is the fracture toughness in mode II. The latter is used as the propagation of the delaminated zone is considered to be of mode II type (Naik et al., 2006).

3.2.2 Model resolution

Once the energetic terms involved in the process are completely defined, it is possible to calculate the main outputs of the model. By substituting the kinetic energy terms, the Equation 3.10 (law of conservation of energy) leads to

$$\frac{1}{2}m_p v_0^2 - \frac{1}{2}m_p v_i^2 = \frac{1}{2}m_{c_i} v_i^2 + E_{tf_{(i-1)}} + E_{ed_{(i-1)}} + E_{dl_{(i-1)}} + E_{mc_{(i-1)}} \tag{3.28}$$

Grouping the non-kinetic terms as follows

$$E_{(i-1)} = E_{tf_{(i-1)}} + E_{ed_{(i-1)}} + E_{dl_{(i-1)}} + E_{mc_{(i-1)}} \tag{3.29}$$

it is possible to rewrite Equation 3.28 as

$$\frac{1}{2}m_p v_0^2 = \frac{1}{2}(m_p + m_{c_i}) v_i^2 + E_{i-1} \tag{3.30}$$

The variable describing the velocity of the projectile at each instant of time is isolated from the previous equation, leading to

$$v_i = \sqrt{\frac{\frac{1}{2}m_p v_0^2 - E_{i-1}}{\frac{1}{2}(m_p + m_{c_i})}} \qquad \text{Projectile velocity} \tag{3.31}$$

Once the projectile velocity is known, the deceleration and displacement of the projectile between two consecutive instants of time are given by the following equations

$$\Delta a_i = \frac{v_{i-1} - v_i}{\Delta t} \qquad \text{Projectile deceleration} \tag{3.32}$$

$$\Delta d_i = v_{i-1} \cdot \Delta t - \frac{1}{2} \cdot \Delta a_i \qquad \text{Projectile displacement} \tag{3.33}$$

Finally the total displacement of the projectile is defined by

$$D_i = \sum_{i=1}^{n} \Delta d_i \tag{3.34}$$

The model just presented requires of an iterative method to be solved. The impact process is divided into small time intervals, usually taken to be $\Delta t = 1\,\mu s$. On each iteration, the energy dissipated by each energetic term is calculated along with the projectile parameters. These parameters are used afterwards as the input needed for the next iteration. Iterations end when the projectile is detained or the target is completely defeated. The algorithm implemented is illustrated in the following figure. Further details can be shown in Appendix B.

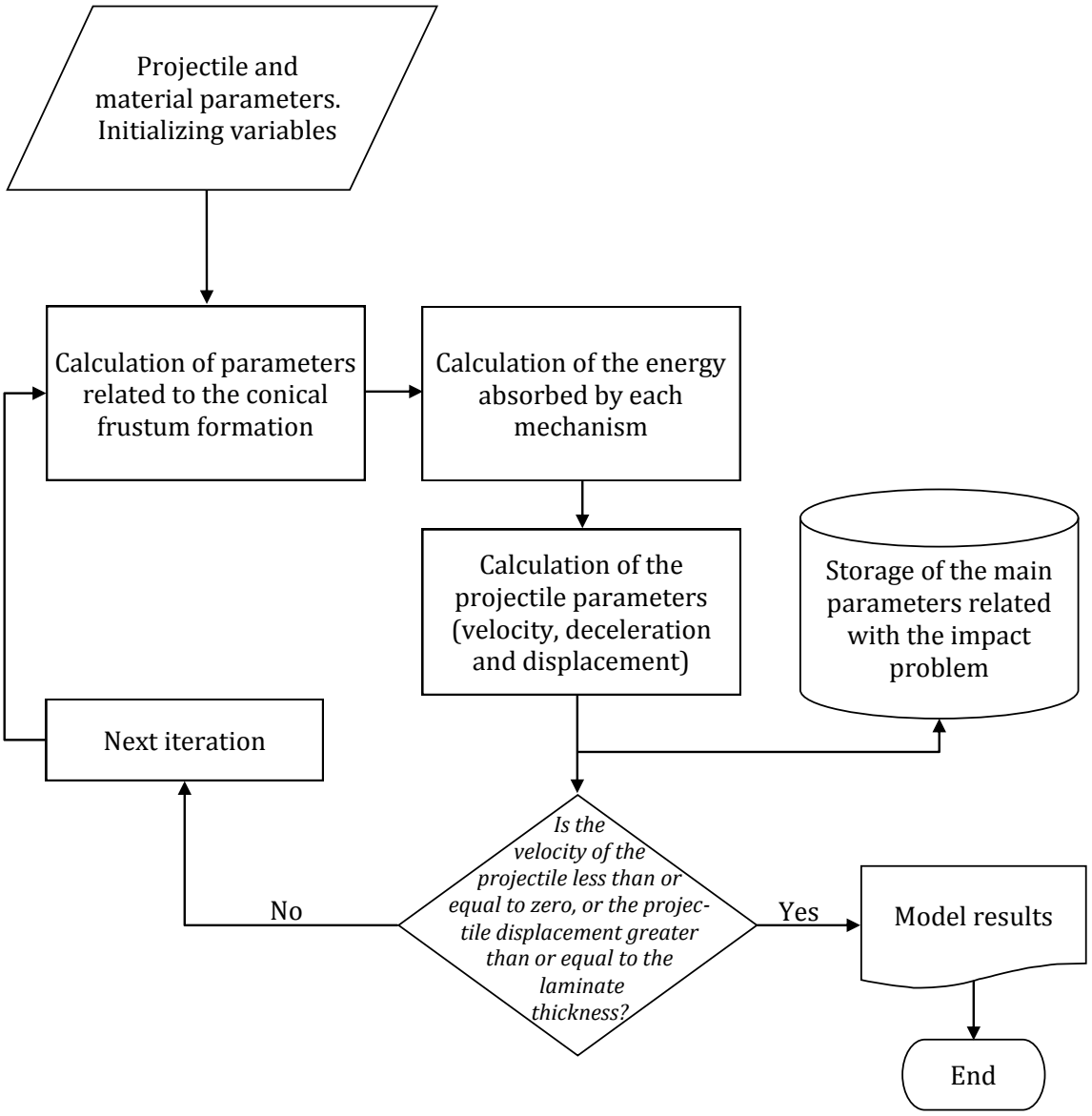

Figure 3.6: Flow chart of the model resolution.

3.3 Results and validation

In the present section, results provided by the analytical model are presented. As in the previous chapter, the performance of the model is evaluated by comparing the model results with experimental data available in the literature.

In order to obtain the results provided by the analytical model, the algorithm presented in Figure 3.6 was implemented in Mathcad 14. Material properties used to validate the model belong to a glass-polyester plain weave laminate with five laminas. The reinforcement is based on glass fiber type E, whilst the matrix used is industrially named as AROPOL FS6902. The properties of this material are proved to be enhanced at high strain rates (Ochoa et al., 2004). Properties of the Eglass/FS6902 woven laminate at high strain rates (10^3 s^{-1}) are reported in Table 3.1.

Property	Unit	Value
E_1	[GPa]	15.2
E_2	[GPa]	15.2
ν_{12}		0.16
X_t	[MPa]	1102
Y_t	[MPa]	1102
G_{II_c}	[J/m^2]	3000
E_{MC}	[J/m^3]	10^6
b		0.9
C		1
ε_f		0.072535
ρ_l	[kg/m^3]	1980
h	[mm]	3.19

Table 3.1: Material properties (Naik et al. (2005) and García-Castillo (2007)).

Results obtained by the model when the material is impacted by a spherical steel projectile of 7.5 mm in diameter and 1.73 g of mass, are shown in Figures 3.7, 3.8, and 3.9. Residual velocity versus impact velocity are shown in the following figure. Ballistic test were performed on the same material by García-Castillo et al. (2009).

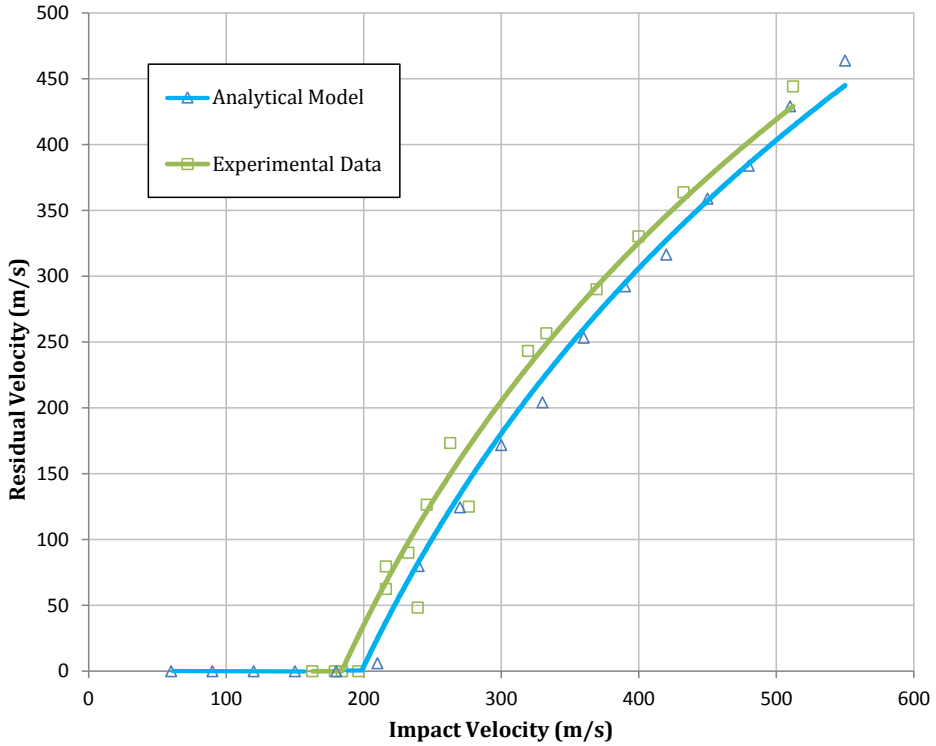

Figure 3.7: Residual velocity versus impact velocity.

The model predicts with reasonable accuracy the response of the material in the range of impact velocities evaluated. By plotting the contact time between projectile and target versus the impact velocity (Figure 3.8), it is possible to observe how, at velocities above the ballistic limit, the time needed by the projectile to completely defeat the target increases when getting close to the ballistic limit. The reason lies on the higher amount of energetic mechanisms involved in dispelling the energy of the projectile at velocities near the ballistic limit (See Figure 3.9(a)). Again, the results obtained are proved to be in good agreement with the experimental data.

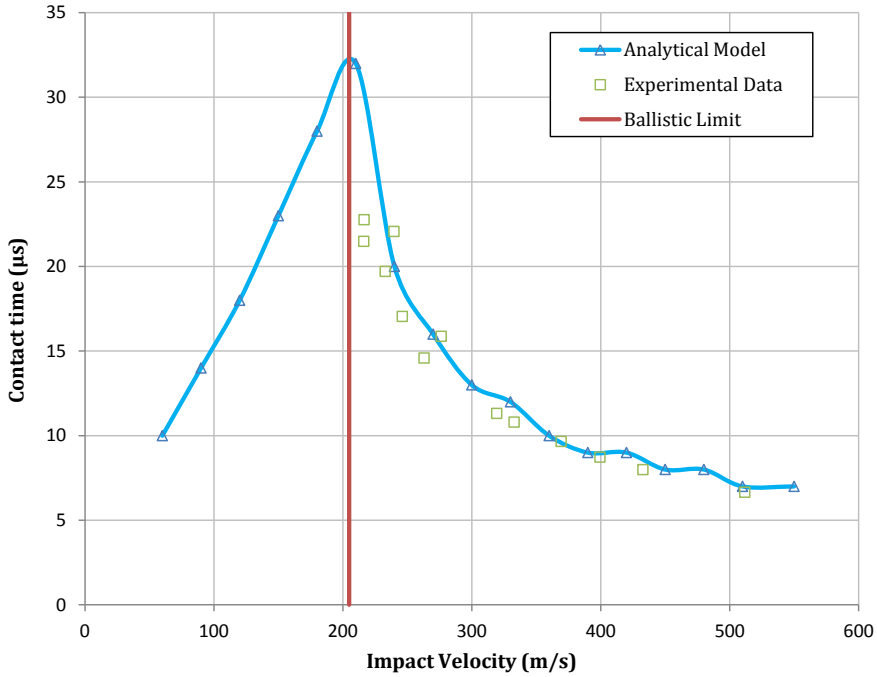

Figure 3.8: Contact time versus impact velocity.

An additional outcome obtained by the model is the one related to the energy absorbed by the different damage and failure mechanisms involved in the process. The energy absorbed by each mechanism at two different velocities, one in the vicinity of the ballistic limit and the other above the ballistic limit, are shown in Figure 3.9.

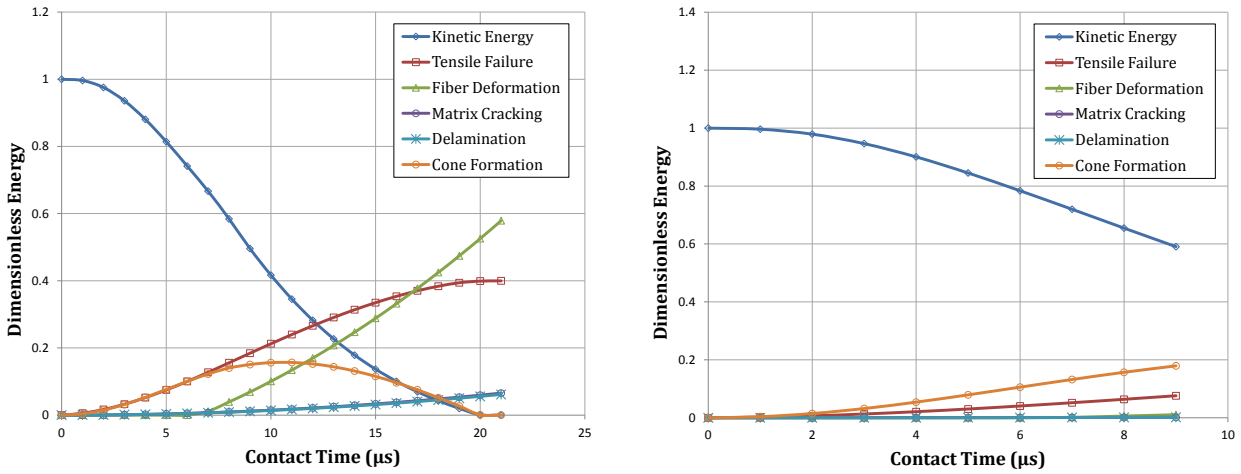

Figure 3.9: Dimensionless energy versus projectile displacement for impact at velocities (a) below the ballistic limit (160 m/s) and (b) above the ballistic limit (400 m/s)

At velocities below the ballistic limit, a material performance dominated by deformation and tensile failure of fibers is revealed. When the velocity of the impactor exceeds the ballistic

limit, the kinetic energy of the conical frustum formed appears to be the prime mechanism involved in the projectile detention. Matrix cracking and delamination are always under the 10 % of the total energy absorbed by the material. This is proved to be in agreement with the empirical assessments carried out by Morye et al. (2000) for woven fabric composites impacted at high velocities.

3.4 Scope of the model

The model described is intended to predict the ballistic performance of flexible fiber composites. Apart from the results presented in the previous section, the model provides an important overview of the ballistic performance of the material under study. Many authors state, for instance, the importance of the matrix in the response under impact of composite materials (Faur-Csukat (2006) and Gopinath et al. (2012)). By using the model, one is able to estimate the effect of changing the matrix in the ballistic performance of composite laminates.

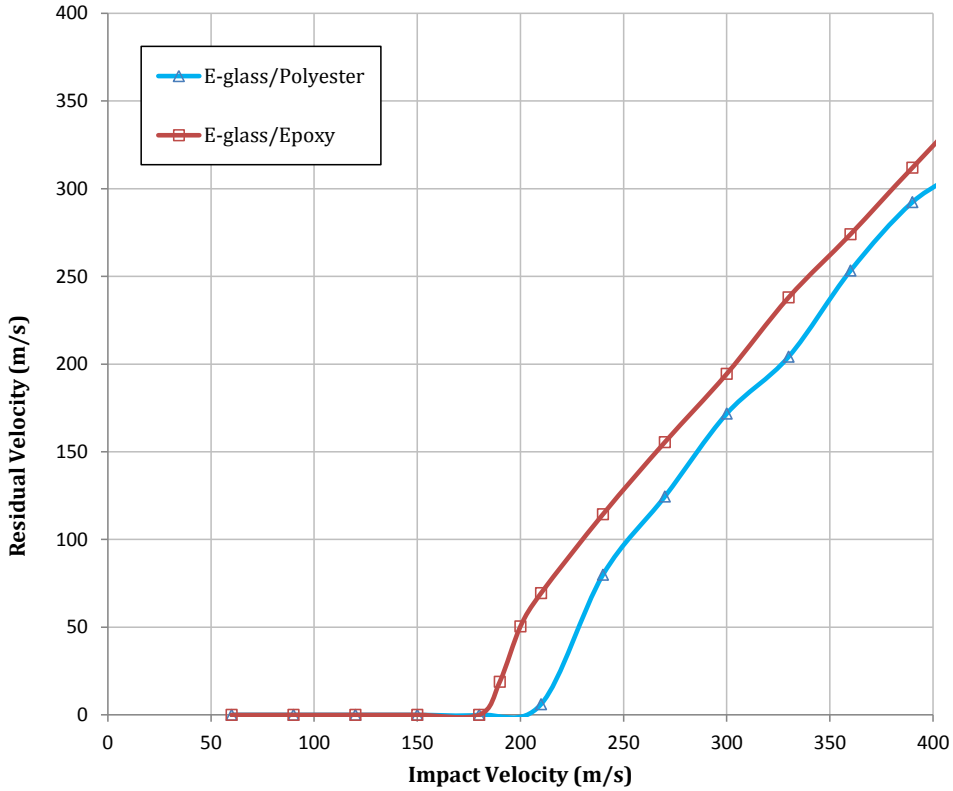

Figure 3.10: Effect of matrix changing in the ballistic performance of the material.

In the previous figure, results provided by the model for a glass fiber-reinforced composite bonded by two different matrices, are illustrated. Properties of the E-glass/polyester composite were presented in the previous section; whereas properties belonging to the E-glass/epoxy are reported in Naik et al. (2006). The rigid behavior of the epoxy as compared with the polyester resin, reduces the overall ballistic performance of the material. Thermoplastic resins have been considered as an alternative on the design of lightweight body armor protection. However, their lower tensile strength force designers to combined thermoplastic resins with high tensile modulus fibers. Also the higher failure strain of thermoplastic matrix-based systems increase the

possibility of blunt trauma injury, when applied on body armor protection, due to the depth of the conical frustum formed (Kulkarni et al., 2013).

As stated before, the model at hand can be used to evaluate the response under impact of polymer fiber composites. Polymeric fibers are used in a broad range of applications. Among others, they stand out in the manufacturing of body armor protection. The most commonly used polymeric fibers are those made of materials such as nylon, aramid and ulta-high molecular weight polyethylene (UHMWPE). These fibers used alone, in the form of multi-layer fabric, or contained within a polymeric matrix, are widely employed in the protection of bodies and structures likely subjected to many different types of dynamic loads (e.g., small calliber bullets, blasts, debris, etc.) (Iremonger and Went, 1996). By using the model, it is possible to estimate the performance under high velocity impact of composite materials reinforced by different types of ballistic fibers. In the following figure, model results are shown on the impact of prepreg systems based on glass, Kevlar® (by DuPont), Zylon® (by Toyobo), Spectra ® (by AlliedSignal/Honeywell), and nylon fibers.

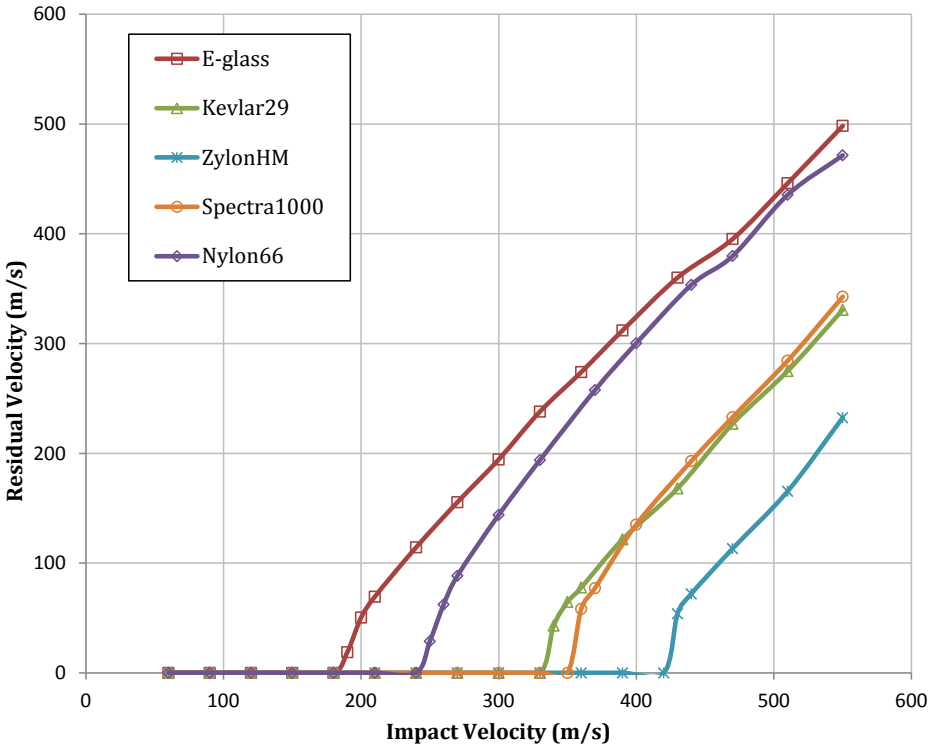

Figure 3.11: Effect of different reinforcements in the ballistic performance of the material.

Based on the results obtained, Zylon® HM (high modulus) fiber has the greatest ballistic performance, followed by Spectra® 1000, Kevlar® 29, Nylon-66, and glass type E fibers. Properties of these materials are reported in Kulkarni et al. (2013). The ballistic performance revealed by the model matches the experimental observations stated in David et al. (2009). Zylon® fibers are made using a liquid crystal polymer commonly referred to as PBO (*poly(p-phenylene benzobisoxazole)*); while Spectra® fibers are made from UHMWPE. Both types of fibers have incredible ballistic features and are extensively used in the manufacturing of modern

lightweight body armors (Kulkarni et al., 2013). However, their applicability is constrained by the high degradation of their properties due to moisture, temperature, UV light and gamma radiation (David et al., 2009).

On the other hand, aramid fibers, like Kevlar®, were developed during the 1960s and since then, they have been highly applied in impact-related systems such as aerospace applications, armor systems and marine structures. The high energy absorption capacity of aramid fibers, related to the their high degree of toughness and damage tolerance, made them suitable for impact resistance applications (Reis et al. (2012) and Woo and Kim (2014)).

Chapter 4

Applicability of models

The creation of a pre-design tool implies a number of steps that need to be performed before the application is ready to be implemented. The most important step is based on a detailed analysis of the content settled behind the application. This means, being able to answer questions like: what is the application main objective? Who is intended to use it? What kind of benefits the application will provide? And most important, does the application content accomplished the sough goals?. On this basis, the need for this work is raised.

The idea of creating a pre-design tool, that supports the design-against-impact of components and structures, stems from the fact that many authors declare the great applicability of their models at early design stages. Undoubtedly, analytical models have much to offer at this level. These models are usually based on relatively simple solutions, which can be run in a normal PC spending no more than a couple of minutes. In the field of mechanics of materials, these models provide, in many cases, a suitable approach to the real behavior of the material under certain conditions, avoiding the need of experimental testing. Less time-consuming and low cost are incredible assets when one starts to think of a structural design. However, some analytical models, which are declared as suitable for pre-design applications, are not always precise fulfilling the previous definitions.

In order to measure whether a given analytical model will be a good option to be implemented into a pre-design tool, three broad requirements must be met. These are:

i. Good predictions. Results provided by the model must be in agreement with results obtained by experimental tests. Moreover, the model must reproduce the overall behavior of the target material with accuracy by precisely handling the physics of the problem.

ii. Broad applicability. One of the main goals of a pre-design tool is providing its users with the chance to avoid experimental testing at early design stages. In order to fulfill this goal, the model must be based on well-known properties for both target and projectile.

iii. Event sensitivity. The model must show up variation on the results obtained when changing one of the parameters related with the impacted material. That could be, for instance, a change on the type of resin used on the composite or a different arrangement of plies. Likewise, the outcome of the model should change when an event condition, such as impact velocity regime or obliquity of the impact, changes.

In the following sections a thorough evaluation of these requirements is presented over the models previously described. The analytical models are referred to as CFRP model, for the model presented in Chapter 2, and GPFRP model, for the model presented in Chapter 3.

4.1 Analysis of the CFRP model

In Chapter 2, a model intended to predict the ballistic performance of carbon fiber reinforced plastics (CFRPs) was presented. Owing to the issues highlighted in Section 2.4, the model at hand does not completely satisfy the minimum requirements for its application to a pre-design tool. A number of improvements must be accomplished.

First, the use of the out-of-plane compressive strength as one of the major properties in charge of the overall behavior of the material becomes one of the main drawbacks. The latter nullify the possibility to verify the good agreement of the model results with experimental tests when a different type of carbon fiber or resin is used. Consequently, the initial crushing process, that comes out at the early stages of the impact even, needs to be rethought in order to meet the required sensitivity.

Second, the model does not completely reproduce accurately the behavior of the material during the impact event. Strain rate sensitivity must be included in order to fulfill this goal. This can be handled by adding to the model the aforementioned Dynamic Enhancement Factor (DIF). Results provided by the model are shown in the following figure.

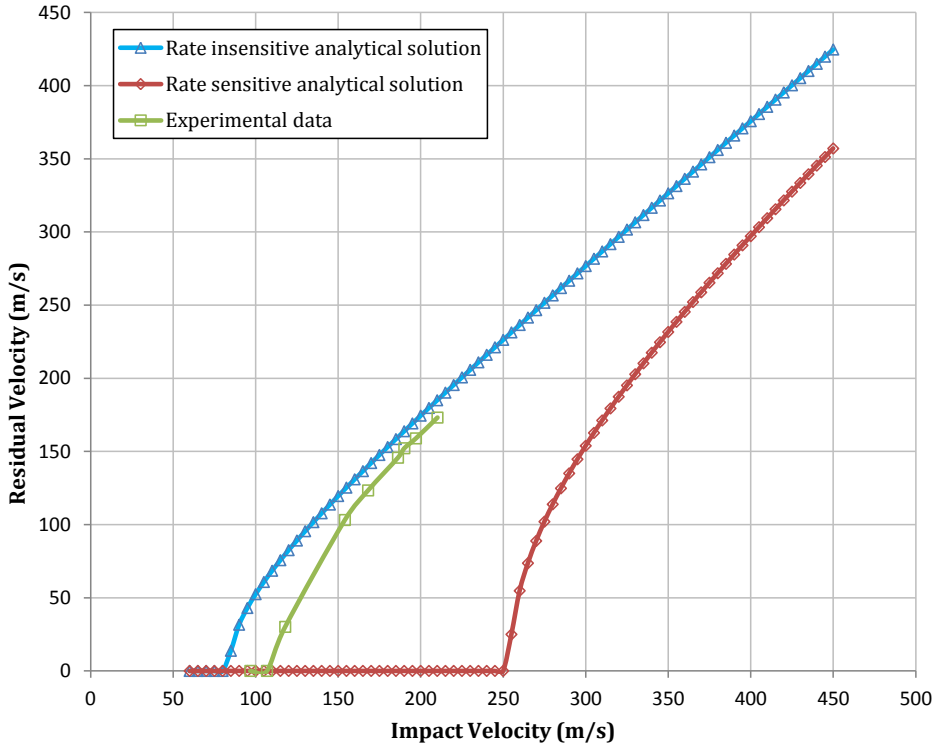

Figure 4.1: Results obtained by adding strain rate sensitivity.

When the model becomes sensitive to the strain rate, the results obtained overestimate the ballistic performance of the material. The addition of DIF is not enough to fulfill the required accuracy. The reason for the discrepancy between model results and experimental data may rely on two facts. The first one is related to the elevated weight taken by the out-of-plane compressive strength in the outcome of the model. The second may be associated with the lack of damage mechanisms considered. Although the amount of energy absorbed by delamination was proved to be small, at impact velocities near the ballistic limit, delamination has some influence on the total energy dissipated by the impacted material. At lower impact velocities, interlaminar damage processes have enough time to show up before the breakage of fibers takes place. Moreover, when an impact occurs at a velocity much higher than the ballistic limit, the shear-out of fibers seems to be the main process leading to the formation of the plug.

The addition of the process of delamination and shear-out drives the model close to the physics of the problem. Besides, the addition of these two energetic terms may also downplay the role of the out-of-plane compressive strength of the material. This could make the evaluation of the model sensitivity easier against different parameters and event conditions, turning it into a suitable model for a pre-design tool.

4.2 Analysis of the GPFRP model

The model presented in Chapter 3 is designed to predict the response under impact of glass and polymer fiber composites. This model appears to accomplish the three requirements needed for its application on a pre-design tool.

Good agreement with experimental data was proved in Section 3.3. The higher number of energy absorption mechanisms considered by the model precisely reproduce the complexity of the impact event. Along with the latter, the simplicity of the model makes it easier to be improved with the aim of reaching a wider range of materials.

The appearance of shear plugging is neglected on the impact of glass and polymer fiber composites. However, the complexity of the dynamic behavior of materials makes this last statement not true in all cases. When glass fibers are bonded by a thermoset resin the material behavior under impact is close to that of a brittle material, where shear-out processes would take place. Also, when polymer fiber composites are impacted a very high velocities, the process of shear plugging appears as well (Patel et al. (2004) and Sikarwar et al. (2013)).

The simplicity of the model allows to improve its scope by adding the effect of shear plugging. The addition of this process makes the model suitable for the characterization of the behavior under impact of most materials. García-Castillo (2007) defined the energy absorbed due to shear plugging between two time intervals by the following equation.

$$\Delta E_{sp_i} = \frac{1}{2}\pi\phi h^2 S_{SP} \tag{4.1}$$

where S_{SP} denotes the out-of-plane shear strength of the material. The total energy absorbed by the end of ith time interval is given by

$$E_{sp_i} = \sum_{i=1}^{n} \Delta E_{sp_i} \tag{4.2}$$

By adding the previous mechanism, the evaluation of the model performance on the impact of CFRPs can be accomplished. Results provided by the model for a thin, carbon/epoxy plain weave composite subjected to high velocity impact are presented in the following figure. The results obtained are shown, along with results provided by the model presented in Chapter 2 and experimental data obtained from López-Puente et al. (2007).

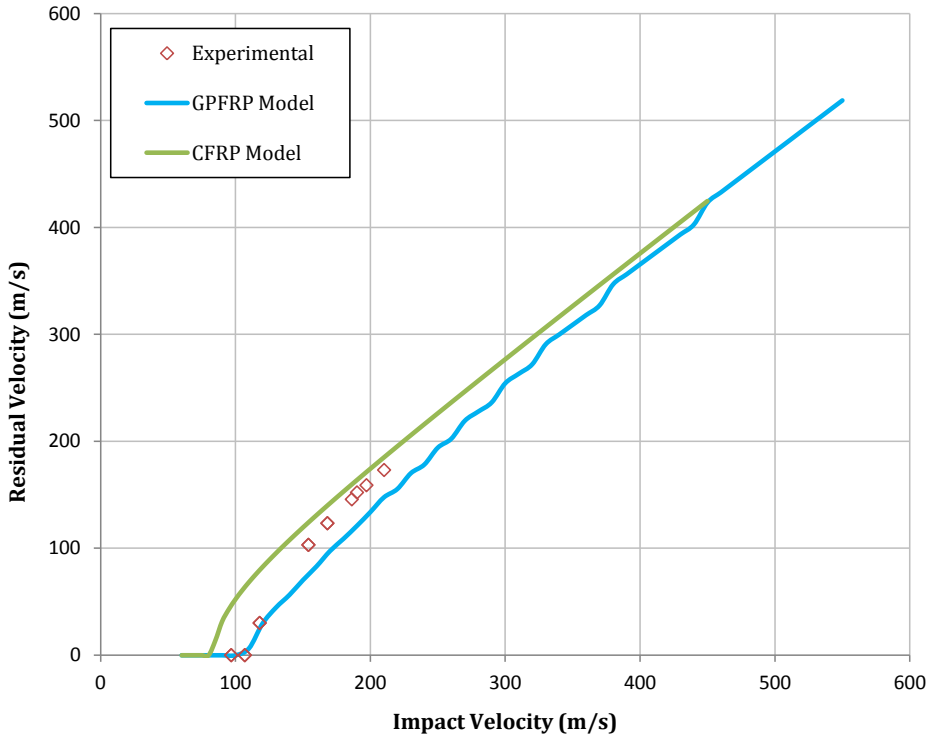

Figure 4.2: Comparison of the results provided by different models

The addition of the shear out process into the model accurately predicts the ballistic limit for a thin, carbon/epoxy woven composite plate transversely impacted by a spherical steel projectile. At velocities above the ballistic limit, the model lightly overestimates the ballistic response of the material. Both models appear to tend to the same results, achieving this goal at velocities over 450 m/s.

As shown, the model can be easily modified in order to predict the ballistic performance of a wide range of materials. This fact proves the second requirement related to the broad applicability of the model.

The last requirement is the most important from a design point of view. Being able to predict how the ballistic performance of the material improves or diminishes when certain parameters change, is a real asset in the design against impact of materials and structures. With

this model, one is able to create trend plots for different types of composite materials. Trends in the ballistic limit of a glass fiber-reinforced composite impacted by a low mass, spherical, steel projectile, are presented below.

The effect of the material failure strain, tensile strength and laminate thickness, in the ballistic performance of the material, are shown in Figure 4.3(a), (b), and (c). This sort of plots gives the designer a quick and valuable overview of the parameters needed to be improved in order to fulfill the required design patterns.

Because of the reasons highlighted throughout this section, the model presented in Chapter 3 is a major candidate in order to be implemented in a pre-design tool on the design of composite material structures subjected to high velocity impacts.

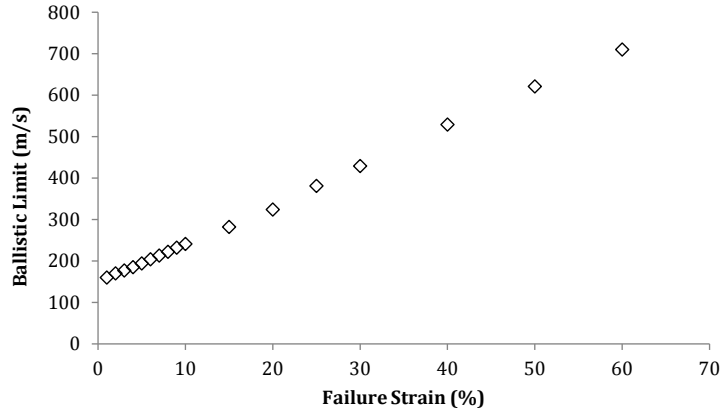

(a)

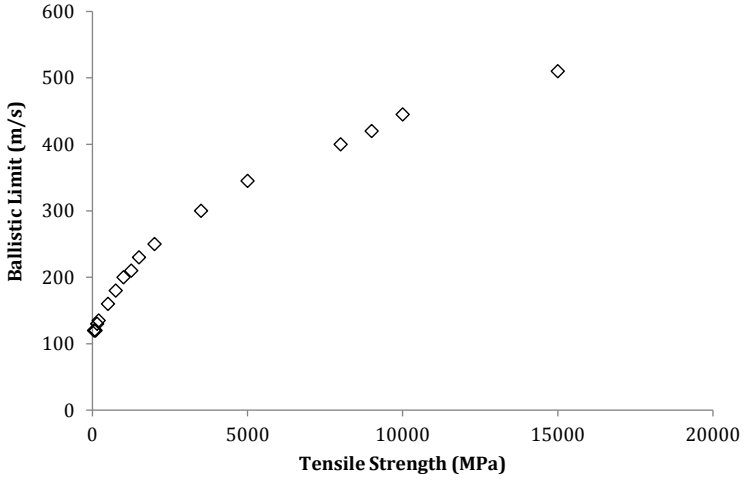

(b)

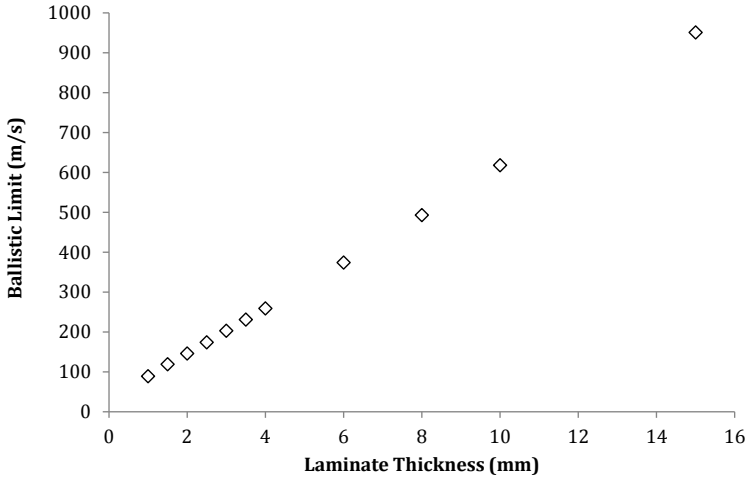

(c)

Figure 4.3: Improvement in the ballistic limit by increasing the (a) failure strain, (b) tensile strength, and (c) laminate thickness.

Chapter 5

Conclusions and future work

The work developed during the present senior thesis was focussed on the evaluation of several analytical models on the impact of composite materials. The main goal of this project was to settle the mainstay for the creation of a pre-design tool. This tool must provide its users with a relatively simple and rapid way to achieve broad results on early designs against impact of structural components.

In Chapter 1, a generic review of the existing literature on analytical models is presented. Since the dynamic behavior of composite materials has begun to interest the scientific community on the 1950s, the literature up to our days is extensive. By selecting two of the most promising models, Chapter 2 and Chapter 3 were devoted to present and disclose the basics of each model, providing theoretical foundations, results and initial findings. In Chapter 4, both models where subjected to a more carefully evaluation applying essential principles for their application into a pre-design tool. Several observations are revealed from this work.

i. Dynamic behavior of materials has drawn the attention of the scientific community for a long time. Due to the prompt development of new and advanced materials and their direct application on different industry sectors, the complete knowledge of their dynamic response has become a valuable goal for their fast and reliable implementation.

ii. Analytical models have set up as benchmark in early design stages, where goals like less time consuming applications and low cost developments are sought. However, many of the anaytical models existing are intended to reproduce one specific case with accuracy, leading to less efficiency or even no possibility to reproduce further environments, leaving aside the broad applicability concept that leads to design applications.

iii. The application of a model into a pre-design tool requires of a bigger approach to the event. Good predictions, along with broad applicability and event sensitivity are the three broad requirements established to decide whether a given model is a good candidate to be applied into a pre-design tool. Some of the models have been found to be easily improved to fulfill the previous requirements.

Based on the conclusions revealed on this project two major paths can be subsequently followed. One is related to the continuous development and improvement of analytical models taking into account the three established requirements. The second is related to the design and

implementation of the pre-design tool.

Regarding the development of new models, future works on the field might focus on:

- Taking into account the three requirements here established in order to make sure that main advantages of analytical methods are well achieved.
- Development of analytical models encompassing a broad range of materials, and further studies on the different mechanisms involved on the projectile-target interaction.
- Performing of experimental tests that better approach the real use of the structural component, moving away from the ideal path. Extreme temperature variations, UV and gamma irradiation, pressure and moisture conditions, multiple impacts, non-flat specimen geometry, and wear and tear of the specimen, are some of the experiments currently been conducted that approach the real use of the final structural component.

Once the basics for the creation of a pre-design tool are established, its implementation can be successfully achieved. Regarding the implementation of the pre-design tool:

- Web applications appear to better fit the needs of this sort of tools. Web applications, like CADEC (Computer Aided Design Environment for Composites), afford to access their content everywhere at any time, providing not only the advantage of the pre-design tool (less time-consuming and low cost) but also the advantage of the on-line accessibility and broadcasting.
- The use of CADEC as the pre-design tool environment also provides an advantage based on the use of its already created interface and database in order to interact with the impact application.
- A web application can be easily modified and improved in order to increase its scope. This can be accomplished by covering up models including different segments like, for instance: low and hyper-velocity impact situations, oblique impacts, projectile type variation, projectile erosion, or under-pressure cylindrical shells.

Bibliography

Abrate, S., 1998. Impact on Composites Structures. Cambridge University Press, Cambridge, UK.

Abrate, S., 2001. Modeling of impacts on composite structures. Composite Structures 51, 129–138.

Akay, M., 1987. Post damage capability of carbon fibre reinforced matrices. In: Proceedings of International Conferences on Polymers for Composites. The Plastics and Rubber Institute, London, UK, pp. 11.1–11.10.

Alves, A., Nascimento, L., Suarez, J., 2005. Influence of weathering and gamma irradiation on the mechanical and ballistic behavior of UHMWPE composite armor. Polymer Testing 24, 104–113.

Atas, C., Icten, B., Küçük, M., 2013. Thickness effect on repeated impact response of woven fabric composite plates. Composites: Part B 49, 80–85.

Barbero, E. J., 2010. Introduction to composite material design, 2nd Edition. CRC Press.

Benloulo, I. C., Sánchez-Gálvez, V., 1998. A new analytical model to simulate impact onto ceramic/composite armors. International Journal of Impact Engineering 21, 461–471.

Bland, P., Dear, J., 2001. Observations on the impact behaviour of carbon-fibre reinforced polymers for the qualitative validation of models. Composites Part A: Applied Science and Manufacturing 32, 1217–1227.

Camponeschi, E., September 1989. Through-thickness strain response of thick composites in compression. Tech. rep., David Taylor Research Center.

Cantwell, W., Morton, J., 1985. Detection of impact damage in cfrp laminates. Composite Structures 3, 241–257.

Cantwell, W., Morton, J., 1986. An assessment of the impact perfomance of CFRP reinforced with high-strain carbon fibres. Composites Science and Technology 25, 133–148.

Cantwell, W., Morton, J., 1989. Comparison of the low and high velocity impact response. Composites 20, 545–551.

Cantwell, W., Morton, J., 1990. Impact perforation of carbon fibre reinforced plastic. Composites Science and Technology 38, 119–141.

Cantwell, W., Morton, J., 1991. The impact resistance of composite mateirals - a review. Composites 22, 347–362.

Carrillo, J., Gamboa, R., Flores-Johnson, E., Gonzalez-Chi, P., 2012. Ballistic performance of thermoplastic composite laminates made from aramif woven fabric and polypropylene matrix. Polymer Testing 31, 512–519.

Christiansen, E., Kerr, J., 2001. Ballistic limit equations for spacecraft shielding. International Journal of Impact Engineering 26, 93–104.

Compton, B. G., Gamble, E. A., Zok, F. W., 2013. Failure initiation during impact of metal spheres onto ceramic targets. International Journal of Impact Engineering 55, 11–23.

Cunniff, P., November 1999. Dimensionless parameters for optimization of textile-based body armor systems. In: 18th International Symposium on Ballistics. San Antonio, TX, pp. 1303–1310.

Curson, A., Leach, D., Moore, D., 1990. Impact failure mechanisms in carbon fiber/PEEK composites. Journal of Thermoplastics Composite Materials 3, 24–31.

Daniel, I., Hsiao, H., Cordes, R., 1995. In high strain rate effects on polymer metal and ceramic matrix composites and other advanced materials. ASME 48, 167–177.

David, N. V., Gao, X. L., Zheng, J. Q., 2009. Ballistic resistant body armor: Contemporary and propspective materials and related protection mechanisms. Applied Mechanics Review 62, 050802/1–20.

den Reijer, P. C., November 1991. Impact on ceramic faced armours. Ph.D. thesis, Delft University of Technology.

ESA, April 2013. Hypervelocity impacts and protecting spacecraft. `http://www.esa.int/Our_Activities/Operations/Space_Debris/Hypervelocity_impacts_and_protecting_spacecraft`, Accessed: 2015-04-03.

Faur-Csukat, G., 2006. A study on the ballistic performance of composites. Advancement in Polymer Composite Technology 239, 217–226.

Florence, A. L., 1969. Interaction of projectiles and composite armour. Part II. Standford Research Institue, Menlo Park, California, USA.

Florence, A. L., Ahrens, T., 1967. Interaction of projectiles and composite armour. Standford Research Institue, Menlo Park, California, USA.

García-Castillo, S., Sánchez-Sáez, S., López-Puente, J., Barbero, E., Navarro, C., 2009. Impact behaviour of cpreloaded glass/polyester woven plates. Composites Science and Technology 69, 711–717.

García-Castillo, S. K., 2007. Análisis de laminados de materiales compuestos con precarga en su plano y sometidos a impacto. Ph.D. thesis, Departamento de Mecánica de Medios Continuos y Teoría de Estructuras. Universidad Carlos III de Madrid.

Godoy, L. A., 1999. Theory of Elastic Stability. Analysis and sensitivity. Taylor & Francis, Department of Civil Engineering, University of Puerto Rico, Puerto Rico, USA.

Gopinath, G., Zheng, J. Q., Batra, R. C., 2012. Effect of matrix on ballistic performance of soft body armor. Composite Structures 94, 2690–2696.

Gu, B., 2003. Analytical modeling for the ballistic perforation of planar plain-woven fabric target by projectile. Composites: Part B 34, 361–371.

Hayhurst, C. J., Hiermaier, S. J., Clegg, R. A., Lambert, W. R. A. M., 1999. Development of material models for Nextel and Kevlar-epoxy for high pressures and strain rates. International Journal of Impact Engineering 23, 365–376.

Hazzel, P., Kister, G., Stennett, C., Bourque, P., Cooper, G., 2008. Normal and oblique penetration of woven CFRP laminates by a high velocity steel sphere. Composites: Part A 39, 866–874.

Hong, S., Liu, D., 1989. On the relationship between impact energy and delamination area. Experimental Mechanics 13, 115–120.

Hosur, M., Alexander, J., Vaidya, U., Jeelani, S., 2001. High strain rate compression response of carbon/epoxy laminate composite. Composite Structures 52, 405–417.

Iremonger, M. J., Went, A. C., 1996. Ballistic impact of fibre composite armour by fragment-simulating projectiles. Composites Part A 27A, 575–581.

Jacob, G., Starbuck, J., Fellers, J., Simunovic, S., Boeman, R., 2004. Strain rate effects on the mechanical properties of polymer composite materials. Journal of Applied Polymer Science 94, 296–301.

Katz, S., Grossman, E., Gouzman, I., Murat, M., Wiesel, E., Wagner, H., 2008. Response of composite materials to hyperveolicty impact. International Journal of Impact Engineering 35, 1606–1611.

Khalili, S., Mittal, R., Panah, N. M., 2007. Analysis of fiber reinforced composite plates subjected to transverse impact in the presence of initial stresses. Composite Structures 77, 263–268.

Kim, H., DeFrancisci, G., Chen, Z., Rhymer, J., Trippmann, J., 2010. Impact damage formation on composite aircraft structures. In: 6th Annual Technical Review Meeting. Federal Aviation Administration Joint Advanced Materials & Structures (JAMS), Seattle, WA.

Kim, H., Welch, D., Kedward, K., 2003. Experimental investigation of high velocity ice impacts on woven carbon/epoxy comopsite panels. Composites Part A: Applied Science and Manufacturing 34, 25–41.

Kistler, L., Waas, A., 1998a. Experiment and analysis on the response of curved laminated composites panels subjected to low velocity impact. International Journal of Impact Engineering 21, 711–736.

Kistler, L., Waas, A., 1998b. Impact response of cylindrically curved laminates including a large deformation scaling study. International Journal of Impact Engineering 21, 61–75.

Kistler, L., Waas, A., 1999. On the response of curved laminated panels subjected to transverse impact loads. International Journal of Solids and Structures 36, 1311–1327.

Kulkarni, S. G., Gao, X. L., Horner, S. E., Zheng, J. Q., David, N., 2013. Ballistc helmets - their deisgn, materials, and performance against traumatic brain injury. Composite Structures 101, 313–331.

Lodeiro, M., Broughton, W., Sims, G., 1999. Understanding limitations of through thickness test methods. Plastics, Rubber and Composites 28, 416–424.

López-Puente, J., October 2003. Análisis y modelizacion de impactos de alta velocidad sobre laminados carbono/epoxi. Ph.D. thesis, Departamento de Mecánica de Medios Continuos y Teoría de Estructuras. Universidad Carlos III de Madrid.

López-Puente, J., Li, S., 2012. Analysis of the strain rate sensitivity of carbon/epoxy woven composites. International Journal of Impact Engineering 48, 54–64.

López-Puente, J., Varas, D., Loya, J., Zaera, R., 2009. Analytical modelling of high velocity impacts of cylindrical projectiles on carbon/epoxy laminates. Composites: Part A 40, 1223–1230.

López-Puente, J., Zaera, R., Navarro, C., 2002a. The effect of low temperatures on the intermediate and high velocity impact response of CFRPs. Composites Part B: Engineering 33, 559–566.

López-Puente, J., Zaera, R., Navarro, C., 2002b. High energy impacts on woven laminates. Journal de Physique IV 110, 639–644.

López-Puente, J., Zaera, R., Navarro, C., 2007. An analytial model for high velocity impacts on thin CFRPs woven laminated plates. International Journal of Solids and Structures 44, 2837–2851.

López-Puente, J., Zaera, R., Navarro, C., 2009. Experimental and numerical analysis of normal and oblique ballistic impacts on thin carbon/epoxy woven laminates. Composites: Part A 39, 374–387.

Manders, P., Harris, W., 1986. A parametric study of composite perfomance in compression-after-impact testing. SAMPE Journal 22, 47–51.

Manzano-Trovamala, J. R., Guerrero, M. G., Velazco, F. A., 2001. Ballistics: Ballistics of effects or ballistics of wounds. Cirujano General 23 (4), 266–272.

Meyers, M. A., 1994. Dynamic Behavior of Materials. John Wiley and Sons, University of California, San Diego, USA.

Mines, R., Roach, A., Jones, N., 1999. High velocity perforation behavior of polymer composite laminates. International Journal of Impact Engineering 22, 561–588.

Misey, J., March 1978. Analysis of the ballistic limit. USA Ballistic Research Laboratory, Maryland, USA.

Morinière, F., Alderliesten, R., Benedictus, R., 2014. Modelling of impact damage in fibre-metal laminates - a review. International Journal of Impact Engineering 67, 27–38.

Morye, S., Hine, P., Duckett, R., Carr, D., Ward, I., 2000. Modelling of the energy absorption by polymer composites upon ballistic impact. Composites Science and Technology 60, 2631–2642.

Moulton, F. R., 1914. An introduction to celestial mechanics. The Macmillan Company, New York, USA.

Nahra, H. K., 1989. Effect of micrometeoroid and space debris impacts on the space station freedom solar array surfaces. NASA-TM-102287.

Naik, N., Doshi, A., 2008. Ballistic impact behaviour of thick composites: Parametric studies. Composite Structures 82, 447–464.

Naik, N., Kavala, V., 2008. High strain rate behavior of woven fabric composites under compressive loading. Material Science and Engineering A 474, 301–311.

Naik, N., Rao, K. V., Veerraju, C., Ravikumar, G., 2010. Stress-strain behavior of composites under high strain rate compression along thickness direction: Effect of loading condition. Materials and Design 31, 396–401.

Naik, N., Shrirao, P., 2004. Composite structures under ballistic impact. Composite Structures 66, 579–590.

Naik, N., Shrirao, P., Reddy, B., 2005. Ballistic impact behaviour of woven fabric composite: Parametrix studies. Materials, Science & Engineering A 472, 104–116.

Naik, N., Shrirao, P., Reddy, B., 2006. Ballistic impact behavior of woven fabric composites: Formulation. International Journal of Impact Engineering 32, 1521–1552.

Navarro, C., 1998. Simplified modelling of the ballistic behaviour of fabrics and fibre-reinforced polymeric matrix composite. Key Engineering Materials, 383–400.

Ochoa, R. O., Marcus, K., Nurick, G. N., Franz, T., 2004. Mechanical behaviour of glass and carbon fiber reinforced composites at varying strain rates. Composite Structures 63, 455–467.

Patel, B., Bhola, S., Ganapathi, M., Makhecha, D., 2004. Penetration of projectiles in composite lamiantes. Defence Science Journal 54, 151–159.

Pernas-Sánchez, J., Artero-Guerrero, J., Varas, D., López-Puente, J., 2014. Experimental analysis of normal and oblique high velocity impacts on cabron/epoxy tape laminates. Composites: Part A 60, 24–31.

Pernas-Sánchez, J., Pedroche, D., Varas, D., López-Puente, J., Zaera, R., 2012. Numerical modeling of ice behavior under high velocity impacts. International Journal of Solids and Structures 49, 1919–1927.

Rakhmatulin, K. A., 1966. Strength under high transient loads. Israel Program for Scientific Translations, Jerusalem.

Rechak, S., Sun, C., 1987. Optimal use of adhesive layers in reducing impact damage in composite laminates. Composite Structures 2, 18–31.

Reis, P., Ferreira, J., Santos, P., Richardson, M., Santos, J., 2012. Impact response of kevlar composites with filled epoxy matrix. Composites Structures 94, 3520–3528.

Rodriguez, J., Chocron, I., Martínez, M., Sánchez-Gálvez, V., 2004. High strain rate properties of aramid and polyethylen woven fabric composites. Composites: Part B 27B, 147–154.

Roylance, D., 1973. Wave propagation in a viscoelastic fiber subjected to transverse impact. Journal of Applied Mechanics Paper No. 72-APM-27.

Schubel, P., Luo, J., Daniel, I. (Eds.), 2006. Through-thickness characterization of thick composite laminates. SEM, Anual Conference & Exposition on Experimental and Applied Mechanics.

Sebaey, T., González, E., Lopes, C., Blanco, N., Costa, J., 2013. Damage resistance and damage tolerance of dispersed CFRP laminates: effect of ply clustering. Composite Structures 106, 96–103.

Shaktivesh, Nair, N., Kumar, C. S., Naik, N., 2013. Ballistic impact perfomance of composite targets. Materials and Design 51, 833–846.

Sikarwar, R. S., Velmurugan, R., Gupta, N. K., 2013. Ballistic performance of kevlar/epoxy composite laminates. Proceedings of the Indian National Science Academy 79, 789–799.

Smith, J., McCrackin, F., Schiefer, H., 1958. Stress-strain relationships in yarns subjected to rapid impact loading: 5. Wave propagation in long textile yarns impacted transversely. Journal of Research of National Bureu of Standards 60, 517–534.

Starley, D., 1999. Determining the technological origins of iron and steel. Journal of Archeological Science 26, 1127–1133.

Stellbrink, K., 1987. Improved impact damaged tolerance. In: Proceedings of European Symposium on Damage Development and Failure Processes in Composite Materials. Belgium.

Stickel, J. M., Nagarajan, M., 2012. Glass fiber-reinforced composites: From formulation to application. International Journal of Applied Glass Science 3, 122–136.

Sun, C., Potti, V., 1996. A simple model to predic residual velocities of thick composite laminates subjected to high velocity impact. International Journal of Impact Engineering 18, 339–353.

Sun, L., Gibson, R., Gordaninejad, F., Suhr, J., 2009. Energy absorption capability of nanocomposites: a review. Composites Science and Technology 69, 2392–2409.

Takeda, N., Sierakowski, R. L., Ross, C. A., Malvern, L. E., 1980. Delamination-crack propagation in ballistically impacted glass/epoxy composite laminates. Experimental Mechanics 22, 19–25.

Tan, V., Lim, C., Cheong, C., 2003. Perforation of high-strength fabric by projectiles of different geometry. International Journal of Impact Engineering 28, 207–222.

Tanabe, Y., Aoki, M., Fujii, K., Kasano, H., Yasuda, E., 2003. Fracture behavior of CFRPs impacted by relatively high-velocity steel sphere. International Journal of Impact Engineering 28, 627–642.

Tolano, M. I. G., February 2008. Introducción a la teoría de perturbaciones. Ph.D. thesis, Universidad de Sonora.

Vinson, J. R., Walker, J. M., 1997. Ballistic impact of thin-walled composites structures. AIAA Journal 35, 875–878.

Vinson, J. R., Zukas, J., 1975. On the ballistic impact of textile body armor. Journal of Applied Mechanics 42, 263–268.

Wang, Y., Chien, X., Young, R., Kinloch, I., Wells, G., 2015. A numerical study of ply orientation on ballistic impact resistance of multi-ply fabric panels. Composites: Part B 68, 259–265.

Wen, H., 2000. Predicting the penetration and perforation of frp laminates struck normally by projectiles with different nose shapes. Composite Structures 49, 321–330.

Will, M., Franz, T., Nurick, G., 2002. The effect of the laminate stacking sequence of CFRP filament wound tubes subjected to projectile impact. Composite Structures 58, 259–270.

Woo, S., Kim, T., 2014. High-strain-rate impact in kevlar-woven composites and fracture anlaysis using acoustic emission. Composites: Part B 60, 125–136.

Woodward, R. L., 1990. A simple one-dimensional approach to modelling ceramic composite armour defeat. International Journal of Impact Engineering 9 (4), 455–474.

Wu, E., Chang, L., 1995. Woven glass/epoxy laminates subjected to projectile impact. International Journal of Impact Engineering 16, 607–619.

Xin, S.-H., Wen, H. M., 2012. Numerical study on the perforation of fiber reinforced plastic laminates struck by high velocity projectiles. Journal of Strrain Analysis 47(7), 513–523.

Yashiro, S., Ogi, K., Nakamura, T., Yoshimura, A., 2013. Characterization of high-velocity impact damage in CFRP laminates: Part i - experiment. Composites: Part A 48, 93–100.

Zaera, R., Sánchez-Gálvez, V., 1998. Analytical modelling of normal and oblique ballistic impacton ceramic/metal lightweight armours. International Journal of Impact Engineering 21, 133–148.

Zhu, G., Goldsmith, W., Dharan, C., 1992a. Penetration of laminated kevlar by projectiles - i. experimental investigation. International Journal of Solids and Structures 29, 399–420.

Zhu, G., Goldsmith, W., Dharan, C., 1992b. Penetration of laminated kevlar by projectiles - ii. analytical model. International Journal of Solids and Structures 29, 421–436.

Zukas, J. A., 1982. Impact Dynamics. John Wiley and Sons, New York, USA.

Appendix A

A.1 Description of the frontal projectile area $A(x)$

In order to achieve the complete description of both, laminate crushing and linear momentum transfer energetic terms, the function that describes the frontal projectile area in contact with the non-crushed laminate should be defined. This function hinges on two facts: the type of projectile defeating the target, and the obliquity between the longitudinal projectile axis and the impacted surface of the plate. For instance, if a flat-nosed cylindrical bullet without stability problems during flight, hits normally onto a rectangular plate, the frontal projectile area will remain constant during the through-thickness penetration.

In this case, the impact is produced by a spherical projectile, so no tumbling effects should be considered. Because of the spherical geometry of the projectile, its frontal area in contact with the non-crushed surface of the target now depends on the depth of penetration. It must be defined in terms of the projectile displacement x.

The Figure A.1 illustrates the complete go-through-the-thickness process. As the frontal projectile area varies with the projectile position, $A(x)$ should be defined in terms of a piecewise-defined function. In the first stage (Figure A.1(a)), the penetration process just get started. Therefore, the frontal projectile area is defined by a circular surface of radius κ.

$$A(0 \leq x \leq h) = \pi\kappa^2 = \pi\left(r^2 - (r-x)^2\right) \tag{A.1}$$

At the second stage (Figure A.1(b)), the projectile reaches the back face of the plate, so that the frontal projectile area is now defined by means of an annulus surface with outer radius κ_o and inner radius κ_i.

$$A(h \leq x \leq r) = \pi\left({\kappa_o}^2 - {\kappa_i}^2\right) = \pi\left((r-x+h)^2 - (r-x)^2\right) \tag{A.2}$$

At the last stage (Figure A.1(c)), the widest part of the projectile penetrates into the target. This means that henceforth, the outer radius of the frontal area is determined by the projectile radius r.

$$A(r \leq x \leq r+h) = \pi\left(\kappa^2 - r^2\right) = \pi(r-x+h)^2 \tag{A.3}$$

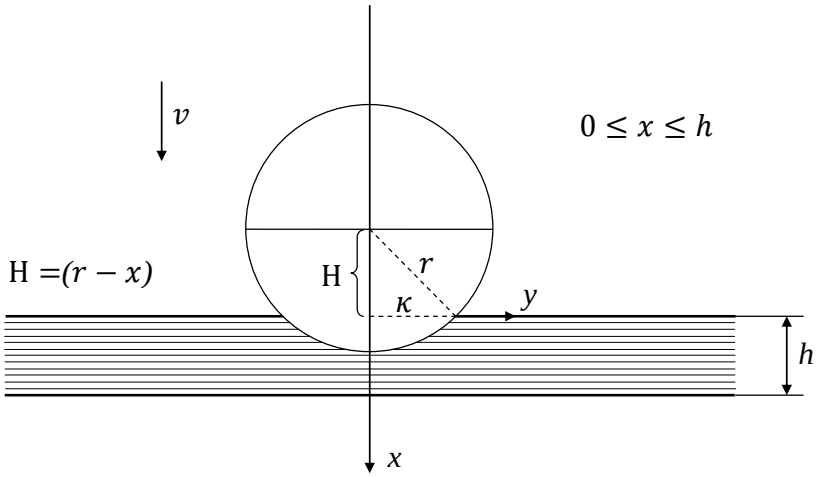

(a)

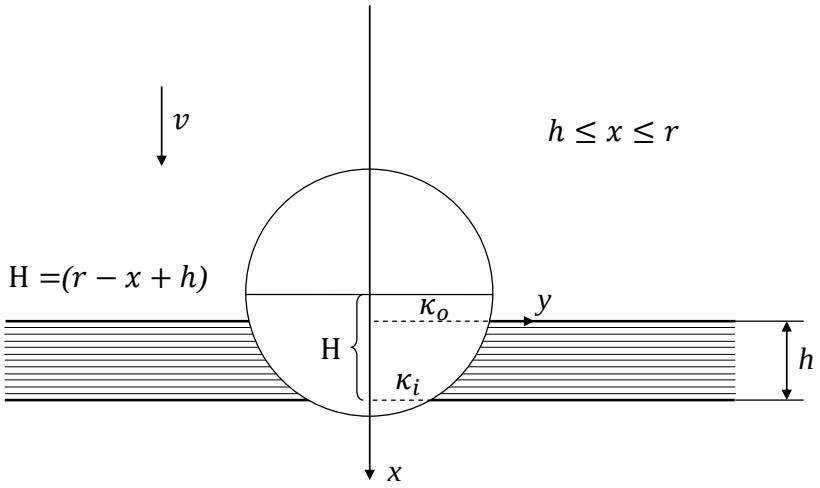

(b)

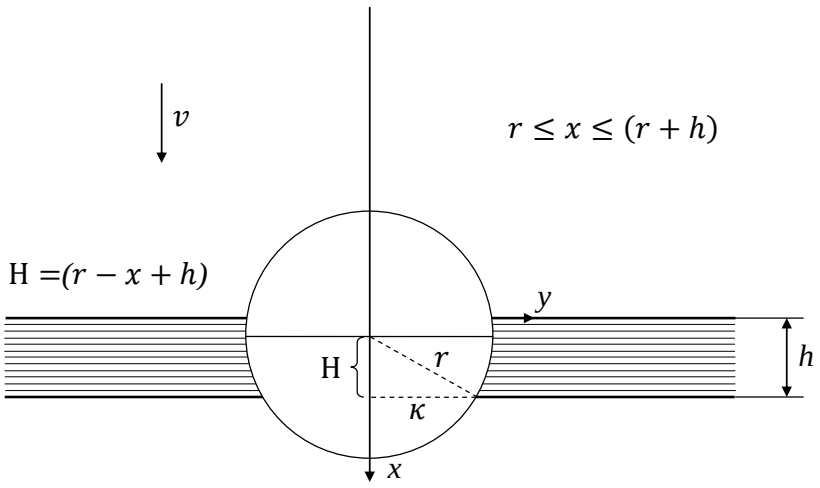

(c)

Figure A.1: Scheme of the penetration process

Gathering the above process into a piecewise function, the frontal projectile area $A(x)$ is completely defined by

$$A(x) = \begin{cases} \pi\left(r^2 - (r-x)^2\right) & \text{if} \quad 0 \leq x \leq h; \\ \pi\left((r-x+h)^2 - (r-x)^2\right) & \text{if} \quad h \leq x \leq r; \\ \pi(r-x+h)^2 & \text{if} \quad r \leq x \leq r+h; \\ 0 & \text{if} \quad x \geq r+h. \end{cases} \tag{A.4}$$

It can be inferred that the dependent energetic terms of this function (laminate crushing and linear momentum transfer) become zero when there is no contact between the projectile and the target plate ($x \geq r + h$). The function $A(x)$, as above described, is only valid when the laminate thickness h is less than the projectile radius r.

A.1.1 Non-Dimensional frontal projectile area $A_c(x^*)$

The frontal projectile area function $A(x)$ can be split up by the product of two terms; as it is described below.

$$A(x) = A_0 A_c(x^*) \tag{A.5}$$

where A_0 is a constant term of value $A_0 = \pi r^2$, and $A_c(x^*)$ is a non-dimensional function in terms of the dimensionless variable $x^* = x/h$; this function is defined as follows

$$A_c(x^*) = \begin{cases} \frac{1}{r^2}\left(2rhx^* - (hx^*)^2\right) & \text{if} \quad 0 \leq x \leq 1; \\ \frac{h^2}{r^2}\left(1 - 2x^* + \frac{2r}{h}\right) & \text{if} \quad 1 \leq x \leq r/h; \\ \left(1 + \frac{h^2}{r^2}\left(x^{*2} + 1 - 2x^*\right) + \frac{2h}{r}\left(1 - x^*\right)\right) & \text{if} \quad r/h \leq x \leq 1 + r/h; \\ 0 & \text{if} \quad x \geq 1 + r/h. \end{cases} \tag{A.6}$$

A.1.2 Primitive of the dimensionless frontal projectile area, $\hat{A}_c(x^*)$

For the complete description of the zero and first order solution, the function $\hat{A}_c(x^*)$ is required. This function is defined as the primitive of the non-dimensional function $A_c(x^*)$

$$\hat{A}_c(x^*) = \int A(x^*)\mathrm{d}x^* \tag{A.7}$$

Previous integration can be accomplished due to the fact that $A_c(x^*)$ is a piecewise continuous function. The notion of area under the graph makes sense due to the finite discontinuities between each piece of the function.

Appendix B

B.1 CFRP model programming code

The code containing the CFRP model, presented in Chapter 2, was programmed using Mathcad 14. This program was used to present the results shown throughout this work. Below, different sections of the code are presented and illustrated in detail.

The program is organized in different tabs or *areas*. By double-clicking on each tab, it is possible to access different sections of the program. The tiresome task of going through all the bulk code is avoided thus, allowing the user to get direct access to the model results.

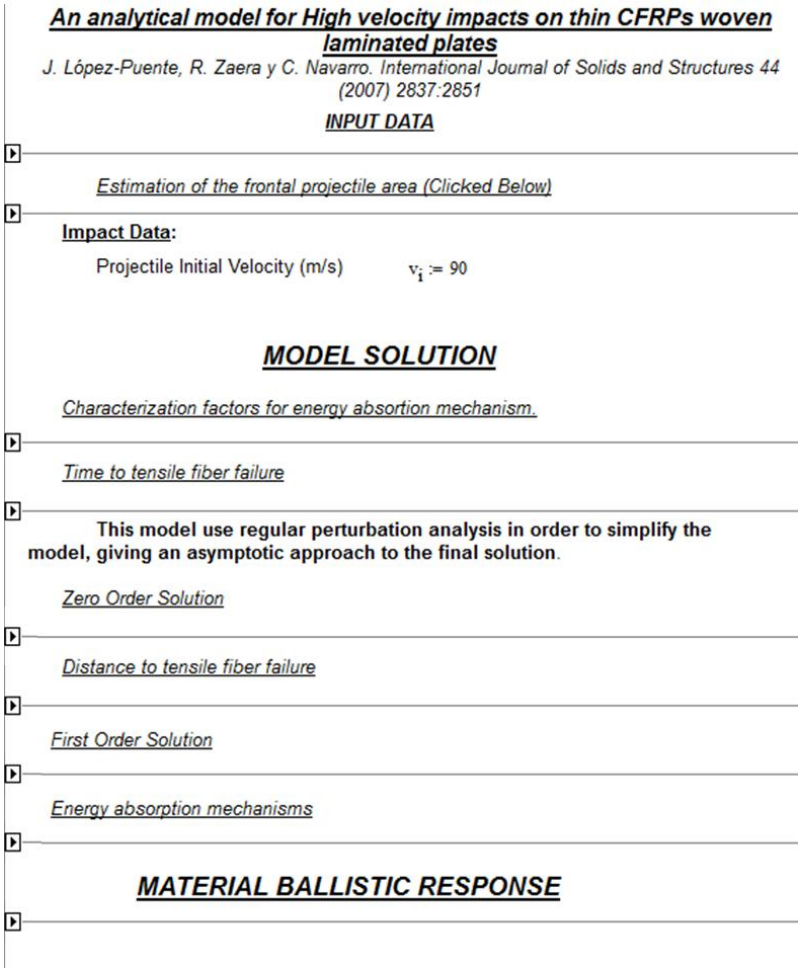

Figure B.1: First look to the CFRP model program.

The first tab that must be opened is the one related to the properties of material and projectile, which defines the program input data.

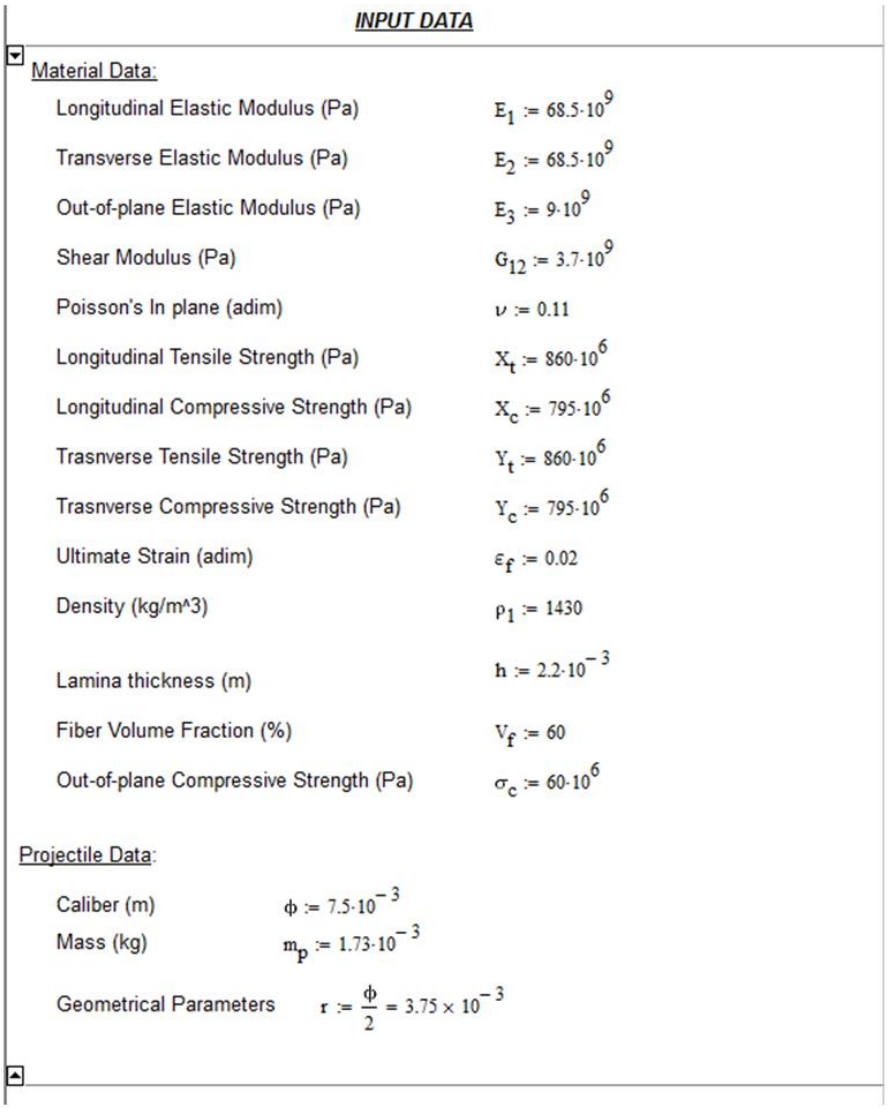

Figure B.2: Input parameters.

Input parameters are followed by a short description of the dimensionless, frontal projectile area (for more details related to this property, see Appendix A). Definition of the program input ends by establishing the projectile impact velocity.

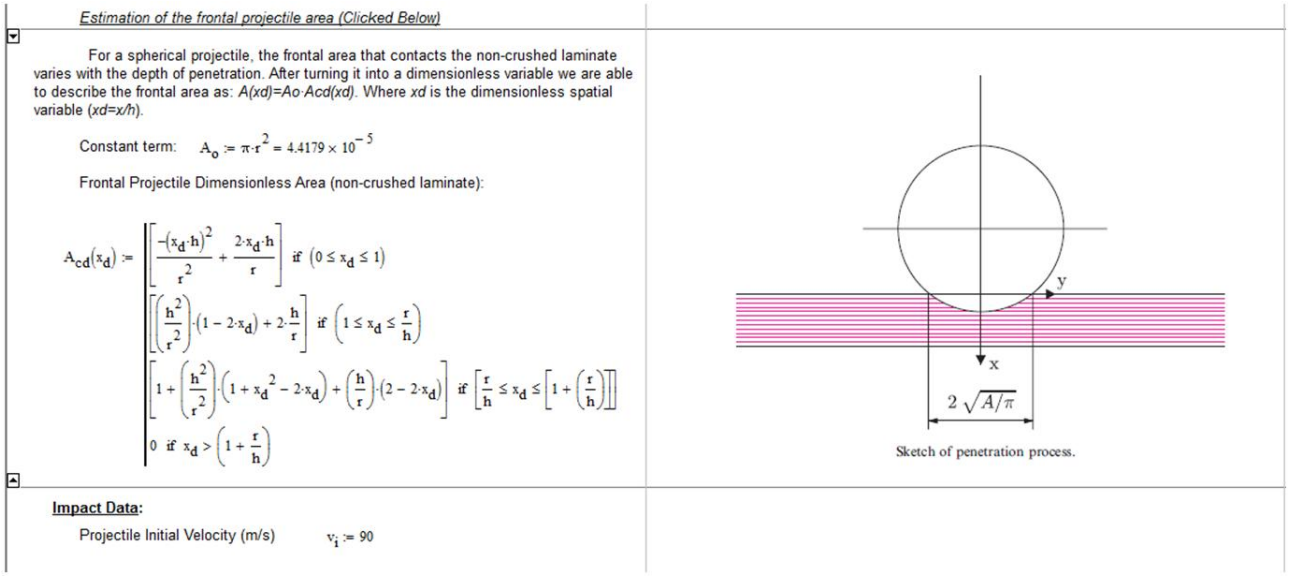

Figure B.3: Frontal area and initial velocity of the projectile.

Once every initial parameter has been declared, model solution is presented. The first section within model solution contains parameters regarding the energy absorption mechanisms characterization factors.

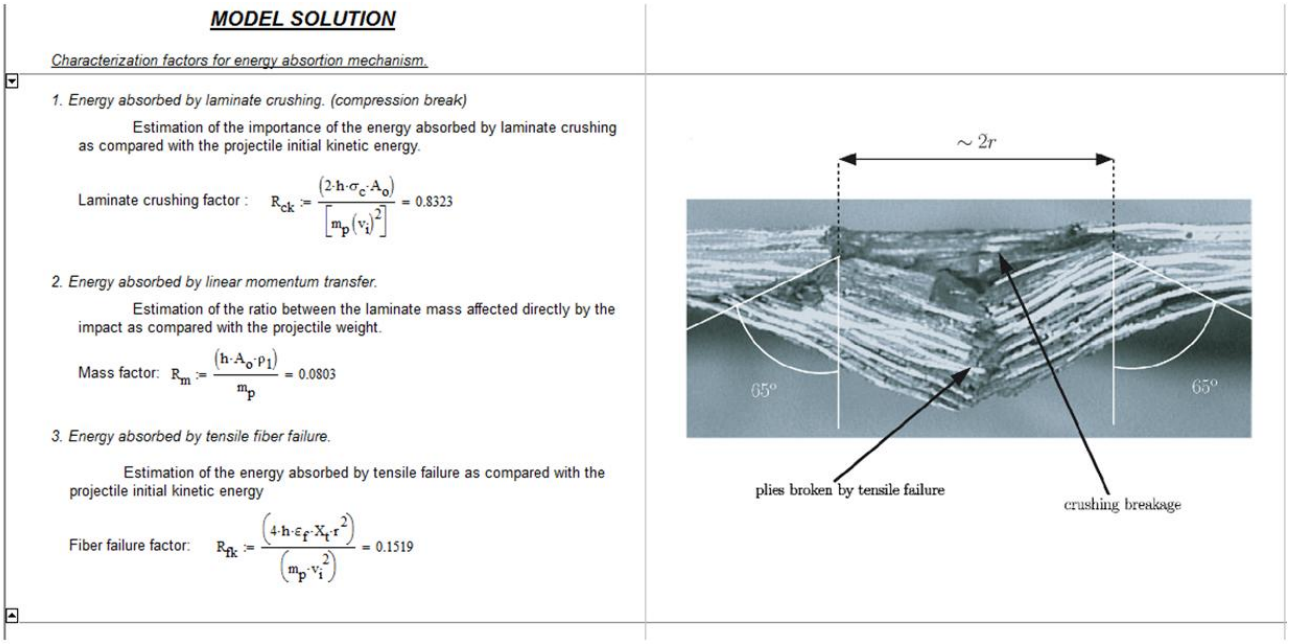

Figure B.4: Characterization factors related to each energy absorption mechanism.

The next tab describes two parameters needed to later define the energy dissipated by tensile fiber failure. Those are, the time up to which this mechanism begins to defeat the target and the cut-off function needed to completely described this failure mechanism.

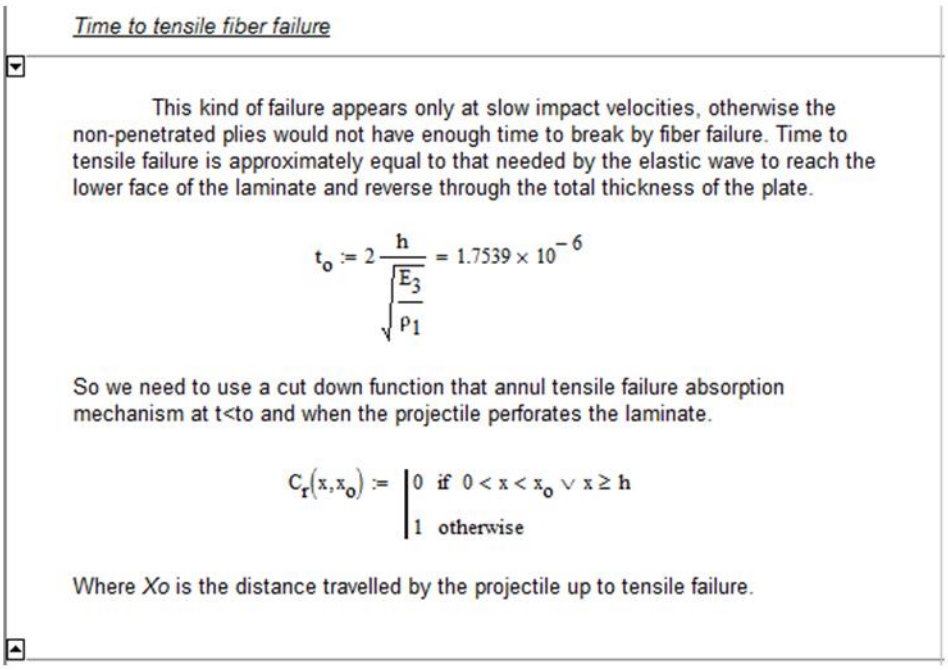

Figure B.5: Time to tensile fiber failure and cut-off function.

In the following sections, the perturbation technique applied in order to solve the model is presented. Zero-order solution and first-order solution are programmed in different tabs so one can compare the improvement obtained by including the latter solution on the asymptotic expansion. A first approach to the ballistic limit and residual velocity of the projectile can be found on the zero-order solution tab.

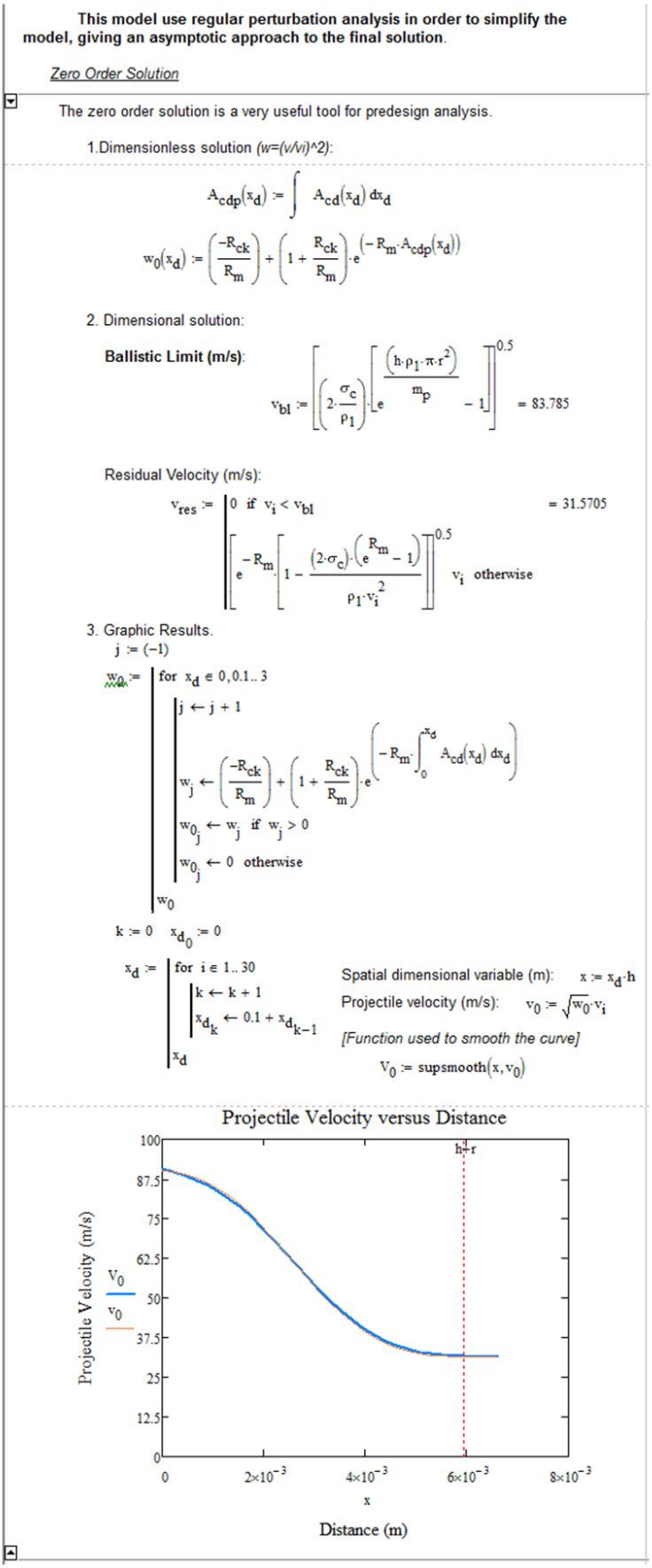

Figure B.6: Zero-order solution.

The distance travelled by the projectile up to which the tensile failure of fibers begins can be obtained right after the zero-order solution. A simple midpoint quadrature rule is used to numerically solve the time to tensile failure equation.

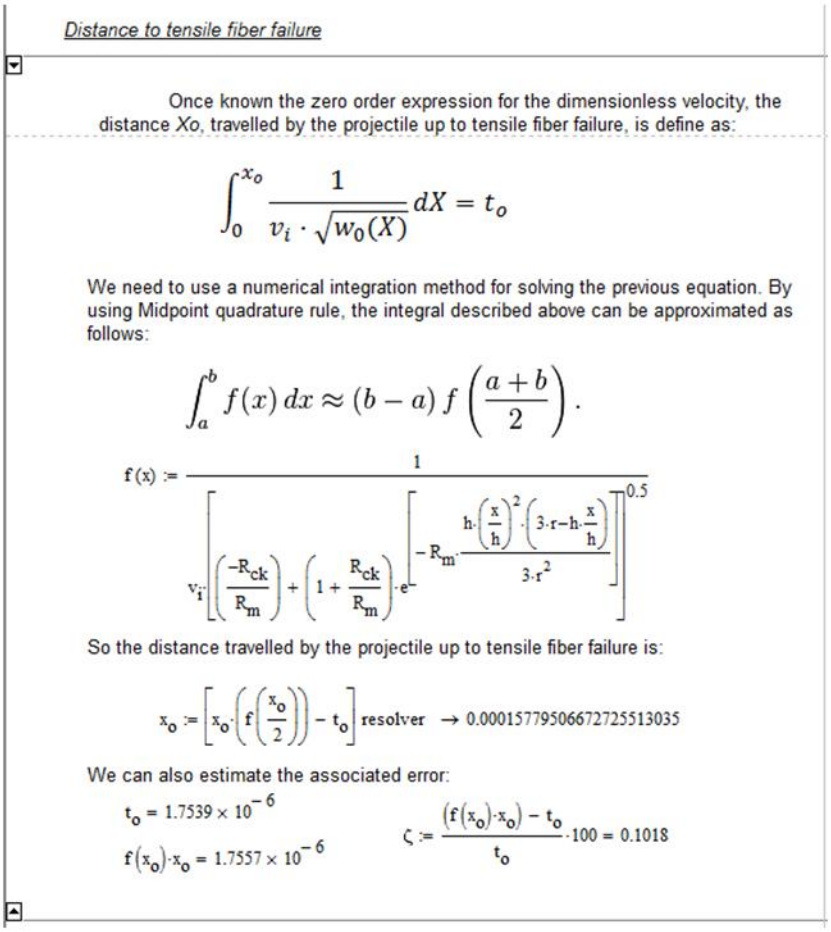

Figure B.7: Distance to tensile fiber failure.

Once the distance to tensile failure is obtained, it is possible to completely define the cut-off function that describes the energy absorbed by tensile failure and therefore, calculate the first-order solution. A chart containing results obtained by the zero-order and first-order solution is also included.

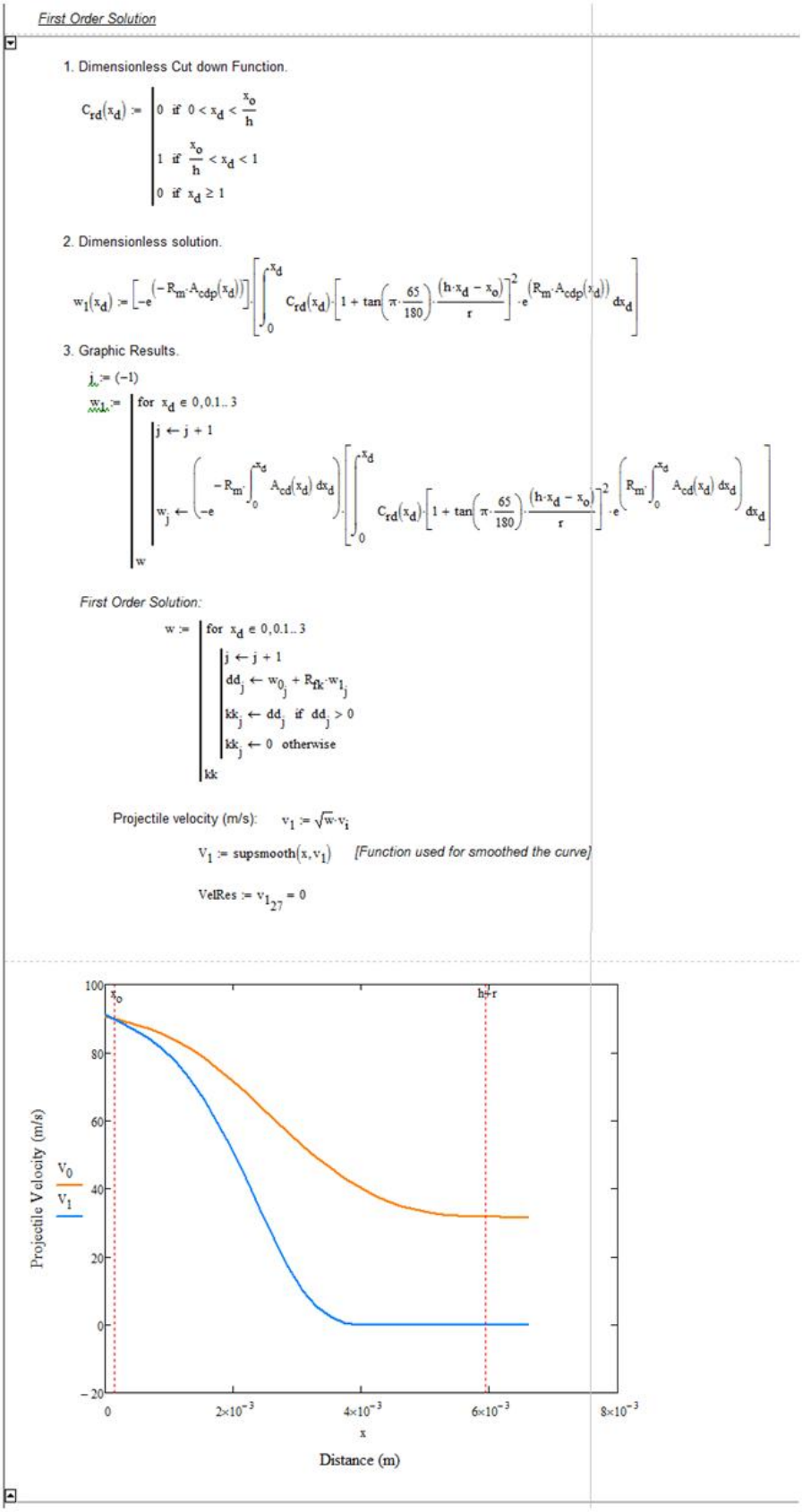

Figure B.8: First-order solution.

With the asymptotic solution totally defined, it is possible to calculate the energy absorbed by each mechanism.

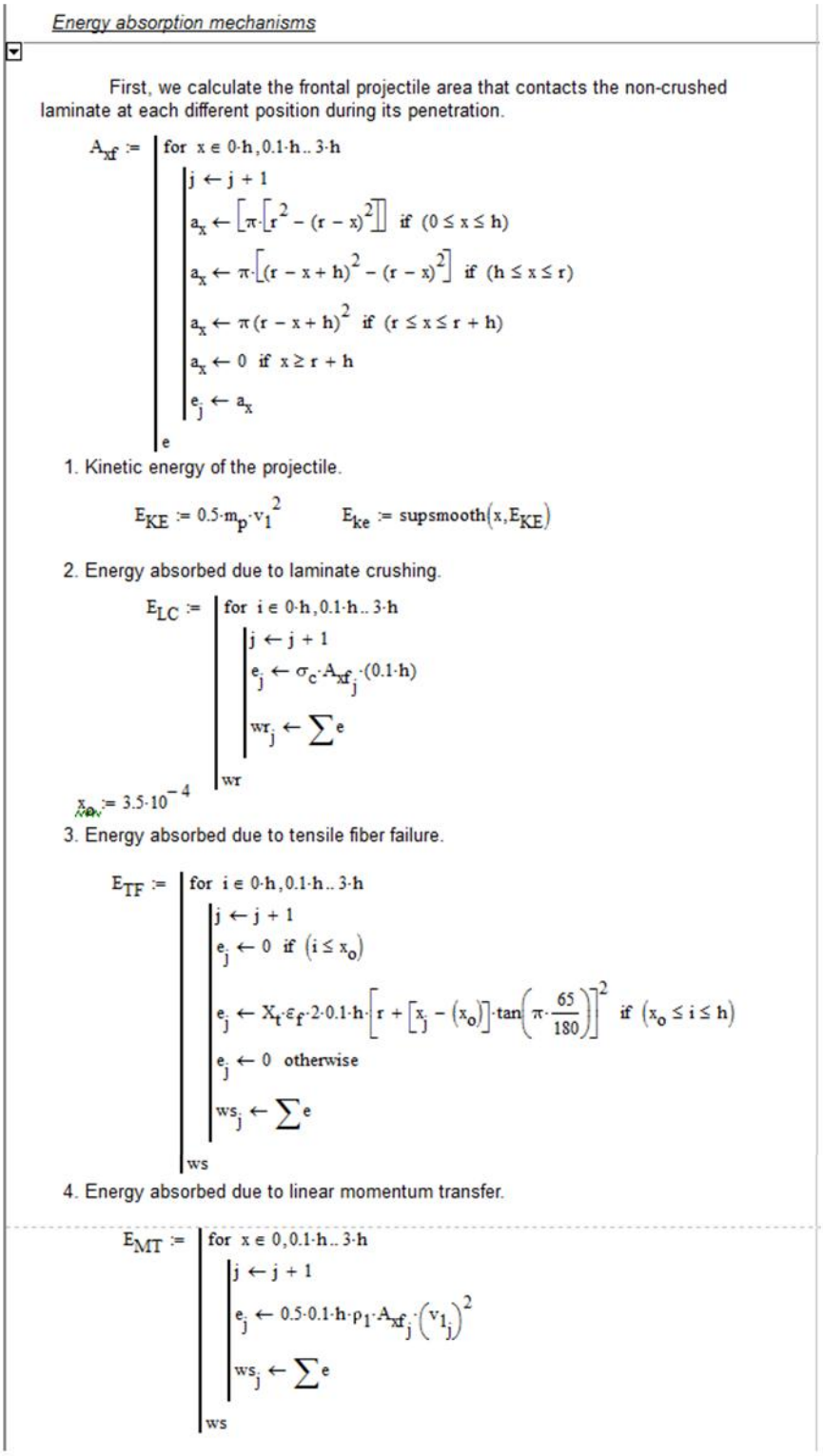

Figure B.9: Energy dissipated by each mechanism.

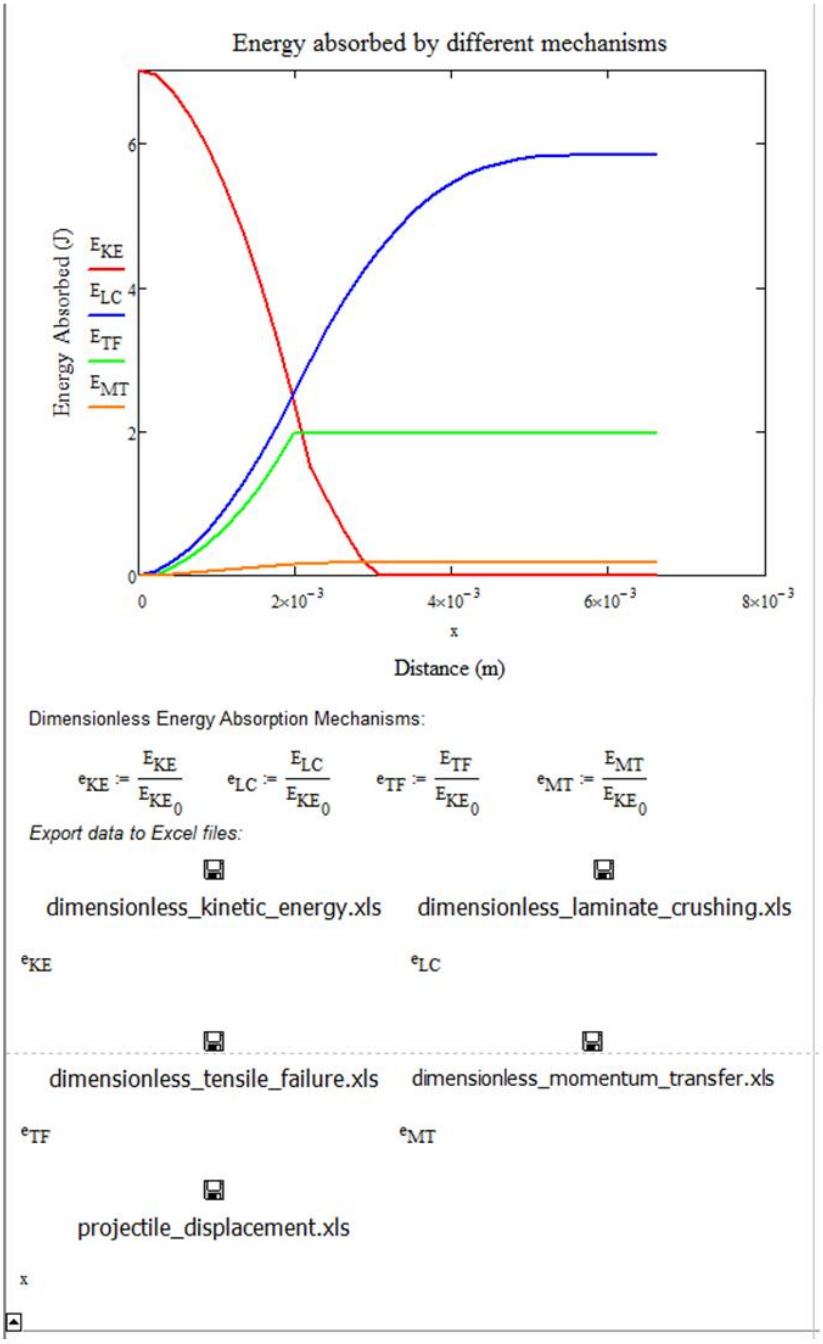

Figure B.10: Energy dissipated with the distance travelled by the projectile.

As shown above, at the end of this section, a plot is featured containing the variation of the energy absorbed by each mechanism with the distance travelled by the projectile. Every data regarding energy mechanisms is sent to an excel file automatically generated where can be easily handled.

Finally, the ballistic response of the material is characterized by the residual velocity of the projectile at different impact velocities.

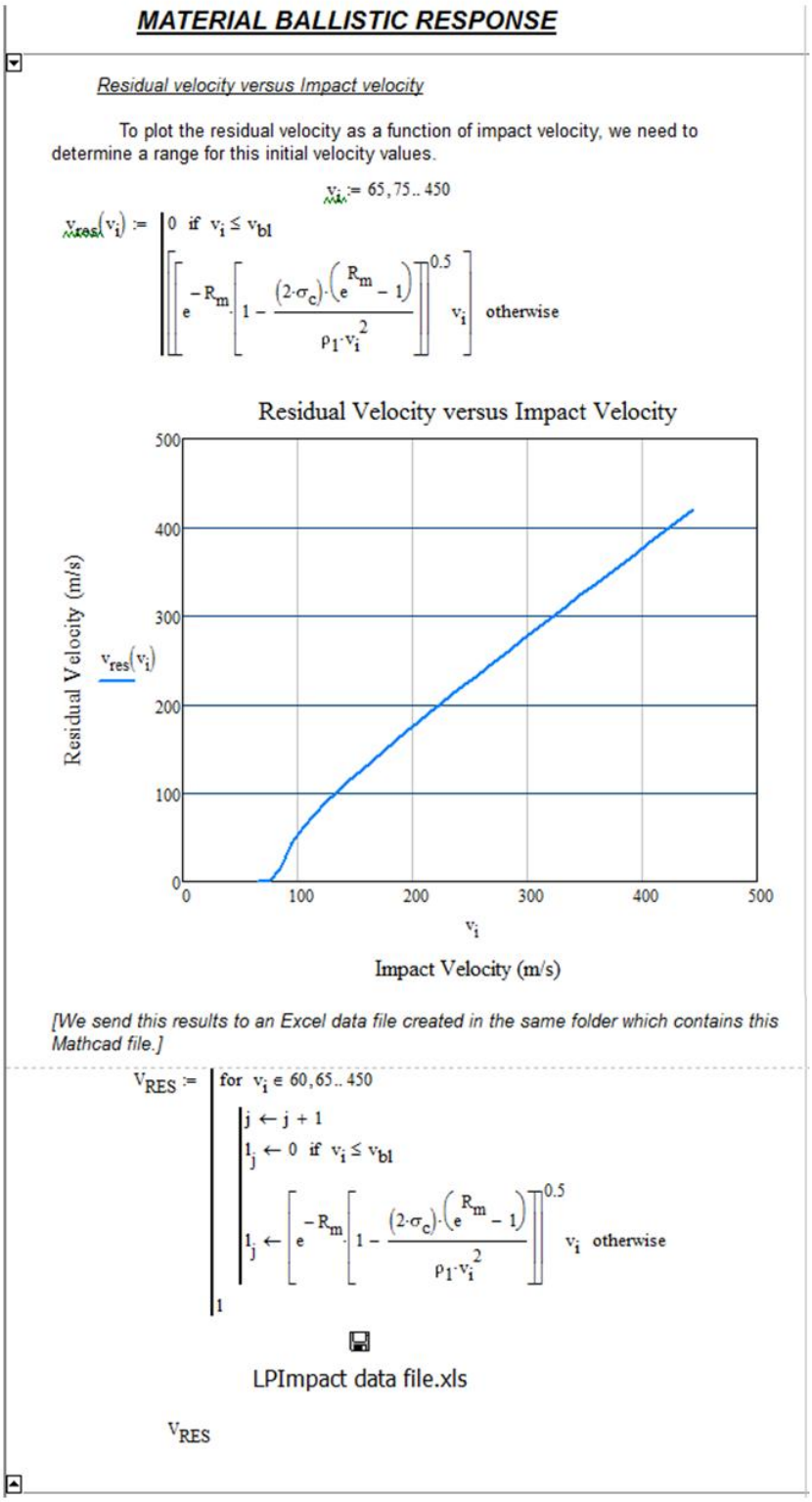

Figure B.11: Ballistic response of the material.

B.2 GPFRP model programming code

The code containing the GPFRP model, presented in Chapter 3, was programmed using Mathcad 14. This program was used to present the results shown throughout this work. Below, different sections of the code are presented and illustrated in detail.

The program code follows the same tab-based structure than in the previous model. As the present model needs of an iterative method to be solved, several differences with the CFRP model can be found along the code. A first look into the program code is shown in the following figure.

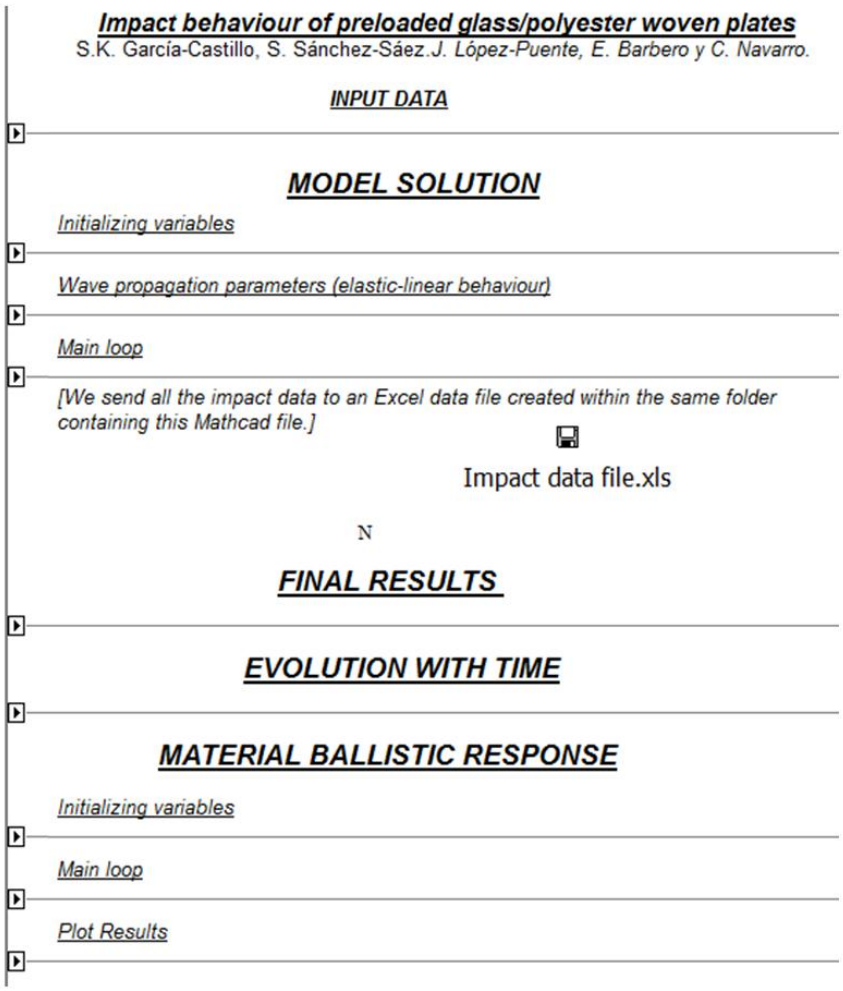

Figure B.12: First look to the GPFRP model program.

The first tab that must be opened is the one related to the properties of material and projectile, which defines the program input data.

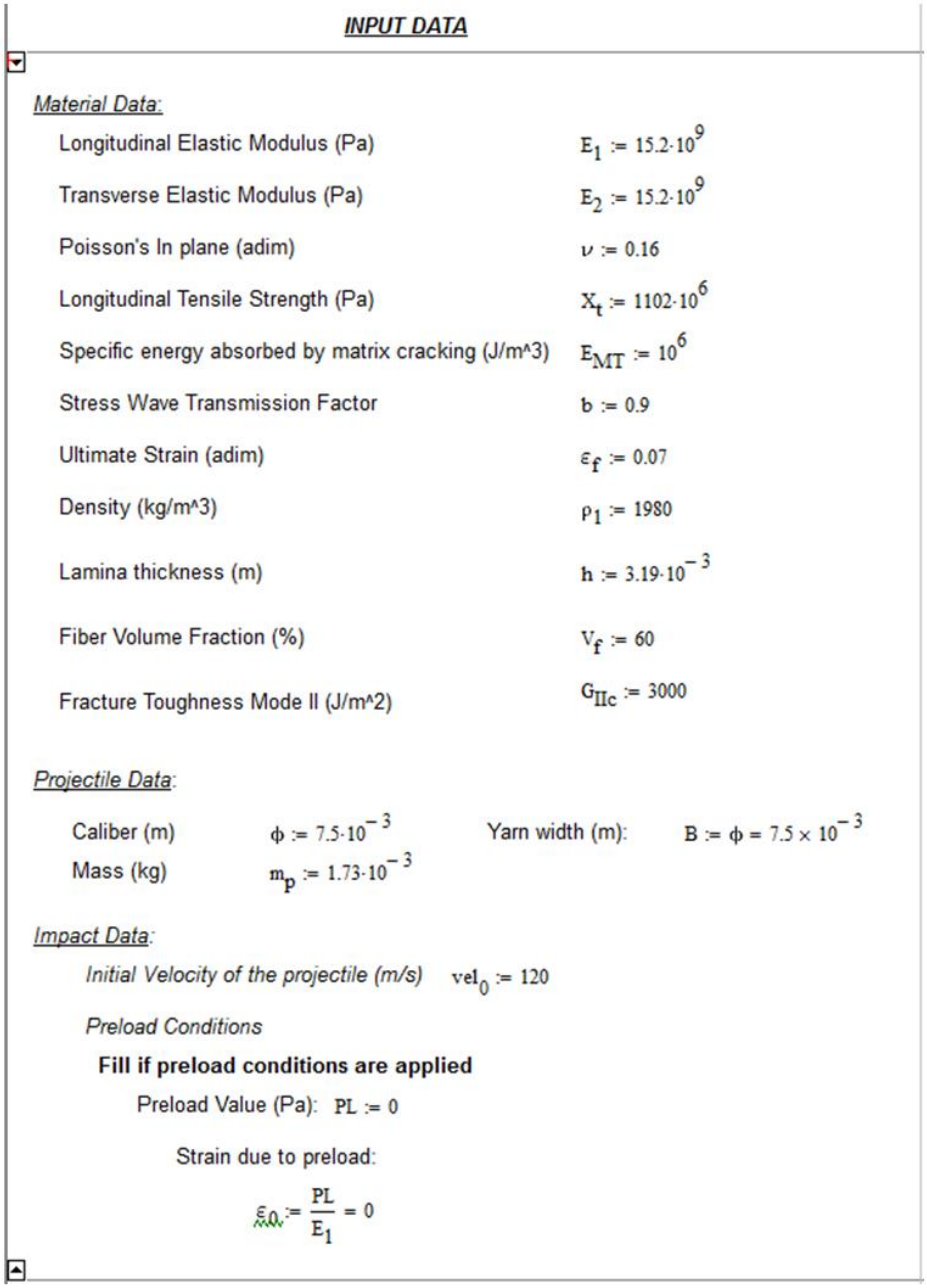

Figure B.13: Input parameters.

The model resolution begins with the initialization of variables. The most important parameter encompassed within this tab is the one related to the time interval. The level of accuracy of the results obtained can be modified by varying the value of this parameter.

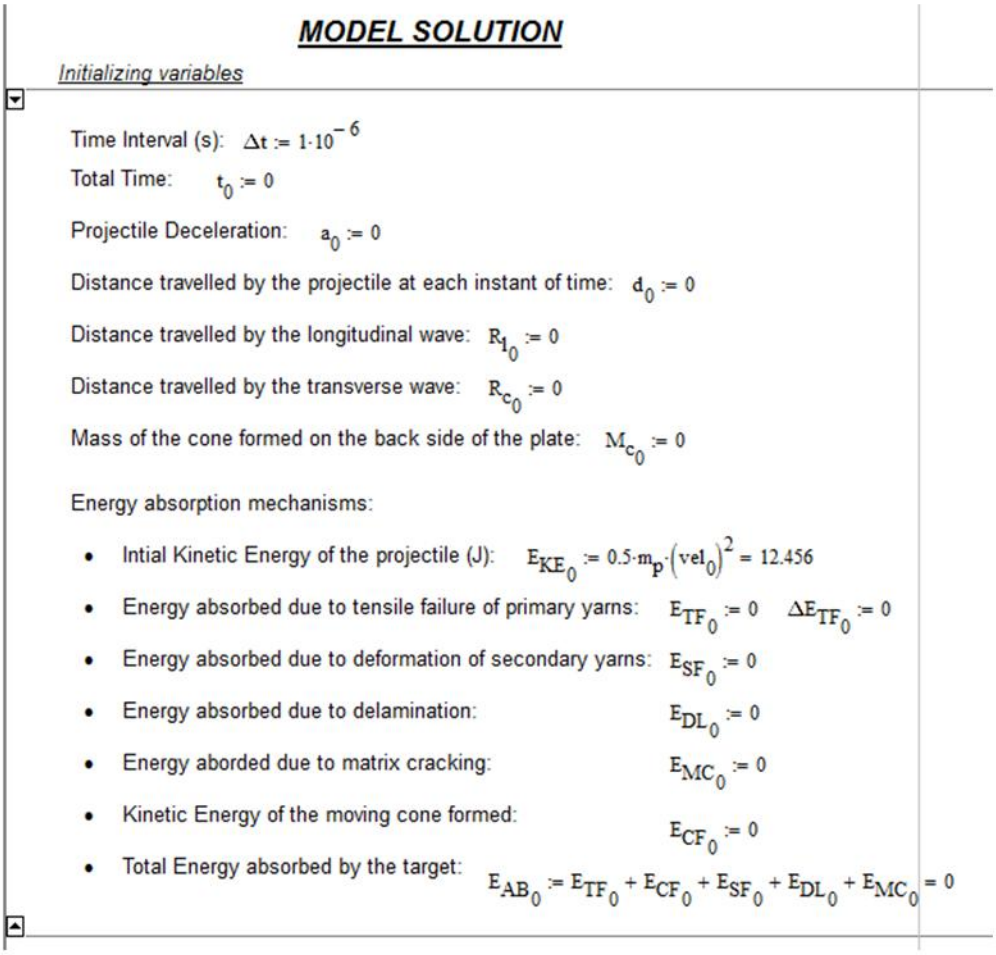

Figure B.14: Initializing variables.

After the initialization of variables, parameters regarding the wave propagation can be found; that is, longitudinal and transverse waves velocities.

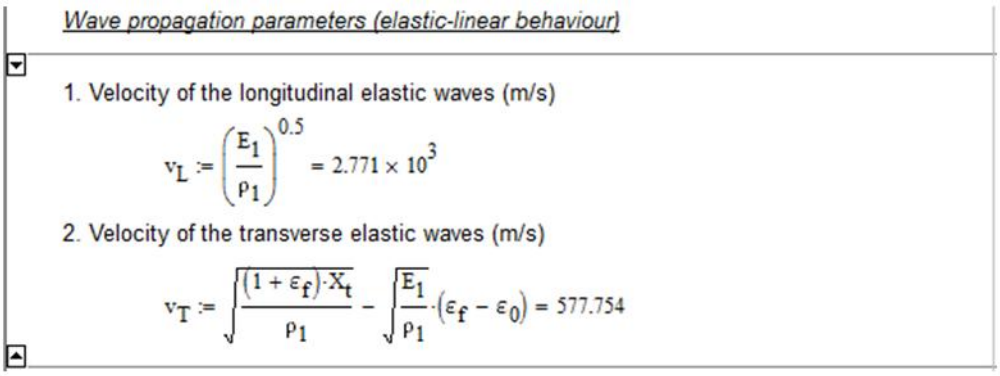

Figure B.15: Wave propagation parameters.

The next tab contains the main code of the program. By this code, several iterations take place until either the projectile has gone through the target or get stuck on it. Results are saved in matrix form in order to handle them easily.

Figure B.16: Main loop of the program code.

Results are sent into an *.xls* file automatically generated so they can be easily managed .

[We send all the impact data to an Excel data file created within the same folder containing this Mathcad file.]

Impact data file.xls

N

Figure B.17: Results exportation.

The final loop results concerning wave, energies, and projectile parameters are gathered into the following tab.

FINAL RESULTS

Distance travelled by the longitudinal and transverse waves

After the initial contact between the projectile and target, longitudinal and transverse waves travel within the plate the following distances.

a) Distance travelled by the longitudinal wave (m):

$R_l := N_{0,3} = 0.044$

b) Distance travelled by the transverse wave (m):

Note that the distance travelled by the transverse wave will be equal to the radius of the cone formed on the back side of plate.

$R_c := N_{0,4} = 9.244 \times 10^{-3}$

As Rc indicates the radius of the cone formed, we are able to estimate the mass (kg) of the cone:

$M_c := N_{0,5} = 1.696 \times 10^{-3}$

Energy absoption mechanisms

0. Initial kinetic energy of the projectile. (J)

$E_{KE} := E_{KE_0} = 12.456$

Once the distances traveled by the waves and the main parameters of the cone formed on the back side of the plate are known, we are able to estimate the amount of energy absorbed by the following mechanisms.

1. Energy absorbed due to delamination.(J)

$E_{DL} := N_{0,6} = 0.805$

2. Energy absorbed due to matrix cracking.(J)

$E_{MC} := N_{0,7} = 0.856$

3. Energy absorbed due to deformation of secondary yarns.(J)

$E_{SF} := N_{0,8} = 7.004$

4. Energy absorbed due to failure of primary yarns.(J)

The energy absorbed by this mechanism depends on the distance travelled by the projectile at each instant of time. In order to estimate it, we must know first the kinetic parameters of the projectile at every time (velocity, aceleration and distance). The velocity of the projectile, in turns, depends on the amount of energy absorbed by the plate at each instant of time. Taking into account all this relationships between variables the energy absorbed due to tensile fiber failure is given by the expression defined in the main loop.

$E_{tf} := N_{0,9} = 4.749$

5. Kinetic of the moving cone formed on the back side of the plate. (J)

$E_{CF} := N_{0,10} = 0$

6. Total energy absorbed by the plate. (J)

$E_{AB} := N_{0,11} = 12.456$

Residual velocity (m/s) and distance traveled by the projectile (m).

$ResVelocity := N_{0,1} = 0$

$Distance := N_{0,2} = 1.282 \times 10^{-3}$

Figure B.18: Outcome of the model.

In the next tab, several plots illustrate the evolution with time of the projectile velocity and energy absorbed by each mechanism.

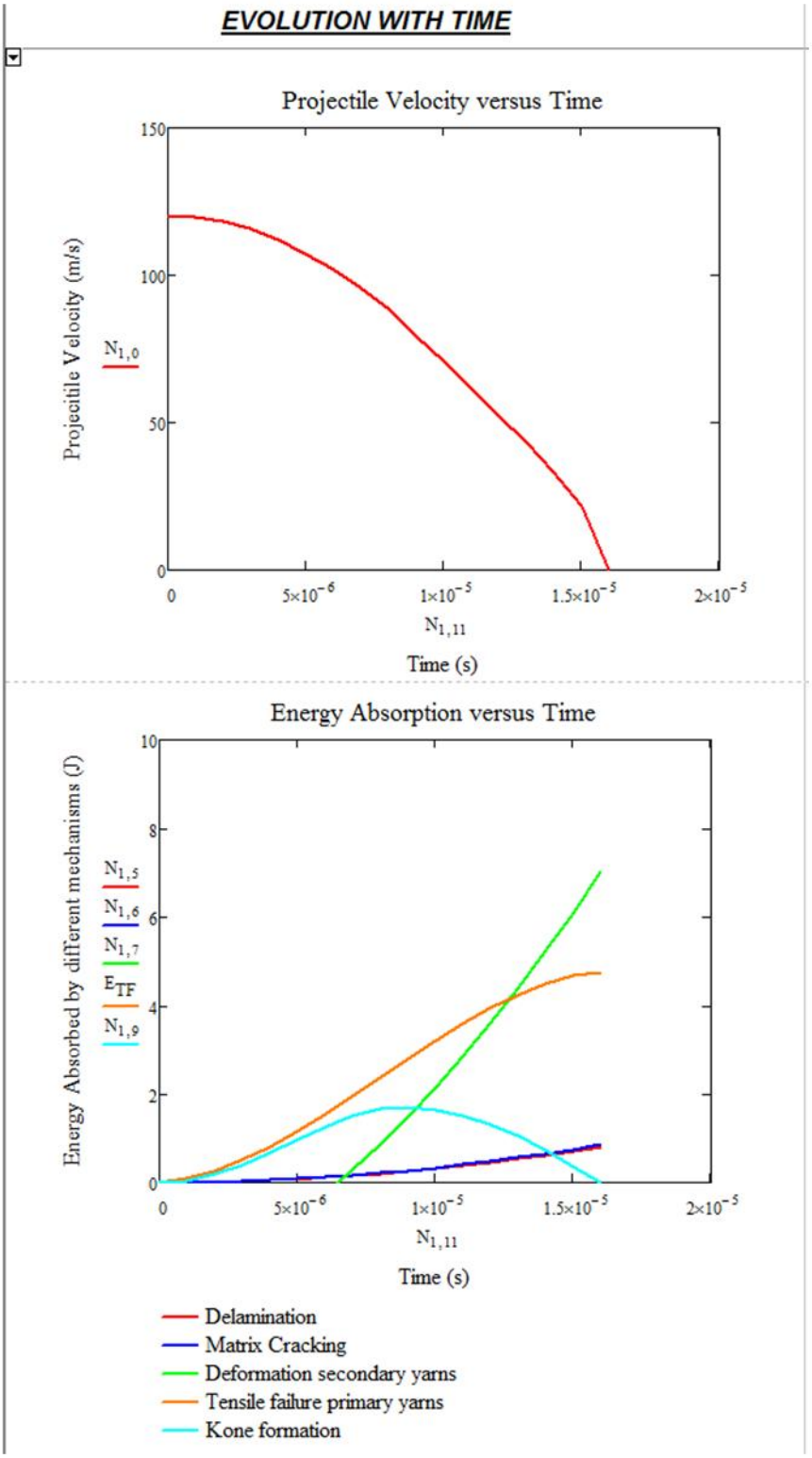

Figure B.19: Evolution of the projectile velocity and energy absorbed with time.

In order to describe the ballistic behavior of the material under study, the main loop has to be redefined as a result of the iterative method.

MATERIAL BALLISTIC RESPONSE

Initializing variables

Main loop

Initial Kinetic Energy of the projectile at different velocities. $E_{KE} :=$ for $l \in 60, 70 .. 550$; $k \leftarrow k + 1$; $mh_k \leftarrow 0.5 \cdot m_p \cdot l^2$; mh

$M :=$ for $l \in 60, 70 .. 550$

$vel_0 \leftarrow 1$

$z \leftarrow vel_0$

$y \leftarrow 0$

$j \leftarrow j + 1$

while $(z > 0 \wedge y < h)$

$i \leftarrow i + 1$

$t_i \leftarrow t_{i-1} + \Delta t$

$R_{l_i} \leftarrow v_L \cdot t_i$

$R_{c_i} \leftarrow v_T \cdot t_i$

$M_{c_i} \leftarrow \left[\rho_1 \cdot \pi \cdot \left(R_{c_i}\right)^2 \cdot h\right]$

$$E_{SF_i} \leftarrow E_1 \cdot h \cdot \pi \cdot \int_{\frac{\phi}{2}}^{R_{c_i}} \left[\frac{\left[2 \cdot \left(R_{c_i} - r\right)\right]}{\left(2 \cdot R_{c_i} - \phi\right)} \cdot \varepsilon_f + \varepsilon_0\right]^2 \cdot r \, dr$$

$$vel_i \leftarrow \left[\frac{\left[E_{KE_j} - E_{AB_{(i-1)}}\right]}{\left[0.5 \cdot \left(m_p + M_{c_i}\right)\right]}\right]^{0.5}$$

$$a_i \leftarrow \frac{\left[vel_{(i-1)} - vel_i\right]}{\Delta t}$$

$$d_i \leftarrow vel_{(i-1)} \cdot \Delta t - 0.5 \cdot a_i \cdot \Delta t^2$$

$$\Delta E_{TF_i} \leftarrow 0.5 \cdot B \cdot d_i \cdot E_1 \cdot \int_0^{R_{l_i}} \left[\left[\varepsilon_f \cdot (b) \frac{x}{B}\right]^2 - \left(\varepsilon_0\right)^2\right] dx$$

$$E_{DLyMCyCF_i} \leftarrow \pi \cdot \left(R_{c_i}\right)^2 \cdot G_{IIc} + \pi \cdot \left(R_{c_i}\right)^2 \cdot E_{MT} \cdot h + 0.5 \cdot \left(M_{c_i}\right) \cdot \left(vel_i\right)^2$$

$$KS_i \leftarrow E_{DLyMCyCF_i} + E_{SF_i} + \sum_{n=0}^{i} \Delta E_{TF_i} \text{ if } E_{SF_i} > 0$$

$$KS_i \leftarrow \left(\sum_{n=0}^{i} \Delta E_{TF_i}\right) + E_{DLyMCyCF_i} \text{ otherwise}$$

$E_{AB_i} \leftarrow KS_i$ if $KS_i < E_{KE_j}$

$E_{AB_i} \leftarrow E_{KE_j}$ otherwise

$z \leftarrow vel_i$

$$y \leftarrow \sum_{k=1}^{i} d_k$$

$$m_j \leftarrow \left(vel_0 \; vel_i \; \sum_{k=0}^{i} d_k \; R_{l_i} \; R_{c_i} \; M_{c_i} \; E_{DLyMCyCF_i} \; E_{SF_i} \; \sum \Delta E_{TF} \; E_{AB_i} \; t_i \; i\right)$$

$i \leftarrow 0$

m

Figure B.20: Main loop for the characterization of the material ballistic response.

Once again, Excel tools are used to easily manage data.

We use Excel tools for organize data.

$$\begin{pmatrix} \text{ImpactVel} \\ \text{ResidualVel} \\ \text{Time} \\ \text{AbsEnergy} \end{pmatrix} :=$$

180	0	0,0025222	0,0831209	0,0173326	0,0059612	5,8420988	24,148186	11,666337	28,026	0,00003
190	0	0,0027542	0,0831209	0,0173326	0,0059612	5,8420988	24,148186	13,039713	31,139079	0,00003
200	0	0,0029973	0,0886623	0,0184881	0,0067825	6,6470102	27,261822	14,518817	34,6	0,000032

$$\begin{pmatrix} M_0 & M_1 & M_2 & M_3 & M_4 & M_5 & M_6 & M_7 & M_8 & M_9 & M_{10} & M_{11} & M_{12} & M_{13} & M_{14} & M_{15} & M_{16} & M_{17} & M_{18} & M_{19} & M_{20} & M_{21} & M_{22} & M_{23} & M_{24} & M_{25} \end{pmatrix}$$

VR := supsmooth(ImpactVel, ResidualVel)

TR := supsmooth(ImpactVel, Time)

Figure B.21: Excel tools used to manage results.

Finally, the ballistic response of the material is gathered up in two plots. These plots display the variation of the residual velocity and contact time with the impact velocity of the projectile.

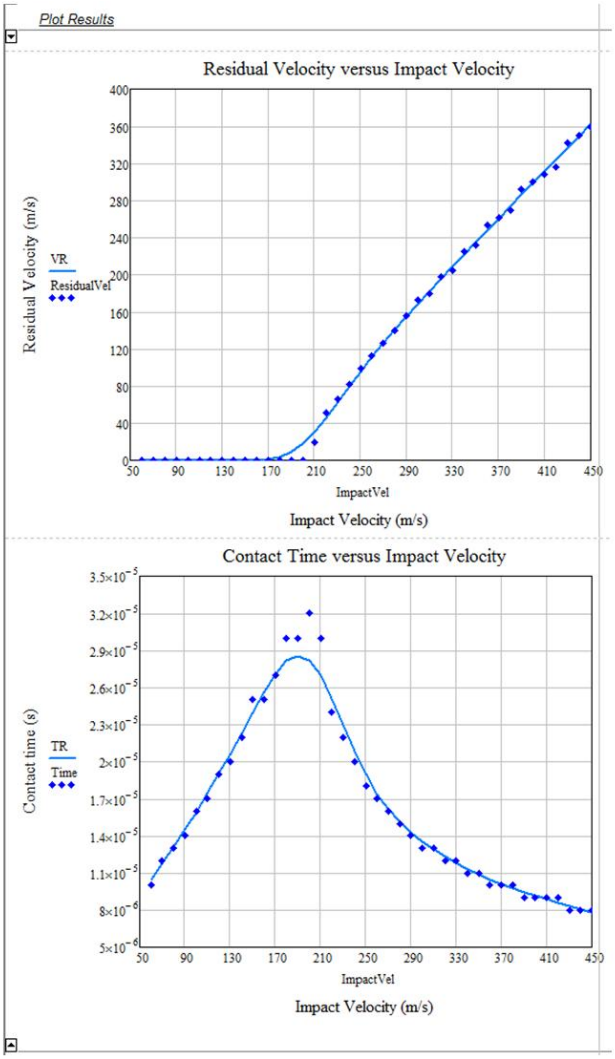

Figure B.22: Ballistic response of the material.